MODELING FILM BOILING AND QUENCHING ON THE OUTER SURFACE OF A CALANDRIA TUBE FOLLOWING A CRITICAL BREAK LOCA IN A CANDU REACTOR

MODELING FILM BOILING AND QUENCHING ON THE OUTER SURFACE OF A CALANDRIA TUBE FOLLOWING A CRITICAL BREAK LOCA IN A CANDU REACTOR

by

JIAN TAO JIANG, B.Eng.

A Thesis Submitted to the School of Graduate Studies

in Partial Fulfillment of the Requirements

for the Degree of

Master of Applied Science

McMaster University

MASTER OF APPLIED SCIENCE (Engineering Physics)

McMASTER UNIVERISTY HAMILTON ONTARIO

TITLE:

MODELING FILM BOILING AND QUENCHING ON THE OUTER SURFACE OF A CALANDRIA TUBE FOLLOWING A CRITICAL BREAK LOCA IN A CANDU REACTOR

AUTHOR:

JIAN TAO JIANG
B. Eng. Electrical Engineering
University of Electronic Science and Technology of China

SUPERVISOR

Dr. John C. Luxat
Department of Engineering Physics
McMaster University

NUMBER OF PAGES

140

Abstract

In a postulated critical break LOCA in a CANDU reactor it is possible that heatup of a pressure tube (PT) causes ballooning contact with the calandria tube (CT). Stored heat in the PT is transferred out, yielding a high PT-CT heat flux, which can cause dryout of the CT and establishment of pool film boiling on the outer surface of the tube. The safety concern associated with this condition is that if the temperature of the CT experiencing film boiling gets sufficiently high then failure of the fuel channel may occur. However, quench heat transfer can limit the extent and duration of film boiling as has been experimentally observed. Current estimates of quench temperatures during pool film boiling are based primarily on experimental correlations. In this dissertation a novel mechanistic model of pool film boiling on the outside of a horizontal tube with diameter relevant to CT (approximately 130 mm) has been developed. The model is based in part upon characterizing the vapor film thickness for steady state film boiling under buoyancy driven natural convection flows around a tube located horizontally in a large liquid pool. Variations in steady state vapor film thickness as a function of the incident heat flux, the temperature of the CT outer wall, and the subcooling of the bulk liquid are analyzed. The calculated effective film boiling heat transfer coefficient is compared to available experimental data. Finally a transient equation is developed which quantifies the instability of the vapor film and a possible occurrence of rapid quench when a step change in governing parameters occurs, such as liquid subcooling. This mechanistic model can be employed in safety analysis to demarcate the conditions under which fuel channel failure will not occur in a postulated critical break LOCA.

Acknowledgements

The following people should be credited with thanks to no end.

My supervisor; Dr. John C. Luxat, a super nice supervisor guiding my study at McMaster University where I spent a couple of unforgettable years in my life. Don't need to mention him being one of the most knowledgeable experts in the field of CANDU safety analysis.

My beloved parents, Shuying Zhan and Shikong Jiang, who have encouraged me to achieve academic excellence and have lightened my pursuit to happiness through hardworking since I was a kid.

My wife, Tian H. Wu, who is always with me and takes care of our two children, Nicholas and Melinda. Without her, I have no way to be here.

The financial support from the following sources is also gratefully acknowledged.

- Natural Sciences and Engineering Research Council (NSERC)
- University Network of Excellence in Nuclear Engineering (UNENE)
- The Eugene G. Bolotkin Scholarships 2006

Table of Contents

List of Figures

List of Tables

List of Acronyms

AECL	Atomic Energy of Canada Limited
CANDU	CANada Deuterium Uranium, a trademark of nuclear reactor in Canada
CT	Calandria Tube
LOCA	Loss Of Coolant Accident
LBLOCA	Large Break LOCA
MFB	Minimum Film Boiling
ODE	Ordinary Partial Differential Equation
PT	Pressure Tube

Nomenclature

a, b, c, c_0	=	constants appearing in Equations
q''_c, q''_{cond}	=	conduction heat flux from CT wall across vapor film
q''_{co}	=	total heat flux from CT wall outer surface
q''_{evap}	=	heat flux used to evaporate saturated liquid
q''_{i-L}	=	heat flux transferred from interface to thin liquid layer
q''_r, q''_{rad}	=	adiation heat flux from CT wall to bulk liquid
q''_{sh}	=	heat flux to superheat steam vapor
q''_w	=	total heat flux emitted from CT outer surface (same as q''_{co})
Q	=	heat rate
h_{fg}	=	latent heat of vaporization
h'_{fg}	=	modified latent heat of vaporization = $h_{fg}+0.5c_{p,v}(T_w-T_{sat})$
g	=	gravity acceleration
h	=	effective heat transfer coefficient
p,P	=	pressure
R	=	calandria tube radius
T	=	temperature
ΔT_{sub}	=	subcooling temperature ($=T_{sat}-T_b$)
T_{mfb}	=	minimum film-boiling temperature ($=\Delta T_{mfb}+T_{sat}$), alternative to quench temperature sometimes in this thesis
u,v,	=	velocity component along r,z axis in Cylindrical polar coordinate system or along x,y in Cartesian coordinate system, respectively
U, V	=	velocity
U_∞, u_∞	=	liquid free stream velocity
$\bar{U}$	=	Average velocity
α	=	thermal diffusivity

β = thermal expansion coefficient

θ = deflection angle

δ = vapor film thickness

$\dot{\delta}$ = moving velocity of vapor-liquid interface

$\ddot{\delta}$ = the acceleration of vapor-liquid interface

δ_L = thickness of laminar liquid boundary layer

ρ = density

κ = conductivity

μ = dynamic viscosity

ξ_L = Liquid transition angle (from laminar to turbulent flow)

ξ_v = vapor transition angle (from laminar to turbulent flow)

σ = the water surface tension

χ = ratio of vapor density to liquid density (ρ_V/ρ_L)

Φ = a potential function

Subscript:

b	=	bulk liquid
br	=	bubble rise
c, cond	=	conduction
c	=	centroid, used in Section 3.5.2
co	=	calandria outer surface
cur	=	curvilinear surface
eff		effective
evap	=	evaporation
i-L	=	two-phase interface to liquid
inf	=	same as ∞

L	=	liquid
mfb	=	minimum film boiling
mp	=	middle point
r, rad	=	radiation
sat	=	saturation condition
sub	=	subcooling condition
sh	=	supper heating condition
v	=	vapor
w, wall	=	wall surface
∞	=	liquid free stream condition

Chapter One

1.0 Introduction

This dissertation presents a model of film boiling and quench heat transfer on the outside surface of a horizontal tube submerged in subcooled water at atmospheric pressure. A mechanistic model for pool film boiling on the outside of a horizontal tube with diameter relevant to calandria tubes (approximately 130 mm in diameter) has been developed. The model is based in part upon characterizing the vapor film thickness for steady state film boiling under buoyancy driven natural convection flows around a tube located horizontally in a large liquid pool. Variations in steady state vapor film thickness as a function of the incident heat flux at the pressure tube inner wall, the temperature of the calandria tube outer wall, and the subcooling of the bulk liquid are analyzed. The calculated effective film boiling heat transfer coefficient is compared to available experimental data. Finally a transient equation is developed which quantifies the stability of the vapor film when a step change in governing parameters, such as inner wall heat flux and liquid subcooling, occurs. The conditions under which the vapor film is destabilized are derived and are applied to establish conduction for which when a rapid quench occurs to force a transition from stable film boiling to surface rewet and nucleate boiling. The dissertation is concluded with potential application in safety analysis to demarcate the conditions under which fuel channel failure will not occur in the postulated critical break LOCA.

1.1 Background to the Problem

In a limiting postulated large break Loss of Coolant Accidents (LOCA) in a CANDU reactor (referred to as a critical break LOCA) it is possible that heatup of a pressure tube (PT) can occur to the extent that creep deformation of the pressure tube occurs. If the internal pressure is sufficiently high then uniform ballooning deformation forces the hot pressure tube into contact with the calandria tube (CT). Following the contact of the hot pressure tube with the calandria tube there is a high heat flux into the calandria tube as stored heat is transferred out of the pressure tube. This high heat flux can cause dryout of the calandria tube and establishment of pool film boiling on the outer surface of the tube. The safety concern associated with this condition is that if the temperature of the calandria tube experiencing film boiling get sufficiently high then failure of the fuel channel may occur. However, quench heat transfer can limit the extent and duration of film boiling as has been experimentally observed. Current estimates of quench temperatures during pool film boiling are based primarily on experimental correlations.

1.2 CANDU Reactor and Fuel Channels

A typical CANDU (CANada Deuterium Uranium) PHW (pressurized heavy water) reactor core, as depicted in Figure 1 [1], consists of about 380 (CANDU 6) or about 480 (CANDU 9) fuel channels laid horizontally inside the calandria vessel, which is a large cylinder with dimensions of 6 m long and inside diameter of 7.6 m (CANDU 6) or 8.5 m (CANDU 9), and filled with large volume (~250,000 liters) of cool D_2O heavy water fluid under atmospheric pressure.

Each fuel channel traverses the calandria vessel from one end to the other, containing 0.7 wt % natural Uranium fuel bundles through which heavy water coolant flows (Refer to Figure 2 [1] and Figure 3 [1]). Each single fuel channel contains twelve nuclear fuel bundles within a pressure tube.

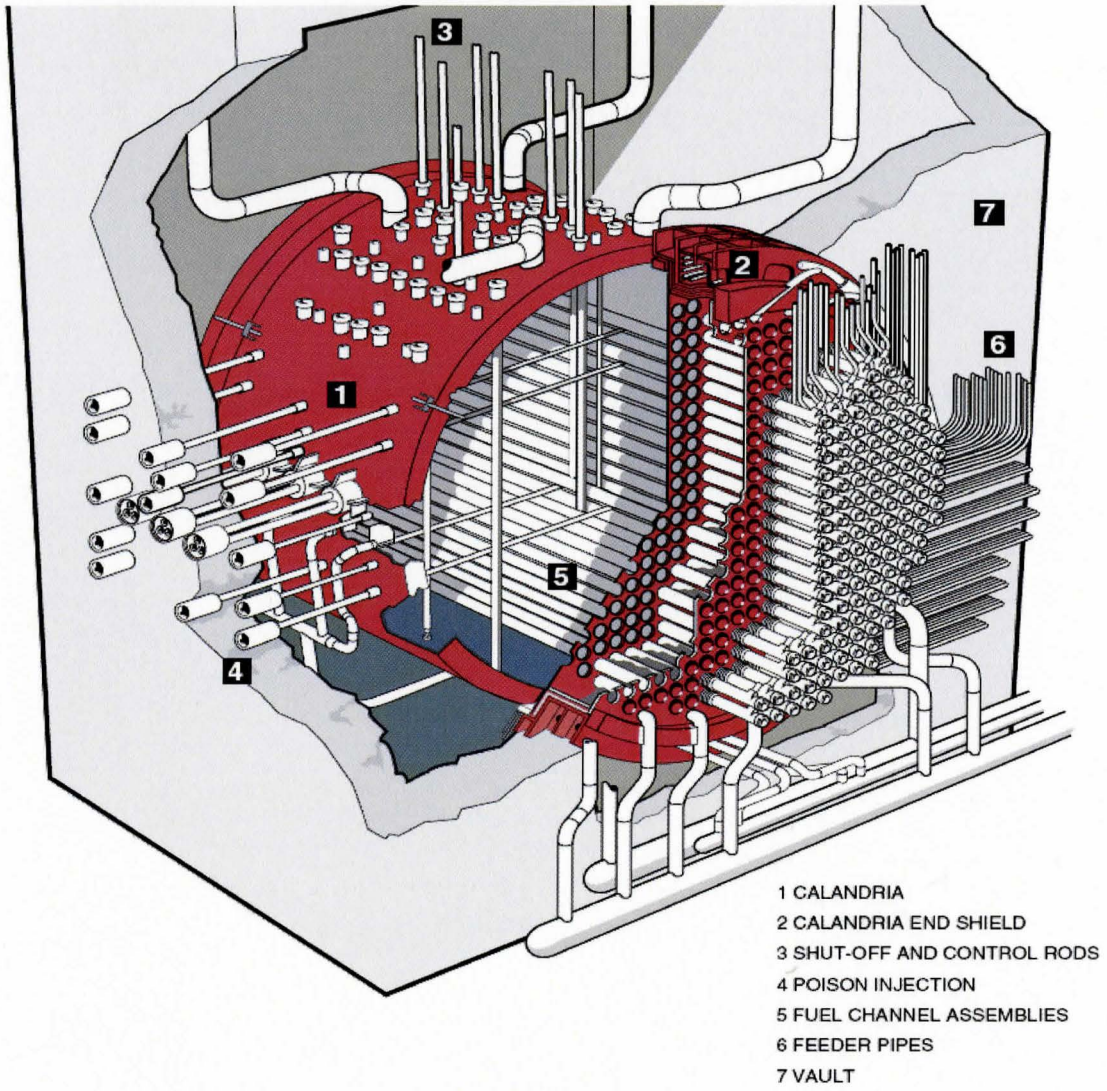

Figure 1: CANDU assembly (AECL[1])

The close-up side view of part of a fuel channel clearly shows the construction. Each fuel channel is composed of an outer CT surrounding a PT, with a gap containing gas CO_2 between them. The PT and CT are separated by four garter springs located along the length of the fuel channel (Figure 3). The CT is made of Zircaloy-2 material and has an inside diameter 129 mm and a wall thickness of 1.4 mm. The PT, which is made up of Zirconium-2.5wt% Niobium, has an inside diameter of 103.4 mm and a wall thickness of 4.2 mm. Each of the 12 fuel bundles in a fuel channel contains 37 identical fuel elements (CANDU 6 and CANDU 9). In normal operation situations the heat generated in the fuel via nuclear fission reactions is removed by the pressurized coolant flowing through fuel channels.

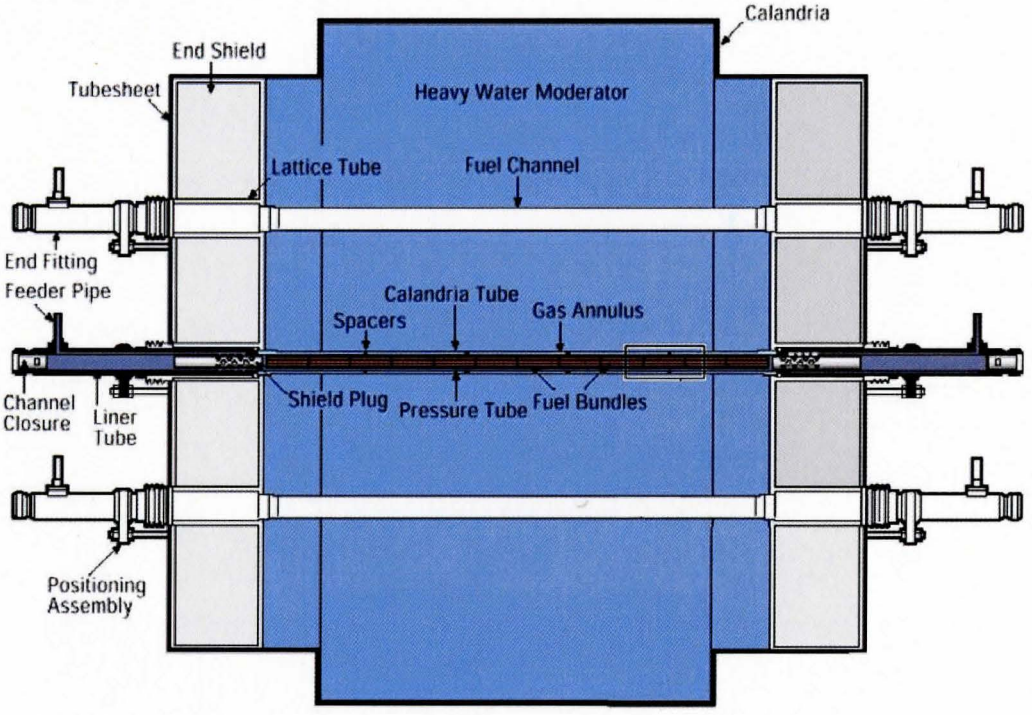

Figure 2: Side view of CANDU calandria and fuel channels (AECL[1])

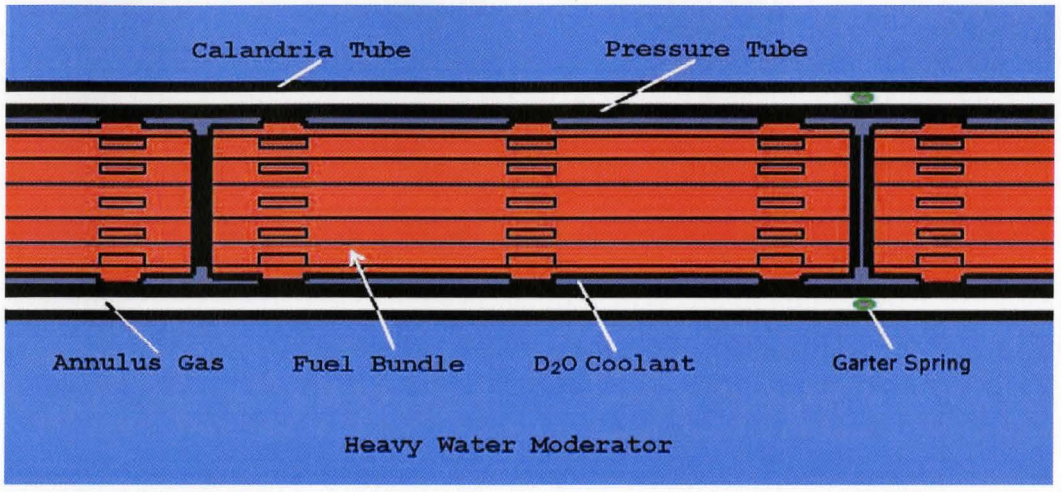

Figure 3: Close-up side view of part of a fuel channel (AECL[1])

The unique CANDU design provides passive safety features that allows heat release from the CT directly to the surrounding fluid should the PT deforms during an accident. The large mass fluid, which is circulated by pumps and cooled by heat exchangers, plays a supplementary role as a heat sink in CANDU reactors. Even if the emergency core cooling is unavailable, fluid is available for stored heat and decay heat removal from heat channels.

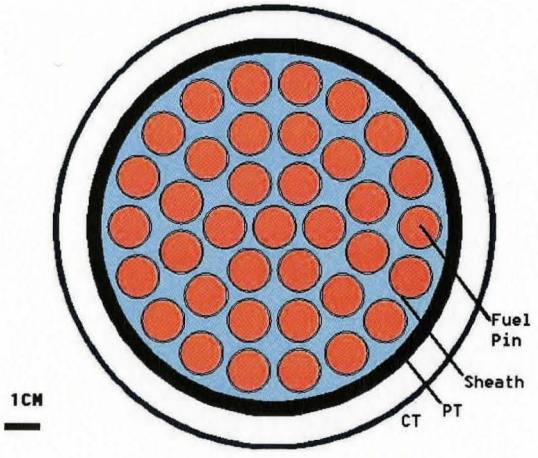

Figure 4: Cross-section of a CANDU 6 fuel channel in normal operational situations

1.3 LOCA and PT/CT Contact

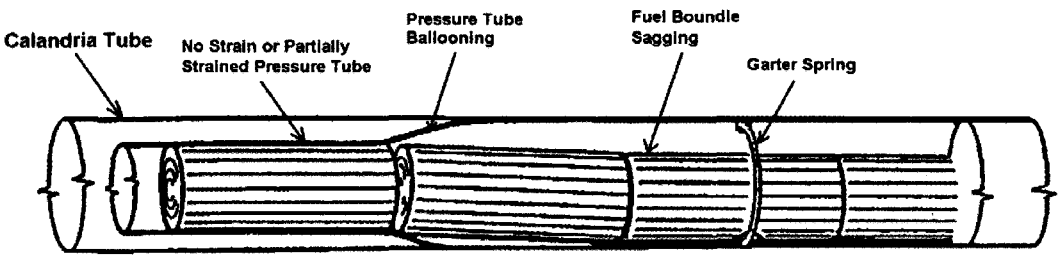

Figure 5: Ballooning of PT into contact with CT and fuel bundle sagging (AECL[2])

A loss of coolant accident (LOCA) involves a break in the primary heat transport system (HTS). The pressure and coolant flow reduce in some fuel channels as the coolant inventory decreases. The reduction of coolant mass flow due to the break results in degradation of heat transfer in fuel channels of particular passes of the HTS. The temperature of nuclear fuel elements will increase because of degraded convective heat transfer. The fission heat, decay heat and heat stored in these fuel elements drives the increase in fuel temperature. Heat is transferred by conduction radially from the uranium fuel pellets to the fuel sheath. The heat transferred from the fuel elements to the PT is mainly by convection in a small LOCA and by a combination of convection and radiation in a large LOCA. Under severe cooling degradation the temperature of the PT can increase significantly. In the conditions of high or intermediate [3]channel pressure, the PT may deform uniformly (so called "ballooning") in large LOCA If PT heatup is delayed then the PT tends to sag into contact with the CT. PT deformation by either mechanism results in partial or complete contact with its associated CT (that is, PT/CT contact) [3].

Figure 5 [4] depicts this scenario in the longitudinal view of a fuel channel. Figure 6 [4] depict this scenario in the cross-section view of a fuel channel. The thermal conductance between the two tubes increases significantly and consequently forms a path for heat removal by conduction with the potential for high heat flux. After PT/CT contact, large amounts of heat can be rejected to the fluid. If the nucleate boiling mechanism on the external CT surface dominates, then the CT will not experience significant increase in temperature. However, if the heat flux is high especially in the initial-contact phase, then the superheated CT wall may experience a rapid transition of boiling heat transfer from nucleate boiling to film boiling. Subsequently the external surface of CT will be blanketed by a vapor film during the post-contact phase.

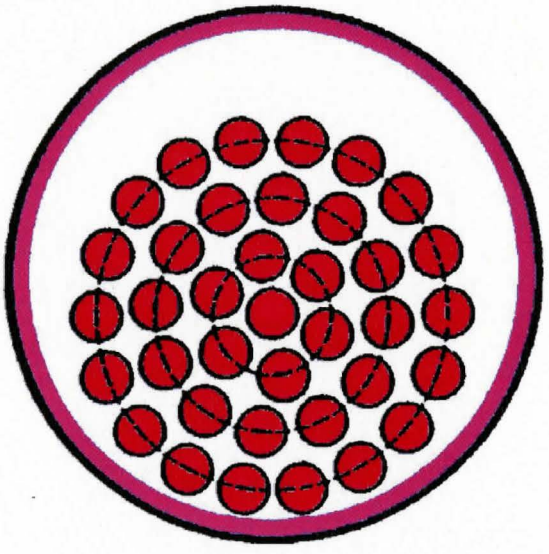

Figure 6: Ballooned PT contacts with CT and fuel bundle sags into contact with PT following a large LOCA (AECL [2])

Obviously, sustained film boiling in the post-contact phase is not desirable since the integrity of fuel channel is challenged by creep strain failures of PT and CT. The

objective of this study is to investigate the characteristics of stable film boiling and triggering effects of quenching mechanism outside of CT submerged in sub-cooled fluid. One of the key issues is to find the critical vapor film thickness over a range of given conditions for which quenching will be initiated. After quenching starts, a small part of CT is wetted by fluid. This may result in a rapid collapse of the vapor film blanket. During this transient collapse process, the stable film boiling regime changes to transition boiling regime and proceeds to nucleate boiling regime as the CT wall superheat is reduced. In order to quantify this process it is necessary to develop an expression for the transient vapor film thickness in terms of various thermal-hydraulic parameters.

1.4 Goals of the Dissertation

The first goal of this dissertation is to develop a mechanic model describing the physical phenomena associated with the film boiling on the calandria tube for the limiting postulated large break LOCA event for a CANDU reactor.

Based on the developed model, the second goal of this dissertation is to analyze the characteristics of vapor film in terms of key parameters, such as subcooling temperature, under the steady state condition.

The third goal is to analyze the vapor film thickness, as well as the heat flux and the wall temperature at the beginning to quench.

The transient behavior of the film thickness given a step change in subcooling is also addressed in this dissertation.

1.5 Dissertation Outline

Chapter one introduces the direction and goals of the dissertation. It describes the characteristics of a LOCA event in a CANDU reactor.

Chapter two provides a review of open literature regarding the theory and empirical investigations associated with film boiling and vapor film thickness. A review of minimum film boiling temperature as linear function of subcooling is also presented.

Chapter three outlines key aspects of fluid mechanics and heat transfer which are essential to the derivation presented in Chapter four.

Chapter four details the theoretical derivation of film boiling and quenching model based on hydraulic pressure and heat transfer balances. An expression for the transient vapor film thickness is given as a second-order, nonlinear and non-homogeneous ODE. A steady state equation is also obtained by assigning the derivatives to be zero. To perform calculation of the transient equation and the steady state equation, two additional theoretical derivations are also provided in this section. One is for the vaporization velocity and the second is for the buoyancy-induced free steam velocity. Both expressions are developed as functions of subcooling temperature.

Chapter five provides results obtained by the film boiling and quenching model under steady state condition. Discussions based on the comparison of the model output and the available film boiling test data is also included in this chapter. In addition, a short discussion about the assumptions is provided.

Chapter six presents a preliminary analysis of the influence of a step change in subcooling temperature to the vapor film thickness oscillation. This is of importance dynamic development of the quench process.

Chapter seven outlines the conclusions and recommendations

In addition, three appendixes are included. The first is the calculation of the calandria tube outer surface heat flux based on PT incident heat flux. The second is a sample of a MatLab code that calculates vapor film temperature at the given steady state vapor film thickness. The third lists tables of thermophysical properties used in this dissertation.

Chapter Two

2.0 Literature Review

2.1 Literature Review on Vapor Thickness of Film Boiling

2.1.1 M. S. Genk and A. G. Glebov

Film boiling from a downward-facing curved surface in saturated and 5°C, 10°C, and 14°C subcooled water was investigated experimentally by Genk and Glebov [5]. Surface rewetting in saturated boiling was hydrodynamically driven, while thermally driven in subcooled boiling. Consequently, surface rewetting in the former occurred earlier at higher minimum heat flux, q_{min}. The critical film thickness, $\delta_{v,crit}$, prior to rewetting was thicker than that at 10°C and 14°C subcooling, but thinner than at 5°C subcooling. Surface rewetting occurred first at lowermost position, θ=0°, then subsequently at higher inclinations. For saturation boiling, the critical film thickness was ~0.085mm at θ=0° and 0.18 mm at θ=8.26°, respectively. For subcooled boiling at θ=0°, the critical film thickness (~0.05±10%mm) at this lowermost position was weakly dependent on subcooling temperatures. The critical film thickness increased, however, with inclination and decreasing subcooling temperature, reaching ~0.175 mm at θ=8.26° and 5K subcooling. The vapor film thickness shown in Table 1 are predicted values based on the Genk and Glebov's correlation.

The experimental condition is worth noting. An oxidation-free treated 237°C copper curved section, with an area of 20.4cm^2 (r= 2.55cm), a thickness of 2cm and a surface curvature radius of 14.8cm, was submerged in a water pool at atmospheric pressure.

Table 1: Vapor film thickness variation with subcooling and inclination angle

	θ=0°	θ=3.29°	θ=4.94°	θ=8.26°
ΔT_{sub}=5°C	0.055mm	0.070mm	0.090mm	0.175mm
ΔT_{sub}=10°C	0.052mm	0.065mm	0.080mm	0.140mm
ΔT_{sub}=14°C	0.050mm	0.060mm	0.070mm	0.110mm

Note that the calculated results from correlation in Table 1 have a much higher degree of resolution than would be supported by experimental data.

In summary, the conclusive results for pool film boiling on this paper are generalized as follows:

- Film boiling quenched earlier at higher water subcooling;
- The lowermost position quenched earlier than other positions;
- The vapor film thickness increased with inclination and was thinnest in the lowermost position, where inclination equals zero;
- The vapor film thickness increased with decreasing subcooling temperature;
- The minimum film boiling heat flux q_{min} increased with subcooling;
- The minimum film boiling heat flux q_{min} increased with decreasing inclination and reached largest at the lowermost position;
- Surface rewetting occurred when the film thickness reached a critical value, which was dependent upon water subcooling and local inclination on the boiling surface;
- The minimum wall superheat, $(\Delta T_{sat})_{min}$, was independent of local inclination due

to high heat conductivity through the wall, and varied between 35 and 42°C corresponding to 5°C -14°C subcooling;

2.1.2 P. J. Berenson

Berenson [6] applied Taylor-Helmholtz hydrodynamic instability theory to film boiling heat transfer from a horizontal surface. He found that the bubble spacing and growth rate, near the minimum film boiling heat flux, is determined by the Taylor instability neglecting the effect of fluid depth and viscosity. Analytical expressions for the minimum film vapor thickness, the heat transfer coefficient near the minimum in film boiling from a horizontal surface were derived based on a simplified geometrical model. The author claimed ±10% agreement with experimental measurements made using n-pentane and carbon tetrachloride fluids.

It is noted that the results based on these two fluids may have additional uncertainties when applied to water.

Berenson's derivation was based on the following assumptions:

- momentum forces are negligible in comparison with the viscous forces;
- The flow is laminar;
- The kinetic energy of the vapor is negligible in comparison with the enthalpy change;
- The average value of vapor properties are equal to those at the average temperature of the hot surface and the saturated liquid;
- Heat is transferred through the vapor film by conduction. Radiation is negligible at

the temperature difference less than 530 °C;

- Vapor flowing to any one bubble is generated in an area of half wavelength of bubble.

Calculations based on experimental results indicated that the film thickness is in the order of 10^{-3}-10^{-2} mm; and that the vapor velocity is relatively low in the order of 0.3 m/sec.

Berenson showed that the characteristic dimension of the bubble is two orders of magnitude greater than the film thickness. Therefore the order of critical film thickness can be roughly estimated from experimental measurements of bubble diameters. The average bubble diameter, cited in the paper [6], was 0.28 inch (0.7cm) for n-Pentane. This implies the critical vapor film thickness to be 0.07mm.

The vapor film thickness near the minimum in film boiling took the form below

$$\delta_{v,MFB} = 2.35\left[\frac{\mu_v k_v \Delta T_{sat}}{h_{fg}\rho_v g(\rho_l - \rho_v)}\sqrt{\frac{\sigma}{g(\rho_l - \rho_v)}}\right]^{1/4} \quad (1)$$

where σ is the surface tension, which was not provided in Berenson's paper [6]. The heat transfer coefficient close to the minimum was expressed as

$$h_{MFB} = 0.425\left[\frac{k_v{}^3 h_{fg}\rho_v g(\rho_l - \rho_v)}{\mu_f \Delta T_{sat}\sqrt{\frac{\sigma}{g(\rho_l - \rho_v)}}}\right]^{1/4} \quad (2)$$

The minimum superheat temperature is characterized by:

$$\Delta T_{MFB} = 0.127 \frac{\rho_v h_{fg}}{k_v} \left[\frac{g(\rho_l - \rho_v)}{\rho_l + \rho_v} \right]^{2/3} \left[\frac{\sigma}{g(\rho_l - \rho_v)} \right]^{1/2} \left[\frac{\mu_v}{\rho_l - \rho_v} \right]^{1/3} \quad (3)$$

The surface tension in Equation (3) is for n-pentane and carbon tetrachloride fluids rather than water. Note that the vapor film thickness presented in Figure 7 is calculated by applying water surface tension. Water surface tension can be found from a steam table written by Liley [7]. Equation (3) needs a specific vapor temperature in order to determine the thermo-physical properties. By assuming the minimum vapor film temperature prior to quench, the critical film thickness can be calculated.

Equation (3) allows one to predict the minimum vapor film temperature prior to quench using iterative technique. If a linear relationship between the vapor temperature and surface superheat is applied, and an arbitrary vapor temperature is initially assumed, a value of wall superheat is determined from Equation (3) by assigning values of temperature-dependent hydraulic and thermo-physical properties; then compare to the value calculated by Equation (4); adjust the estimated value of vapor temperature until a convergence occurs.

$$T_v = \frac{(T_w + T_{sat})}{2} = \frac{1}{2}\Delta T_{sat} + T_{sat} \quad (4)$$

Or

$$\Delta T_{sat} = 2\,(T_v - T_{sat}) \quad (5)$$

It is worth noting that Berenson's model ignored the heat loss by conduction and convection to subcooled liquid, so this model is applicable for only saturated pool boiling

condition but not for subcooled conditions. In subcooled pool boiling, vapor film thickness will decrease. Therefore the prediction of Berenson model overestimates the vapor film thickness. Berenson's model also did not consider the radiation heat transfer effects on vapor film thickness. Because the effect of radiation heat transfer tends to increase as the vapor film thickness increases, the Berenson model will hold for wall superheat less than around 500°C, which is claimed in his paper [6]. However, Berenson did not prove why the radiation heat transfer can be ignored at the temperatures below around 500°C. Personally, I doubt this assumption.

2.1.3 L. A. Bromley

Bromley derived a natural convection stable film boiling heat transfer coefficient [8] from a horizontal tube by an approach similar to Nusselt's equation for condensers. Later Bromley et al. proposed the condition of $U\cdot(gD)^{-0.5} < 1.0$ to fit for forced convection film boiling problems [9]. The heat transfer coefficient in the vapor film without radiation effects is given by:

$$h_c = 0.62 \sqrt[4]{\frac{k_v^{\,3}(\rho_l - \rho_v)\rho_v \; g \left[h_{fg} + 0.4C_{p,v}(T_w - T_{sat})\right]}{D\mu_v(T_w - T_{sat})}} \tag{6}$$

where D = tube diameter,

$C_{p,v}$ = specific heat of vapor at its average temperature,

$C_{p,l}$ = specific heat of liquid at boiling temperature.

For heavy water,

$C_{p,l} = 1.903\ kJ/(kg\cdot K)$ (at boiling point),

$C_{p,v} = -3x10^{-14}T_v^{\,5} + 6x10^{-11}T_v^{\,4} - 5x10^{-8}T_v^{\,3} + 2x10^{-5}T_v^{\,2} - 4.5x10^{-3}T_v + 2.1481\ [kJ/(kgK)]$

From the relation of heat transfer coefficient and vapor film thickness we have

$$h_c = \frac{k_v}{\delta_v} \tag{7}$$

Combining equation (6) and (7), yields the following expression for film thickness:

$$\delta_v = 1.613 \sqrt[4]{\frac{k_v D \mu_v (T_w - T_{sat})}{(\rho_l - \rho_v)\rho_v \; g\left[h_{fg} + 0.4 C_{p,v}(T_w - T_{sat})\right]}} \tag{8}$$

Applying Equation (8) results in a steady state thickness of 0.277mm at wall temperature 277°C. This is much larger than predictions of other investigations.

If a Nusselt's number, Nu, is given at the minimum film boiling on a horizontal tube, one may calculate the corresponding heat transfer coefficient via the definition of Nusselt's number:

$$h_{conv} = Nu \frac{k_v}{D} \tag{9}$$

The corresponding vapor film thickness can be calculated as

$$\delta_v = \frac{k_v}{h} = \frac{k_v}{h_{conv} + h_{rad}} \tag{10}$$

where h is the combined heat transfer coefficient. The radiation heat transfer coefficient, h_{rad}, is defined as

$$h_{rad} = \frac{\sigma_{s\text{-}b}}{\frac{1}{\varepsilon_w} + \frac{1}{\varepsilon_L} - 1} \cdot \frac{\left(T_w^4 - T_{sat}^4\right)}{\left(T_w - T_{sat}\right)} \tag{11}$$

where $\sigma_{s\text{-}b}$ is the Stefan-Boltzmann constant.

Equation(10) may suggest that, in the case of constant incident heat flux from the tube wall surface, the inclusion of radiation heat transfer effect would result in a thinner vapor film thickness in Equation(10) than in Equation (8) that ignores radiation heat transfer.

2.1.4 Y. P. Chang

Chang [10] analyzed heat transfer for natural convection film boiling from a horizontal and a vertical surface from the viewpoint of wave theory. A critical wave length was suggested as

$$l_{cr} = 2\pi\left[\frac{\sigma}{g(\rho_l - \rho_v)}\right]^{\frac{1}{2}} \tag{12}$$

The vapor should break the interface in a spacing approximately equal to this critical wave length during the development of a thin vapor film.

The critical film thickness is to be determined by

$$\delta_{cr} = \left[\frac{8\pi^2\mu_v\alpha_c}{g(\rho_l - \rho_v)}\right]^{\frac{1}{3}} \tag{13}$$

where α_c is the equivalent thermal diffusivity. For subcooling less than 10°C, α_c is defined as

$$\alpha_c = \frac{\Delta T_{sat} k_v}{2\left(h_{fg}\rho_v + \Delta T_{sub} c_{p,l}\rho_l\right)} \tag{14}$$

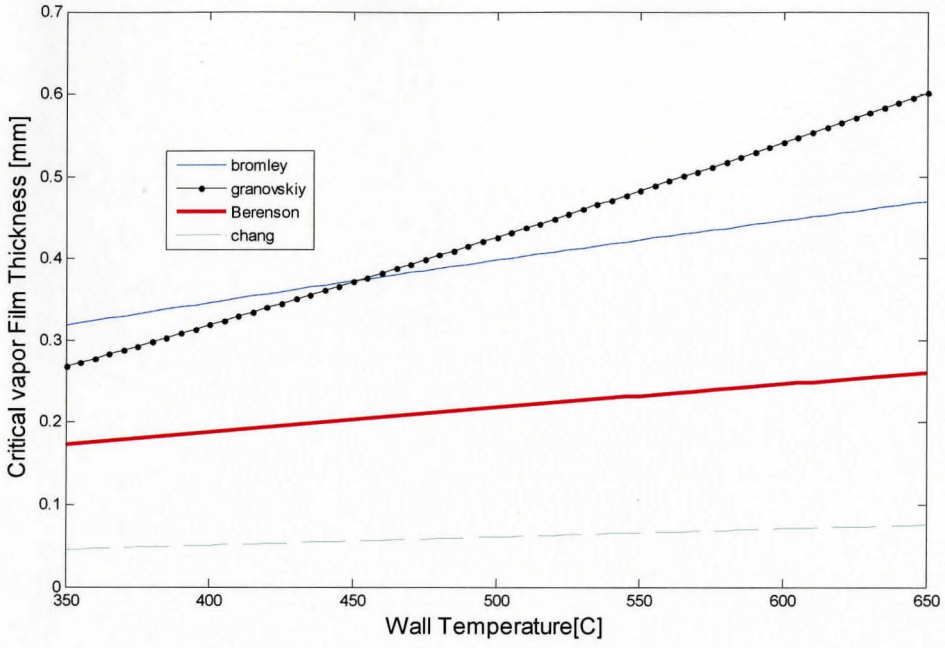

Figure 7 : Literature review of critical vapor film thickness in saturated water pool boiling

Figure 7 represents the critical vapor film thickness in terms of metal wall temperature in the conditions of saturated water pool boiling. It is observed that

- the vapor film thickness is not for subcooled pool boiling
- these vapor film thickness values vary significantly.

2.2 Literature Review on Empirical Correlation of Quench Temperature in Terms of Subcooling.

A number of experimenters suggested empirical correlations of minimum film boiling temperature as function of water subcooling on various metal surfaces using the equation $\Delta T_{MFB}=a\Delta T_{sub}+b$, where a and b are constants.

The most representative one was performed by M. Mori [11] in 1980 for water on Zircloy-4 rods.

$$\Delta T_{MFB} = 7.5\Delta T_{sub} + 140 \quad (15)$$

This simple equation agrees perfectly with the data of Mori et al and is adequate for bottom reflood of LWR fuel assemblies.

Other empirical correlations are available from the literature for minimum film billing temperature as a function of fluid subcooling as follows.

Bradfield [12] :

$$\Delta T_{MFB} = 6.15\Delta T_{sub} + 200 \quad (16)$$

Adler [13]:

$$\Delta T_{MFB} = 7\Delta T_{sub} + 175 \quad (17)$$

Lauer, Hufschmidt [14]:

$$\Delta T_{MFB} = 5.893\Delta T_{sub} + 228.6 \quad (18)$$

Groeneveld and Stewart [15,,16]]

$$T_{MFB} = 284.7 + 44.1P - 3.72P^2 - \frac{10^4 C_{p,l}\Delta T_{sub}}{(2.82 + 1.22P)h_{fg}}$$

where P is pressure in MPa. At atmospheric pressure (0.101MPa), the Groeneveld and Stewart correlation is fitted by simpler linear relationship with subcooling, given by:

$$\Delta T_{MFB} = 6.3\Delta T_{sub} + 189 \quad (19)$$

Ohnishi [17]

$$\Delta T_{MFB} = 5.1\Delta T_{sub} + 350 \quad (20)$$

Dhir and Purohit [18]

$$\Delta T_{MFB} = 8\Delta T_{sub} + 201 \tag{21}$$

Nishio [19] predicted that the minimum film boiling temperature is a constant for saturated water at atmospheric pressure based upon the temperature-controlled hypothesis as

$$\Delta T_{MFB} = 100 \tag{22}$$

Figure 8 shows those empirical correlations except Nishio empirical correlation.

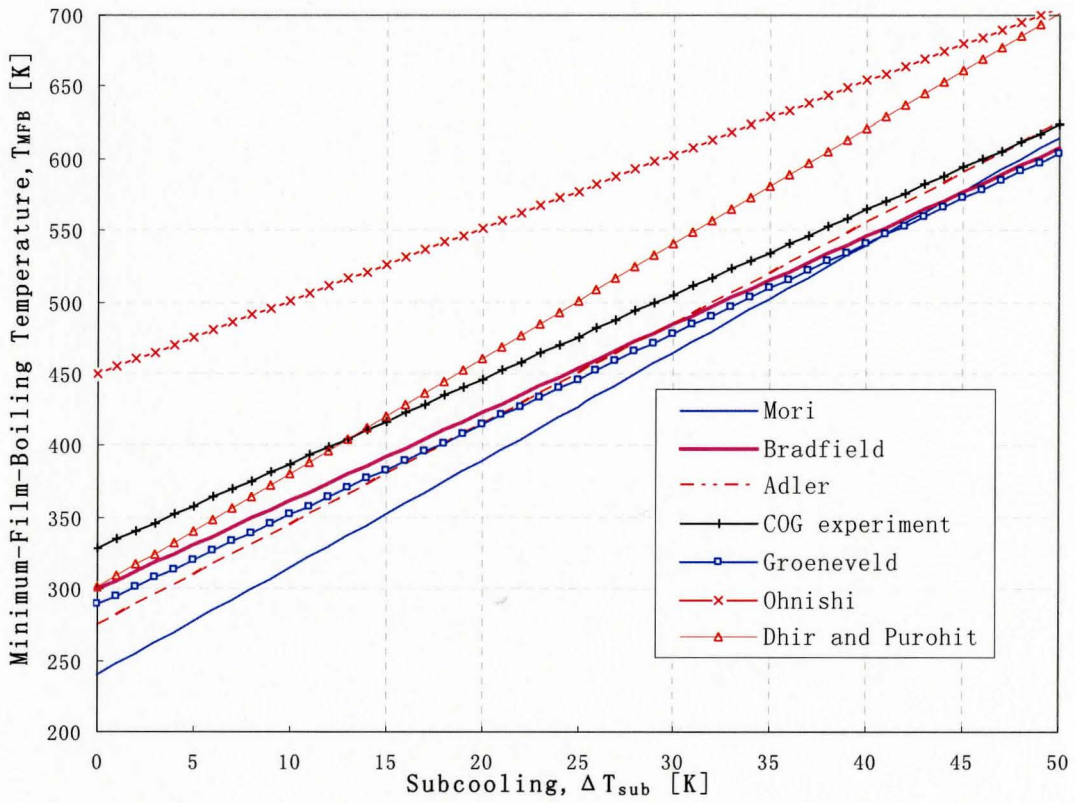

Figure 8: Review of minimum film boiling temperature correlations ($T_{MFB} = \Delta T_{MFB} + T_{sat}$, T_{sat} =100˚C at atmospheric pressure)

Chapter Three

3.0 Fluid Mechanics and Heat Transfer

This chapter provides a short description of relevant theory in fluid mechanics and heat transfer pertinent to the problem of interest. Section 3.1 introduces a potential flow over a cylinder, which provides a relationship between free stream flow velocity and tangential velocity at the cylinder surface. Section 3.2 contains classification of hydrodynamic pressures (static pressure and dynamic pressure). The result will be used in Chapter Four. Section 3.3 provides the heat transfer mechanisms, namely conduction, convection and radiation heat transfer, with special consideration of cylindrical geometry. Section 3.4 discusses the film boiling mechanism and Sideman's "thin liquid layer conduction" theory. This theory will be used in the next chapter to evaluate heat transfer from the vapor-liquid interface to the subcooled bulk liquid. The concept of latent heat and superheat are covered in Section 3.4. In section 3.5, the quench mechanism is introduced. Lastly, thermal properties of heavy water, steam and zircaloy as functions of temperature are given. This treatment facilitates iteration calculations of computer codes.

3.1 Potential Flow over a Cylinder

Of interest is the velocity and pressure distribution for inviscid flow over a cylinder. Invisid flow does not satisfy the no-slip condition, and boundary layers do not form on the cylinder surface.

3.1.1 Velocity Potential and Stream Function

A potential function ϕ is defined such that $\vec{V} = \nabla\phi$

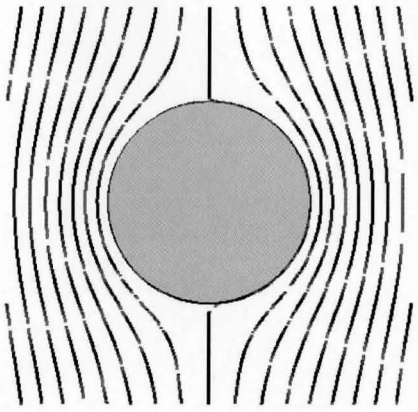

Figure 9: Cylinder in a uniform flow

If ϕ is two dimensional and satisfies the conditions of irrotationality and incompressibility, then

$$u = \frac{\partial \phi}{\partial x} \quad \text{and} \quad v = \frac{\partial \phi}{\partial y} \tag{23}$$

Likewise, a stream function ψ can be defined such that continuity equation is automatically satisfied for incompressible flow.

$$u = \frac{\partial \psi}{\partial y} \quad \text{and} \quad v = -\frac{\partial \psi}{\partial x} \tag{24}$$

Equations (23) and (24) are for Cartesian coordinates system, In cylindrical coordinates, the following expressions are obtained:

$$u_r = \frac{\partial \phi}{\partial r} \quad \text{and} \quad u_\theta = \frac{1}{r}\frac{\partial \phi}{\partial \theta} \tag{25}$$

$$u_r = \frac{1}{r}\frac{\partial \psi}{\partial \theta} \quad \text{and} \quad u_\theta = -\frac{\partial \psi}{\partial r} \tag{26}$$

3.1.2 Uniform Flow

For a uniform flow in x direction shown in Figure 10 [20], $u = U$, and $v = o$.

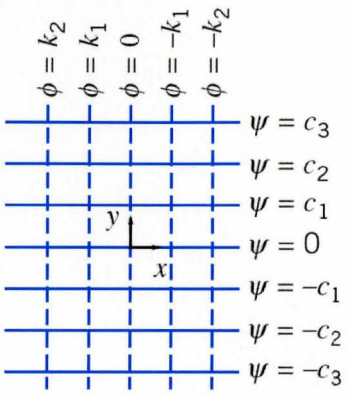

Figure 10: Uniform flow

Equation (23) gives $u = \frac{\partial \phi}{\partial x} = \mathrm{U}$ and $v = \frac{\partial \phi}{\partial y} = 0$. So that

$$\phi = Ux + f(y) + const \xrightarrow{\partial\phi/\partial y = 0} \phi = Ux + const$$

Similarly, from equation (24)

$$\psi = Uy + g(x) + const \xrightarrow{v = -\partial\psi/\partial x = 0} \psi = Uy + const$$

For convenience, let the constants to be zero. Hence

$$\phi = Ux \quad \text{and} \quad \psi = Uy$$

In cylindrical coordinates,

$$\phi = Ur\cos\theta \quad \text{and} \quad \psi = Ur\sin\theta \tag{27}$$

3.1.3 Point Source and Point Sink

A point source is a point where in a two-dimensional system a constant mass flow enters this point and leaves out in all directions in a plane. Cylindrical coordinates are the best coordinates for this flow. For incompressible flows with constant volumetric flow rate, if q' represents the volumetric flux per unit length with direction into the page, then $q'=2\pi r u_r$ and $u_\theta = 0$, where u_r is the velocity in the radial direction, u_θ is the velocity perpendicular to radial direction, and r is the radial coordinate.

Using equation(26) one has

$$u_r = \frac{q'}{2\pi r} = \frac{\partial \phi}{\partial r} = \frac{1}{r}\frac{\partial \psi}{\partial \theta}$$

So

$$\phi = \frac{q'}{2\pi}\ln r, \text{ and } \psi = \frac{q'}{2\pi}\theta$$

By contrast, a point sink is a point where fluid exits the flow field and fluid enters equally from all directions. The volumetric flux per unit length is negative, so there exist

$$\phi = -\frac{q'}{2\pi}\ln r, \text{ and } \psi = -\frac{q'}{2\pi}\theta$$

3.1.4 Source-Sink Pair: Doublet

A useful flow results from letting the distance 2L between a source sink pair tend to zero while allowing their strengths q' to tend to infinity so that the product $q'L$ remains constant. This product is defined as the strength of the doublet. By adding a uniform fluid

stream to the doublet in the positive x direction, the most inner streamline can be a perfect circle. These streamlines represents the velocity distribution around a cylinder (Figure 11)

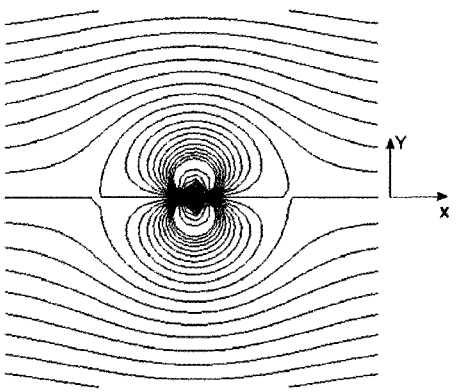

Figure 11: Streamlines of a doublet in a uniform stream [21]

Without loss of generality, assume that the distance between source and sink is 2L. A combined source-sink pair satisfies

$$\psi = -\frac{q'}{2\pi}(\theta_1 - \theta_2)$$

The source is labeled with subscript 2 and the sink with subscript 1 in the above equation and in Figure 12.

When the source and the sink are close enough such that the distance 2L is small, $\theta_1 - \theta_2$ is small too, we have $\theta_1 - \theta_2 \approx 2L\sin\theta / r$. So

$$\psi = -\frac{q'}{\pi}\frac{L\sin\theta}{r} = -\frac{K}{r}\sin\theta \qquad (28)$$

where K can be a constant and equals $q'L/\pi$. Under these conditions, this kind of source-sink pair is the doublet. The velocity potential of a doublet is defined as $\phi = K\cos\theta / r$ in fluid mechanics

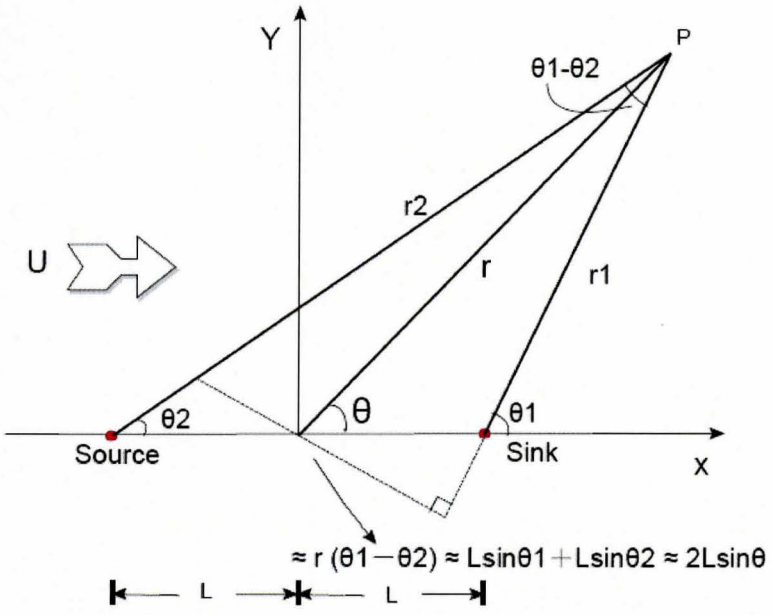

Figure 12: Combination of a source and a sink

3.1.5 Flow Over a Cylinder: Superposition of Uniform Flow and Doublet

Flow over a cylinder can be simulated by a superposition of uniform flow and doublet. This is shown in Figure 13.

Adding the stream function for a uniform flow with velocity U in the direction of the positive x axis (Equation(27)) to the stream function for a doublet (Equation(28)) yields:

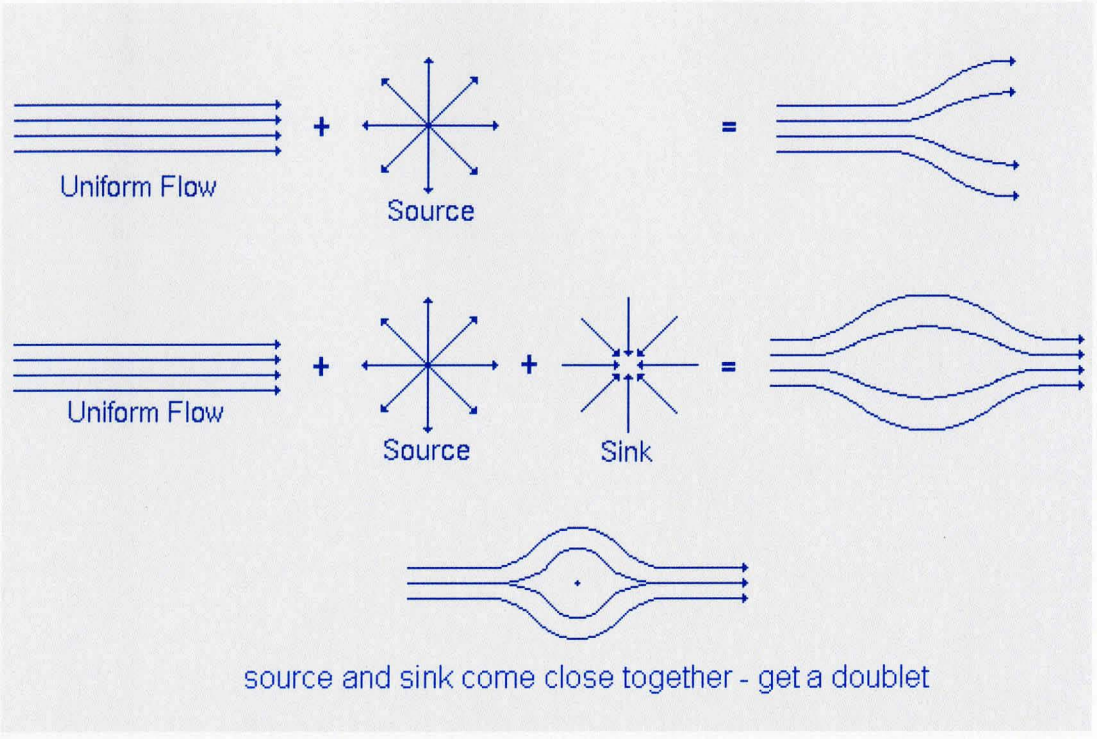

Figure 13: Superposition of uniform flow and doublet

$$\psi = Ur\sin\theta - \frac{K}{r}\sin\theta = Ur\sin\theta\left(1 - \frac{K/U}{r^2}\right) \tag{29}$$

Substituting Equation(29) into Equation(26), yields

$$u_r = \frac{1}{r}\frac{\partial\psi}{\partial\theta} = U\cos\theta\left(1 - \frac{K/U}{r^2}\right)$$

and

$$u_\theta = -\frac{\partial\psi}{\partial r} = -U\sin\theta\left(1 + \frac{K/U}{r^2}\right) \tag{30}$$

$r = (K/U)^{1/2}$ on the surface of the cylinder, so $u_r = 0$ and

$$u_\theta = -2U\sin\theta \tag{31}$$

This is to say, radial velocity u_r on the surface is 0 since the surface is a stream line. The tangential velocity (or surface velocity) u_s on the surface is variant to angle. The minus sign is due to angle θ defined as positive anti-clockwise (refer to Figure 12). If we redefine the angle θ* as clockwise deviation from x axis, which is same as the direction of flow, equation (31) becomes

$$u_T = 2U \sin\theta \ * \tag{32}$$

where u_T stands for tangential velocity. For convenience, thereafter the star sign * on the angle θ will be dropped, but it must keep in mind that the angle is clockwise deviation from the flow direction.

As shown in Figure 14 , the normal velocity and tangential velocity around the circular surface has the relationship:

$$u_N^2 = u_\infty^2 - u_T^2 \tag{33}$$

Combining equation(32) and (33), yields,

$$u_N^2 = u_\infty^2 - u_T^2 = u_\infty^2(1 - 4\sin^2\theta) \tag{34}$$

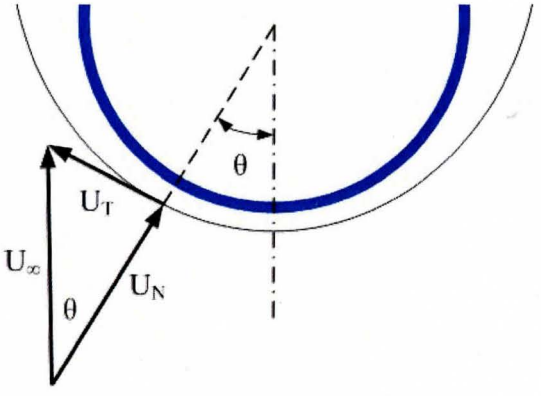

Figure 14: Normal and tangential velocity

This result is applicable to a solid cylindrical surface. Accounting for the movement of vapor-liquid interface with velocity $\dot{\delta} = \partial\delta / \partial t$, then

$$u_N^2 = (u_\infty + \dot{\delta})^2(1 - 4\sin^2\theta) \tag{35}$$

3.2 Hydrodynamic Pressures

According to the conservation law for fluid momentum, the following one dimensional expression for linear momentum of a fluid applies:

$$\rho u \frac{du}{dx} = -\frac{dP}{dx}$$

where ρ is the density of the fluid, P is the pressure, x is the direction of the flow, and u is the velocity in the x direction. Rearranging the above equation yields:

$$\frac{dP}{dx} + \rho u \frac{du}{dx} = 0$$

For a constant density (incompressible flow) the density and viscosity terms can be placed inside the differential:

$$\frac{dP}{dx} + \frac{d}{dx}\left(\frac{1}{2}\rho u^2\right) = 0$$

and then gathering all the terms, yields:

$$\frac{d}{dx}\left(P + \frac{1}{2}\rho u^2\right) = 0$$

Integrating this differential equation:

$$P_{static} + \frac{1}{2}\rho u^2 = \text{constant} = P_{total}$$

This equation has the same form as the incompressible Bernoulli equation. Each term in this equation has the dimensions of a pressure (force/area); P_s is the static pressure, the constant P_t is the total pressure, and $1/2(\rho u^2)$ is the dynamic pressure associated with the flow velocity, u. Assigned the letter P_{dyn} for the dynamic pressure,

$$P_{dyn} = \frac{1}{2}\rho u^2$$

The dynamic pressure is a defined property of a moving flow. We have performed this simple derivation to determine the form of the dynamic pressure. In Chapter 4, the relationship between dynamic pressure and static pressure will be applied to describe the flow motion passing around horizontal cylinder submerged in liquid.

3.3 Heat Transfer

Heat transfer is a process of energy transfer. Whenever there exists a temperature difference, heat transfer must occur. The basic modes of heat transfer process are classified. The first mode is *conduction* which occurs across a medium. The medium may be a solid, a liquid fluid or a stationary gaseous substance. The second mode convection refers to heat exchange between a surface and a moving fluid when they are in different temperature level. The third mode we use the term *thermal radiation* to account for the cases between two or more surfaces in which an intervening medium is absent. All surfaces of finite temperature emit energy in the form of electromagnetic waves; therefore a net heat transfer exists between two surfaces at different temperatures.

The energy transferred in the above three mechanisms is sensible energy by the indications of temperature difference. When a medium experiences a phase change, for example, boiling of a liquid or condensation of a gas, the temperature remains unchanged at a fixed pressure. But there exists heat gain for a liquid during boiling process or heat loss for a gas during condensation process. The two reverse processes are referred to phase-change problem and usually associated with the term *latent heat*.

3.3.1 Conduction Heat Transfer

Heat Conduction is induced by temperature difference between molecules by which a molecule at higher temperature imparts energy or heat to adjacent molecules at lower temperature levels. This type of heat transfer occurs in solid, liquid, or gas system in which temperature gradients exists. Fourier in 1822 first stated a formula describing this phenomenon:

$$q_x'' = \frac{q_x}{A} = -k\frac{dT}{dx} \tag{36}$$

where q_x is the heat transfer rate in x direction with SI unit Watt (W); A is the area normal to the direction of heat flow with SI unit m^2; q_x'' is heat flux in x direction with SI unit W/m^2; the negative sign indicates that the heat flow is in the direction of a negative temperature gradient. k is the thermal conductivity with SI unit W/(m.K), it depends on space, temperature, varying significantly with pressure only in the case of gases subjected to high pressures. At atmospheric pressure and for isotropic materials, k is a function of temperature alone. Under a steady-state conditions and the temperature distribution is linear, the temperature gradient becomes

$$\frac{dT}{dx} = \frac{T_{low} - T_{hi}}{\delta} \tag{37}$$

where δ is the thickness of the medium in the x direction. Substituting equation(37) into equation(36), yields

$$q_x'' = k\frac{T_{hi} - T_{low}}{\delta} \tag{38}$$

To account for a temperature-dependant k an average thermal conductivity may be simply calculated as:

$$\bar{k} = \frac{\int_{T_1}^{T_2} k(T)\, dT}{T_2 - T_1} \tag{39}$$

A more general expression of conduction heat transfer can be written as

$$\vec{q}'' = \frac{\vec{q}}{A} = -k\nabla T \tag{40}$$

Equation(40) is the vector form of Fourier rate equation, often referred to as Fourier's law of heat conduction.

3.3.2 Convection Heat Transfer

Convection heat transfer mode contains two mechanisms. Besides of heat transferred by random molecular activity that is similar to the mechanism of conduction heat transfer, heat is also transferred due to bulk fluid motion. Frequently the later mechanism is called advection heat transport.

Convection heat transfer is often classified based on the nature of the flow. We speak of *natural convection* or *free convection* when the flow is induced by buoyancy forces, which arises from density differences caused by temperature variations in the fluid flow. As a contrast, *Forced convection* is used when the flow is caused by external means, such as a pump. A *combined* type of natural convection and forced convection may exist in industry.

A general expression, regardless of particular nature of the convection heat transfer process, is known as *Newton's law of cooling*

$$q'' = h(T_w - T_\infty) \tag{41}$$

where q", the convective heat flux with a SI unit of W/m^2, is proportional to the difference between the wall surface and the fluid temperature, T_w and T_∞, respectively; the proportionality constant, h with SI unit W/(m^2·K), is the *convective heat transfer coefficient*. It is affected by geometry of the wall surface, nature of the fluid flow, an assortment of thermodynamic properties and the boundary layer conditions. In engineering applications, the average heat transfer coefficient is often of interest, for example, as in the case of calculating the total heat transfer coefficient of a heat exchanger. The convective heat transfer coefficient, h, is the parameter that will be examined in the paper for the film boiling prior to quench and be compared to available experimental data.

3.3.3 Radiation Heat Transfer

While either conduction or convection requires the presence of a material medium to transfer heat, radiation does not. The medium can be a vacuum, air or steam. Heat flux

emitted by a real surface with temperature T_w is less than that of a blackbody at the same temperature and is given by

$$E = \varepsilon E_b = \varepsilon \sigma_{s-b} T_w^4 \tag{42}$$

where E_b is the heat flux emitted by a blackbody; σ_{s-b} is the Stefan-Boltzmann constant (= 5.67×10^{-11} $kW/m^2/K^4$); and ε is the surface emissivity, with a value in the range between 0 and 1. It depends strongly on surface material and finish. For an unoxidized calandria tube made of Zircaloy-2, a typical value of 0.15-0.19 [22] is applicable for the surface emissivity. In the case of a surface at temperature T_w being completely surrounded by a much larger, isothermal surface at temperature T_{sur}, the net radiation heat flux can be expressed as

$$q''_{rad} = \varepsilon \sigma_{s-b} (T_w^4 - T_{sur}^4) \tag{43}$$

where ε effective emissivity between the wall and the surroundings, both T_w and T_{sur} are the absolute temperatures (K). As depicted in Figure 15, for a two-surface enclosure of long (infinite) concentric cylinders with emissivities of ε_1 and ε_2, and with radii r_1 and r_2, respectively. The effective emissivity, ε, defined in Equation (43), is given as [20]:

$$\varepsilon = \left[\frac{1}{\varepsilon_1} + \frac{1 - \varepsilon_2}{\varepsilon_2} \left(\frac{r_1}{r_2} \right) \right]^{-1} \tag{44}$$

We need to choose a value of ε for the case of film boiling outside of a calandria tube. In the case of film boiling, the media between the two surfaces is steam vapor, which can be roughly treated as transparent. The water surrounding vapor film has a thermal

emissivity of ε_2 = 0.95. The calandria tube wall, which is made of Zircaloy-2 material, has an emissivity of approximately ε_1 = 0.19 under non-oxidized condition (Figure 16 [22]).

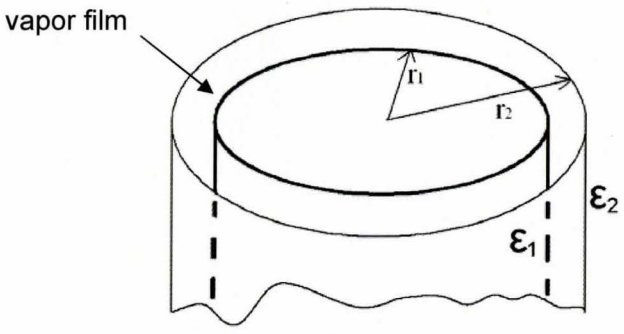

Figure 15: Long concentric cylinder experiencing film boiling

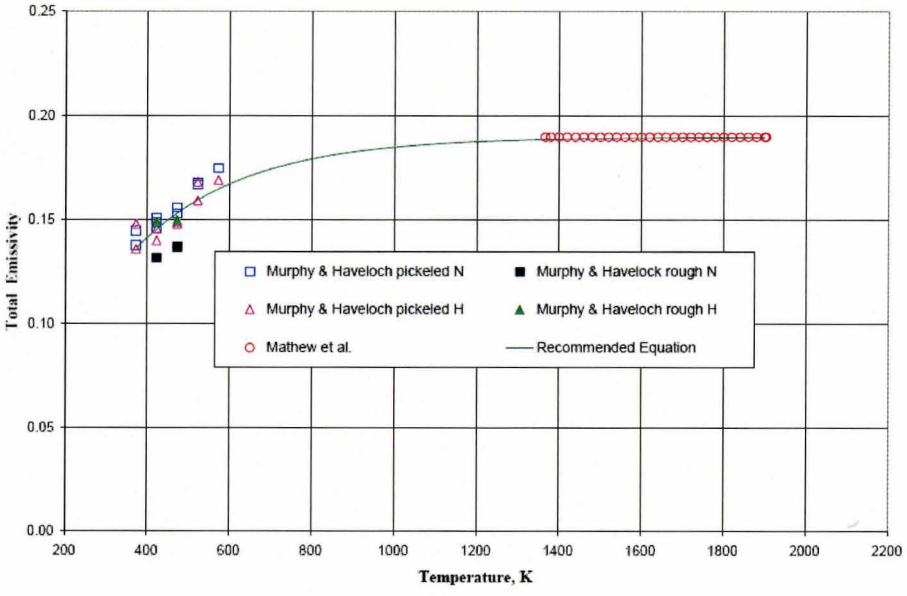

Figure 16: Total emissivity of unoxidized Zircaloy [22]

In addition to thermal emissivities, $r_1$and r_2 are almost equal in that the thickness of vapor film is extremely thin compared to the radius of calandria tube. Therefore the effective emissivity can be simplified as:

$$\varepsilon \approx \varepsilon_1 \tag{45}$$

3.3.4 Heat Balance and Effective Heat Transfer Coefficient

Consider a configuration of two-phase involved heat transfer in which heat is generated in an infinitely large hot metal plate submerged in a quiescent liquid. Outside of the metal plate there is a thin vapor film. The interface between vapor and liquid is at the saturation temperature associated with pressure. The direction of heat transfer is from the outside surface of the metal plate to the vapor film to the interface, then from the interface to the bulk liquid. Conduction heat transfer is dominated by the heat transfer mechanism in the vapor layer. Heat transfer from the interface to the bulk liquid is mainly by convection; while radiation heat transfer occurs from the hot solid outer surface to the surrounding environment. Referring to Equations (38), (41) and (43), the three heat transfer fluxes can be rephrased as following

Conduction: $q_{cond}'' = k\frac{T_w - T_{sat}}{\delta}$

Convection: $q_{conv}'' = h(T_{sat} - T_b)$

Radiation: $q_{rad}'' = \varepsilon\sigma_{s-b}(T_w^4 - T_b^4)$

where T_w, T_{sat}, T_b are the wall temperature of metal plate, the saturation temperature and the bulk liquid temperature, respectively.

The total heat transferred from the metal plate can be expressed as

$$q_w" = h_{eff}(T_w - T_b)$$

where h_{eff} is called the effective heat transfer coefficient.

From the perspective of heat balance, and assuming that there are no other heat losses, all heat transferred out of the metal plate should be equal to the above three heat losses.

$$q_w" = q_{cond}" + q_{rad}"$$

Note that the convection heat transferred from the vapor-liquid interface to bulk liquid is part of the conduction heat transferred out from the metal plate, and therefore it is included in conduction heat.

Therefore the effective heat coefficient can be calculated as

$$h_{eff} = \frac{q_w"}{T_w - T_b} = \frac{k}{\delta}\frac{T_w - T_{sat}}{T_w - T_b} + h\frac{T_{sat} - T_b}{T_w - T_b} + \varepsilon\sigma_{s-b}(T_w^2 + T_b^2)(T_w + T_b)$$

The application of effective heat transfer coefficient provides a "lumped" method to describe the overall heat transfer coefficient for some complicated cases. For example, it was a common engineering practice to analyze heat exchangers with turbulent two-phase flow. It is useful when the detailed heat transfer mechanisms are not of the interest.

3.4 Boiling Regime

This subsection first introduces typical boiling curve and boiling regime, followed by introduction to film boiling and transition boiling.

3.4.1 Nikiyama Boling Curve

The pool boiling mode was first proposed by Nukiyama in 1935. The existence of several boiling modes over a wire was recognized and these modes are plotted as in Figure 17.

There are three basic modes of boiling, nucleate boiling, transition boiling, and film boiling. Each occurs over a range of superheats. Superheat is defined as the temperature difference that the temperature of wall surface exceeds the liquid saturation temperature. Regime AC in Figure 17 is called nucleate boiling, the most commonly observed and most efficient boiling mode initiated by a small superheat (about 3 to 30°C). This mode is characterized by the formation of bubbles from preferred sites randomly distributed over the surface. These preferred sites are termed nucleate sites where the vapor phase develops with less energy required than in the bulk. The increase in superheat results in more and more activated bubble from nucleate sites and therefore rapid increase in heat flux. With further increase in superheat the second mode, transition boiling, occurs. Bubbles begin to coalesce and local patches forms with intermittent explosions of bubbles. Heat flux decreases with increasing superheat. The transition boiling is represented as regime CD in Figure 17. At higher superheats, say several hundred Celsius degrees, a continuous blanket of vapor film covers heating surface with intermittent departure of bubbles at regular frequencies. This mode is called film boiling. The film boiling features following characteristics:

- Since a vapor blanket covers the surface during the film boiling, the heat transfer coefficient is greatly less than that of other boiling regimes due to the relatively much lower thermal conductivity of the vapor layer.

- The surface temperature in the film boiling regime is considerably high compared to that of nucleate boiling and transition boiling.
- Since the high surface temperature, the radiation heat transfer may not be ignored anymore.

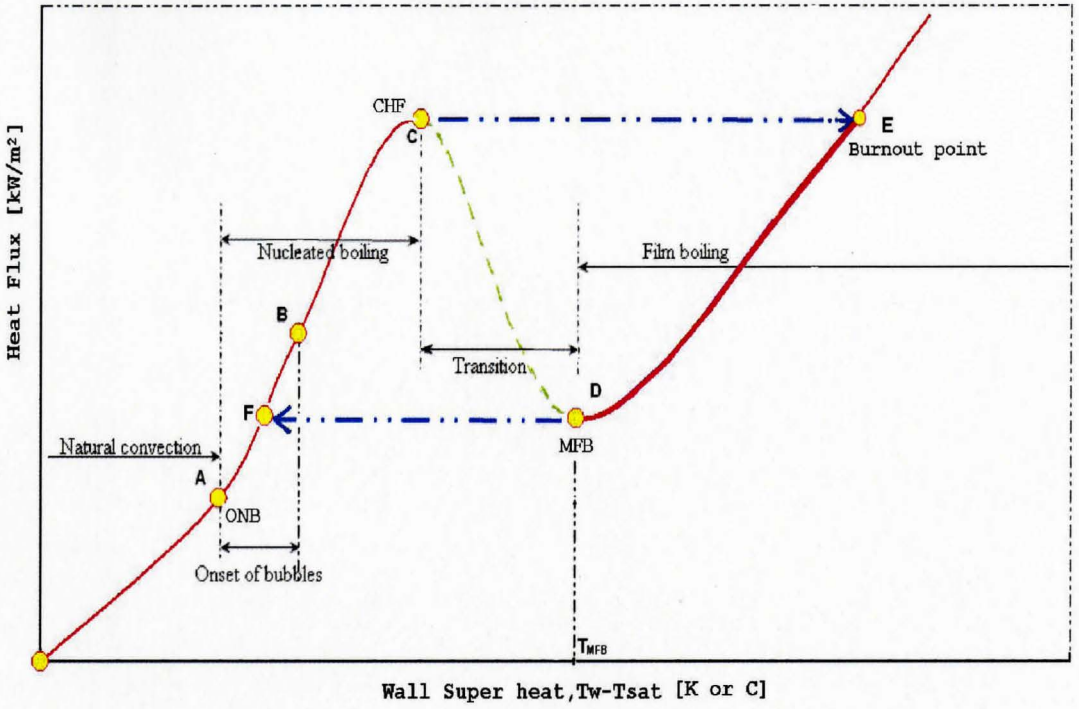

Figure 17: Typical boiling modes in terms of heat flux and wall superheat

3.4.2 Film Boiling and Transition Boiling

In Figure 17, the range of wall superheat temperature between the Critical Heat Flux (CHF) and Minimum Film Boling (MFB) on the boiling curve (between point C and D) is usually termed the transition boiling regime. The mechanism of film-transition boiling is totally different from that for nucleate-transition boiling. The film-transition boiling usually

occurs with quenching. Quenching experiments were used to investigate film-transition boiling data. There are relatively less experiments for transition boiling than for experiments dealing with other boiling regimes.

The description proceeded in Section 3.4.1 is under a temperature-controlled surface. If the heating surface is heat flux controlled, the independent variable is the heat flux rather than temperature. Ramping up of the heat flux would bring the nucleate boiling directly into film boiling with a large increase of superheat through dotted path CE in Figure 17. Point E is called burnout point. For the opposite condition, reducing the heat flux would bring the film boiling directly into nucleate boiling through the dotted path DF, rather than path DCF as occurred in temperature-controlled process. Point D is termed by different names, such as minimum film boiling (MFB) temperature, rewet superheat temperature, or Leidenfrost superheat temperature. This implies the quenching heat transfer is a complex transfer mechanism and it affects the heat transfer boiling regimes in a very rapid manner.

3.5 Vapor Superheat and Vapor-Liquid Interface

The vapor-liquid interface demarcates the superheat temperature and the subcooled temperature. On one side the temperature of the superheated vapor decreases from the highest value on the metal surface to the lowest saturation temperature on the vapor-liquid interface. On the other side, subcooled liquid temperature decreases from the saturation temperature to bulk liquid temperature. In this subsection we are going to introduce the vapor superheat and then discuss the representative vapor temperature.

3.5.1 Superheat and Latent Heat

Before quenching occurs, evaporation from the vapor-liquid interface supports vapor generation and maintains the existence of film boiling. The vapor gradually absorbs energy as heat conducts from the metal surface to outside. Therefore, the vapor becomes superheated. The superheated temperature is higher than the boiling point temperature corresponding to the pressure. The temperature that can represent the varying vapor temperature will be discussed in Section 3.5.2.

The amount of energy in the form of heat absorbed or released by a substance during a change of phase is called latent heat. Liquid phase at the interface absorbs the latent heat and evaporates to vapor phase. The vapor phase can absorbs more heat to become superheated.

3.5.2 Representative Vapor Temperature

Assume that a smooth vapor film layer blanket a horizontal calandria tube as shown in Figure 18. The dashed line represents the centroidal line of the vapor area at temperature T_c. This temperature may best describe the average vapor temperature. Assume that the CT has radius R_w and temperature T_w; the outmost solid circular line is the vapor-liquid interface at the temperature T_{sat}; δ_v is the vapor film thickness; and δ_c is the distance from the centroid normal to the CT tube surface.

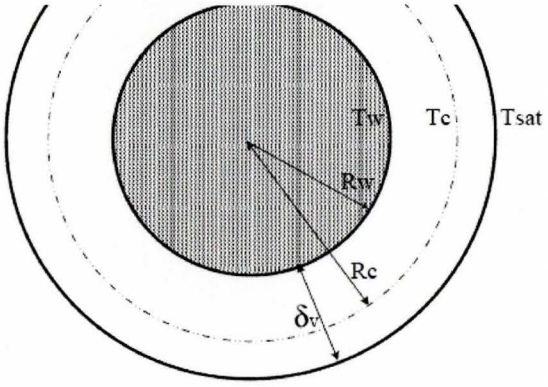

Figure 18: Vapor film layer outside CT

Since the conduction heat transfer dominates in the vapor steam film layer, the temperature profile across the vapor film, strictly speaking, is not a straight line, instead, is a curve in terms of the cylindrical coordinates. Figure 19 shows the curvature profile of the vapor film thickness across the vapor film. The temperature at any point inside the vapor film is given as [23]:

$$T(r) = \frac{T_w - T_{sat}}{\ln\left[R_w / (R_w + \delta_v)\right]} \ln\left(\frac{r}{R_w + \delta_v}\right) + T_{sat} \tag{46}$$

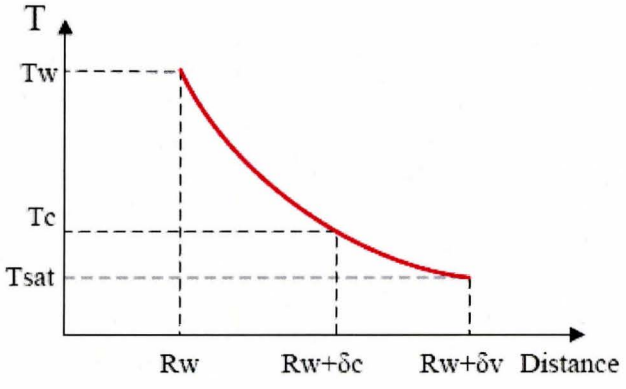

Figure 19: Temperature drop across the vapor film

The radius of the centroid line can be calculated through the relation of mass. The centroid line separates the total vapor mass into halves, so there exist

$$\pi\left(R_c^{\,2} - R_w^2\right) L\rho_v = \frac{1}{2}\pi\left[(R_w + \delta_v)^2 - R_w^2\right] L\rho_v$$

where L is the unit length perpendicular to the paper. Solving the above equation one obtains

$$R_c = \sqrt{R_w^2 + R_w\delta_v + \frac{1}{2}\delta_v^2} \tag{47}$$

Letting $r=R_c$ and Substituting Eq.(47) into Eq.(46), yields the temperature at centroid:

$$T_c = \frac{T_w - T_{sat}}{\ln\left[R_w / (R_w + \delta_v)\right]} \ln\left(\frac{\sqrt{R_w^2 + R_w\delta_v + \frac{1}{2}\delta_v^2}}{R_w + \delta_v}\right) + T_{sat} \tag{48}$$

One may define the average temperature as the integral of the temperature function over a whole range of the vapor film and then be divided by vapor film thickness. This yields:

$$\bar{T} = \frac{\int_{R_w}^{R_w+\delta_v} T(r)dr}{\delta_v} \tag{49}$$

where T(r) is given by Equation(46).

Another way to estimate the representative vapor film temperature is to use the middle point temperature of the vapor film. After applying $R_{mp}=R_w+0.5\delta_v$ to Equation (46), it follows that

$$T_{mp} = \frac{T_w - T_{sat}}{\ln\left[R_w / (R_w + \delta_v)\right]} \ln\left(\frac{R_w + 0.5\delta_v}{R_w + \delta_v}\right) + T_{sat} \tag{50}$$

The last approach is to assume a linear temperature profile across the vapor film. The temperature at the midpoint can be calculated as

$$T_v = \frac{1}{2}(T_w - T_{sat}) + T_{sat} = \frac{1}{2}(T_w + T_{sat}) \tag{51}$$

Now there are four methods to calculate the representative vapor film temperature. A comparison among vapor film temperatures as function of vapor film thickness, δ_v, ranging from 0.05mm to 0.35mm, is given in Table 2.

Table 2: Comparison of vapor temperature results of four methods

Tw=200 C						Tw=300 C			
Rw[mm]	**δv[mm]**	Tc	T_ave	Tmp	Tv	Tc	Tave	Tmp	Tv
65.88	**0.05**	149.98	149.99	149.99	150.00	199.96	199.99	199.98	200.00
65.88	**0.10**	149.96	149.99	149.98	150.00	199.92	199.97	199.96	200.00
65.88	**0.15**	149.94	149.98	149.97	150.00	199.89	199.96	199.94	200.00
65.88	**0.20**	149.92	149.97	149.96	150.00	199.85	199.95	199.92	200.00
65.88	**0.25**	149.91	149.97	149.95	150.00	199.81	199.94	199.91	200.00
65.88	**0.30**	149.89	149.96	149.94	150.00	199.77	199.92	199.89	200.00
65.88	**0.35**	149.87	149.96	149.93	150.00	199.74	199.91	199.87	200.00

Tw=400 C						Tw=500 C			
Rw[mm]	**δv[mm]**	Tc	Tave	Tmp	Tv	Tc	Tave	Tmp	Tv
65.88	**0.05**	249.94	249.98	249.97	250.00	299.92	299.97	299.96	300.00
65.88	**0.10**	249.89	249.96	249.94	250.00	299.85	299.95	299.92	300.00
65.88	**0.15**	249.83	249.94	249.91	250.00	299.77	299.92	299.89	300.00
65.88	**0.20**	249.77	249.92	249.89	250.00	299.70	299.90	299.85	300.00
65.88	**0.25**	249.72	249.91	249.86	250.00	299.62	299.87	299.81	300.00
65.88	**0.30**	249.66	249.89	249.83	250.00	299.55	299.85	299.77	300.00
65.88	**0.35**	249.60	249.87	249.80	250.00	299.47	299.82	299.74	300.00

Tw=600 C						Tw=700 C			
Rw[mm]	δv[mm]	Tc	Tave	Tmp	Tv	Tc	Tave	Tmp	Tv
65.88	0.05	349.91	349.97	349.95	350.00	399.89	399.96	399.94	400.00
65.88	0.10	349.81	349.94	349.91	350.00	399.77	399.92	399.89	400.00
65.88	0.15	349.72	349.91	349.86	350.00	399.66	399.89	399.83	400.00
65.88	0.20	349.62	349.87	349.81	350.00	399.55	399.85	399.77	400.00
65.88	0.25	349.53	349.84	349.76	350.00	399.43	399.81	399.72	400.00
65.88	0.30	349.43	349.81	349.72	350.00	399.32	399.77	399.66	400.00
65.88	0.35	349.34	349.78	349.67	350.00	399.21	399.74	399.60	400.00

From the above table one can find that the largest deviation occurs when CT wall temperature T_w=700°C and δ_v=0.35mm, the temperature at centroid line is 399.21°C. Compared to the temperature 400°C by linear approximation method, the maximum error is less than 0.2%. As shown in the Table all the four methods result in little difference between calculated vapor temperatures. The reason for this stems from the vapor film thickness being extremely thin in comparison to the CT wall radius.

In conclusion, the simplest method is the fourth method, which is the linear approximation shown in Equation(51). This will provide a simple computational approach.

The calculated data in the Table above shows that the assumption of linear temperature drop is feasible, so the following expression for heat conduction flux across the vapor film is employed in Chapter Four.

$$q''_c = -k_v \left.\frac{\partial T_w}{\partial r}\right|_{r=R_{CT}} = k_v \frac{T_w - T_{sat}}{\delta} = k_v \frac{(2T_v - T_{sat}) - T_{sat}}{\delta} = k_v \frac{2(T_v - T_{sat})}{\delta} \qquad (52)$$

3.6 Thin Layer Heat Conduction from Interface to Subcooled Bulk Liquid

In this subsection we are going to introduce Sideman's Investigation on Thin Layer Heat Conduction [24] near the vapor-liquid interface. The conclusion will be applied in heat balance equation in Section Four.

Considering mass transfer, Sideman examined the apparent equivalence between penetration theory and potential flow theory but only under restricted conditions. One such condition limits the transfer to a narrow layer near the interface where constant velocity may be assumed regardless of the existing boundary on the other side of the flowing liquid. The other condition is for large Péclet numbers. The Péclet number is defined as

$$Pe \equiv \frac{velocity \cdot characteristic\ length}{thermal\ diffusivity} \equiv \frac{VL}{\alpha} \equiv \mathrm{Re} \cdot \mathrm{Pr}$$

The Péclet number, Pe, is a product of Reynolds number and Prandtl number. It is also a measurement of ratio between the advection and diffusion. Note that in engineering applications the Peclet number is often very large. In such situations, the dependency of the flow upon downstream locations is diminished, and variables in the flow tend to become 'one-way' properties. Thus, when modelling certain situations with high Péclet numbers, simpler computational models can be adopted [25]

For a 2-dimensional curvilinear spherical coordinates, the local flux was calculated as

$$\left.\frac{\partial C}{\partial y}\right)_{y=0} = \alpha_L \frac{c_0}{\sqrt{\pi}} \frac{\sin^2\theta^+}{\sqrt{\left(2\,\mathrm{R_c}\alpha_L \int_0^{\theta^+} \sin^3\theta^+ d\theta^+\right) / (3u_\infty)}}$$

where α = thermal diffusivity

c_0 = interfacial concentration

θ^+ = zenith angle

R_c = radius of curvilinear surface

u_∞ = free stream liquid velocity

L.C. Witte [26] extended the result to heat transfer in a cylindrical coordinates for a horizontal cylinder. The liquid temperature gradient close to the vapor-liquid interface was given as:

$$\left.\frac{\partial T_L}{\partial y}\right)_{y=\delta} = -\sqrt{\frac{2\,u_\infty}{\pi R\alpha_L(1-\cos\theta)}} \cdot \sin\theta \cdot \Delta T_{sub} \tag{53}$$

where T_L = liquid temperature

R = calandria tube radius

δ = local vapor film thickness

θ = inclination angle

ΔT_{sub} = subcooling temperature $(T_{sat} - T_b)$

An expression of the heat flux from the interface to the bulk liquid is thus derived from the above equation and will be applied in Chapter Four as

$$q''_{i-L} = -k_L \left.\frac{\partial T_L}{\partial y}\right)_{y=\delta} = 2k_L \sqrt{\frac{u_\infty + \dot{\delta}}{\pi R\alpha_L}} \cdot \cos\frac{\theta}{2} \cdot \Delta T_{sub} \tag{54}$$

where a conversion is applied in Equation (53) to arrive Equation (54),

$$\frac{\sin\theta}{\sqrt{1-\cos\theta}} = \frac{2\sin\frac{\theta}{2}\cos\frac{\theta}{2}}{\sqrt{2}\sin\frac{\theta}{2}} = \sqrt{2}\cos\frac{\theta}{2}$$

The free stream velocity u_∞ is relpalced by $u_\infty + \dot{\delta}$ with consideration of interface movement of the vapor film in Chapter Four.

3.7 Thermalhydraulic Properties of Vapor as Function of Temperature

Thermalhydraulic properties of heavy water and steam may be expressed as functions of temperature and pressure. Under the fixed pressure condition, the properties can be plotted as functions of temperature by adopting well recognized tabulated data. From each plot a trend-line of a specific property as a polynomial function of the temperature can be obtained. The reason of choosing polynomial functions, when computer-based coding and calculation are involved, relies on the fact that polynomial functions have better stability than other functions such as exponential, logarithmic or trigonometric functions.

Figure 20 to Figure 24 are obtained by applying heavy water properties data (Hill, MacMillan and Lee, AECL [27]). The copies of these data are presented in Appendix C.

Those thermalhydraulic properties of saturated D_2O steam include density, specific heat, dynamic viscosity, thermal conductivity, and thermal diffusivity.

Figure 20 shows the D_2O steam density as a function of steam temperature and can be expressed by

$$\rho_v = -10^{-9}T_v^{\,3} + 3\times10^{-6}T_v^{\,2} - 2\times10^{-3}T_v + 0.8237$$

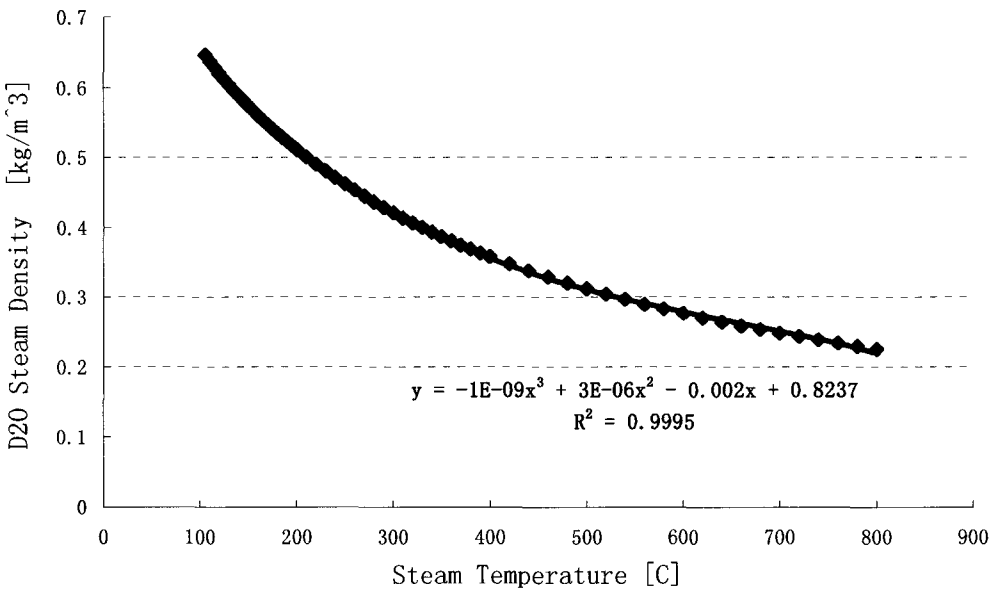

Figure 20: D_2O steam density in terms of steam temperature (Hill, AECL [27])

Figure 21 gives the relationship between D_2O specific heat and temperature as

$$c_{p,v} = -3\times10^{-14}T_v^{\,5} + 6\times10^{-11}T_v^{\,4} - 5\times10^{-8}T_v^{\,3} + 2\times10^{-5}T_v^{\,2} - 4.5\times10^{-3}T_v + 2.1481$$

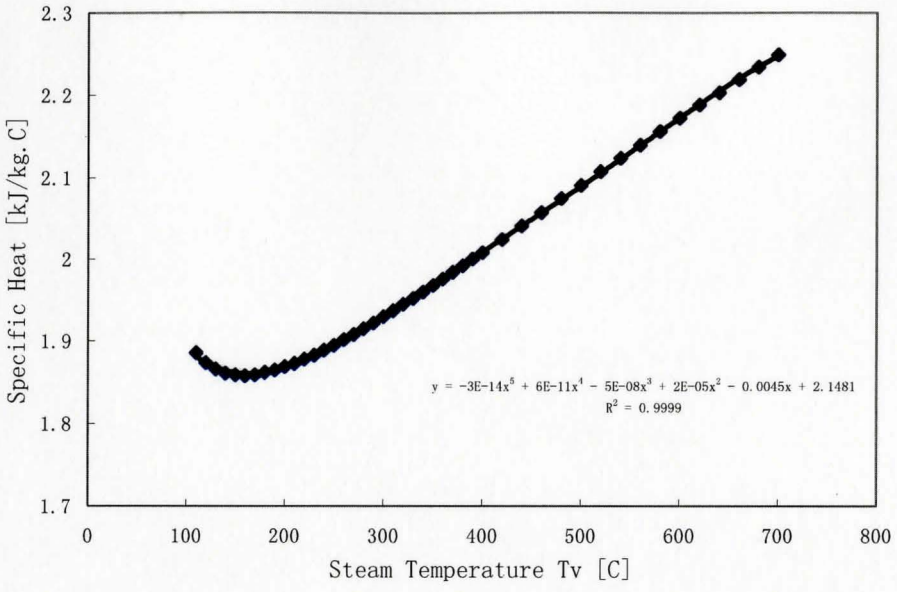

Figure 21: D_2O steam specific heat in terms of temperature (Hill, AECL [27])

Figure 22 provides an expression of D_2O dynamic viscosity in terms of temperature:

$$\mu_v = 4 \times 10^{-8} T_v + 8 \times 10^{-6}$$

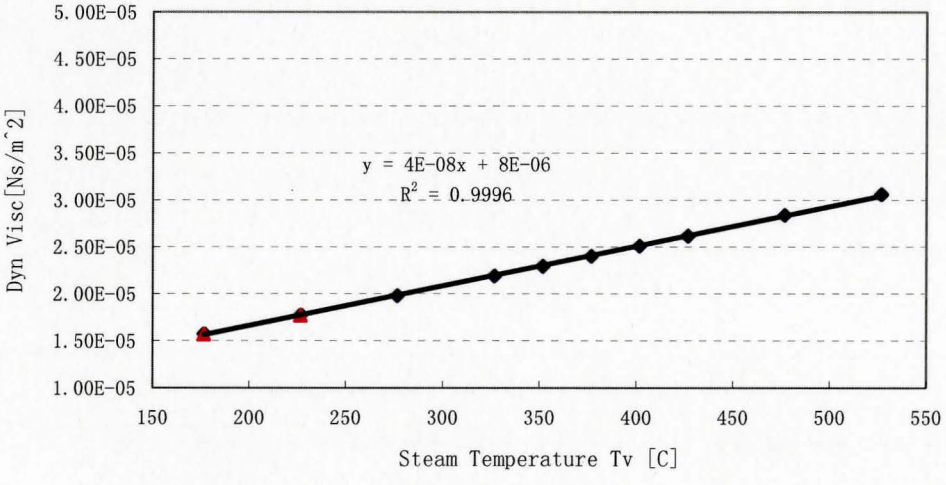

Figure 22: D_2O steam dynamic viscosity in terms of temperature (Hill, AECL [27])

Note that the data available is in the temperature range from about 175 °C to 525 °C. The values of dynamic viscosity can be obtained by interpolation for temperature lower than 175 °C and higher than 525 °C .

Figure 23 shows the D_2O Thermal Conductivity, K_v, as a function of temperature and can be expressed as

$$K_v = 10^{-10} T_v^2 + 5 \times 10^{-8} T_v + 2 \times 10^{-5} \quad (55)$$

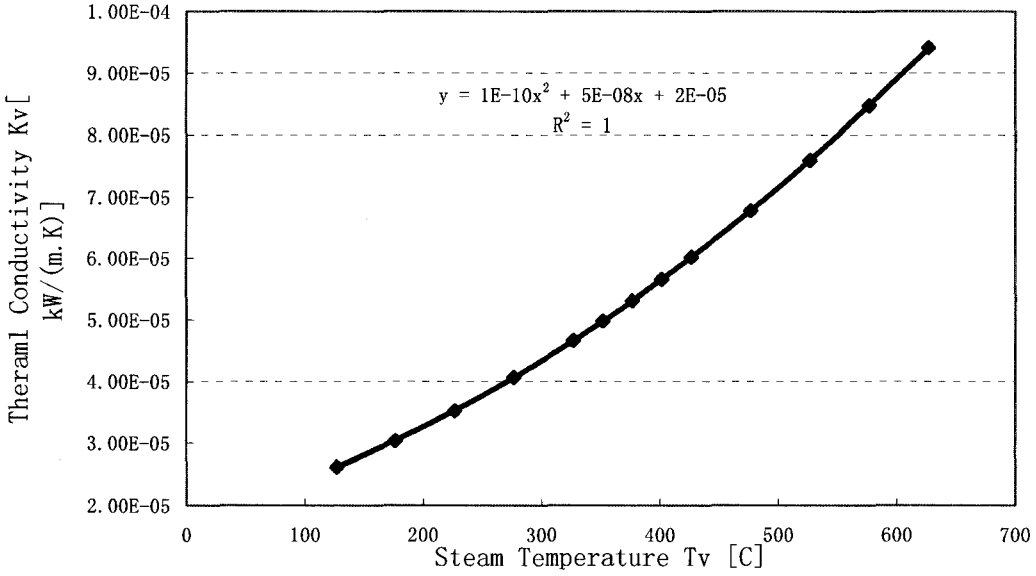

Figure 23: D_2O steam thermal conductivity in terms of temperature (Hill, AECL [27])

Figure 24 gives the D_2O thermal diffusivity as a quadratic function of temperature.

$$a_v = 3 \times 10^{-10} T_v^2 + 2 \times 10^{-8} T_v + 2 \times 10^{-5}$$

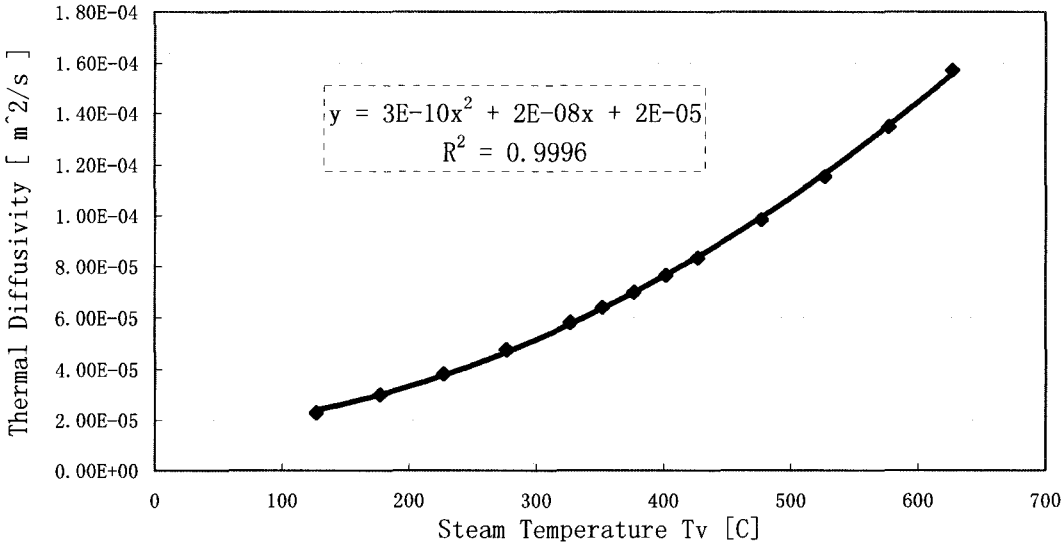

Figure 24: D_2O steam thermal diffusivity in terms of temperature (Hill, AECL [27])

Chapter Four

4.0 Transient Vapor-Film-Thickness Equation

In this chapter a transient vapor-film-thickness equation will be derived based on dynamic pressure and heat balances. A physical model and associated assumptions will be introduced first, then an intermediate equation resulting from pressure balance will be derived. An analysis of heat balance then follows. Then a resultant expression for vaporization from heat balance will be substituted into the intermediate equation. In the end a transient vapor-film-thickness equation will be derived.

4.1 Physical Model

4.1.1 Description of the Physical Model

Film boiling on a horizontal CT is characterized by the existence of a continuous vapor film surrounding the heated CT outer surface. The region of the stagnation point at the lowest part of the CT is dominated by mass transfer. Continuous vapor formation sustains a vapor blanket along the CT outer surface. Vapor departs from the upper part of the cylinder, as showed in Figure 25. The vapor transient separation angle, ξ_v, indicates the position at which the vapor transitions from laminar to turbulent flow. Similarly, there exists a liquid transient separation angle, ξ_L, in the liquid zone.

The cylindrical coordinates system given in Figure 26 is appropriate for this geometric configuration. The reference point is taken at the bottom of the CT. Vector z is normal to the surface and vector r is tangential to the surface. The stagnation point is located at the

lowest point of the vapor-liquid interface just beneath the origin point. The velocity components u and v are along with r and z axes, respectively.

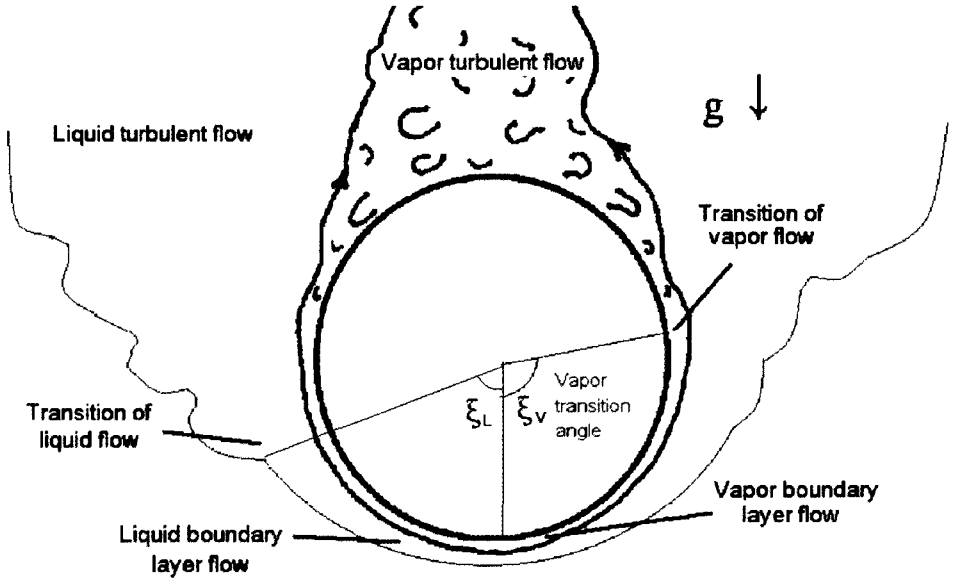

Figure 25: Cross-section of CT experiencing laminar film boiling

$P_0(0, \delta)$ is the liquid side static pressure at the stagnation point; $P_{x,total}(d, \delta-\Delta h)$is the liquid side total pressure of point X at the interface. $P_{x,staticl}(d, \delta-\Delta h)$ is the liquid side static pressure of point X at the interface. Point X is in the neighborhood of the stagnation point. The angle θ indicates the vicinity of stagnation point. At the vicinity of the stagnation point, the variation in vapor film thickness can be ignored. The pressure inside the vapor film, p_v, is assumed uniformly distributed.

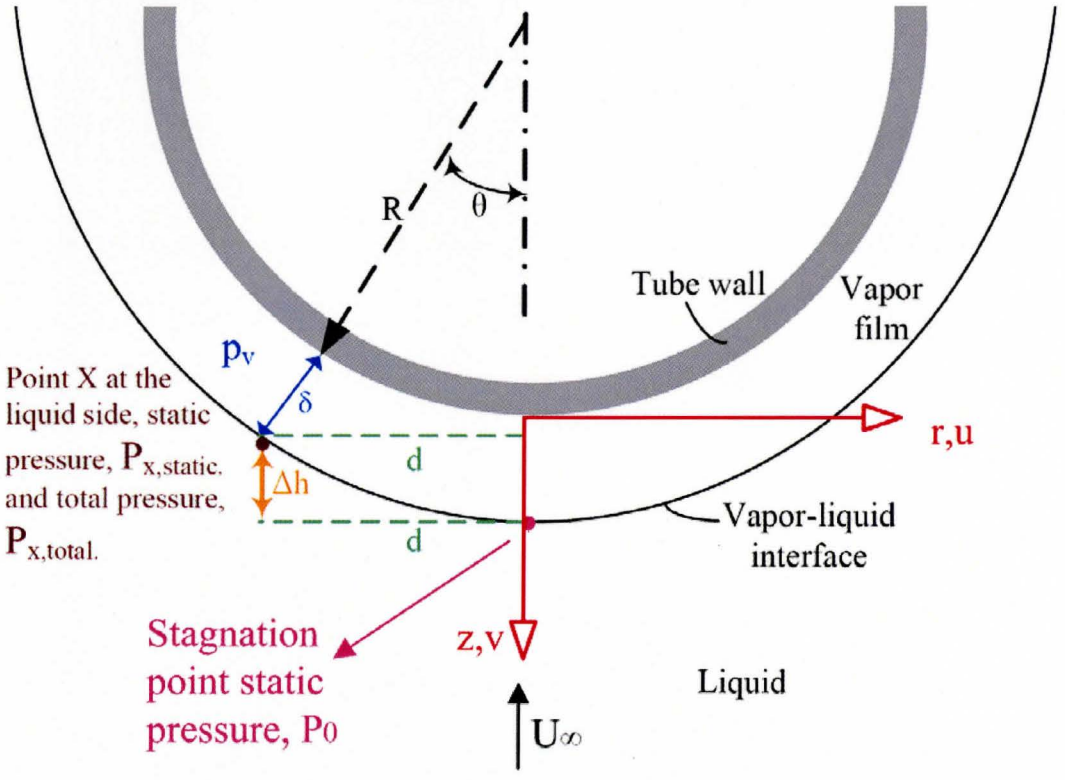

Figure 26: Physical model of vapor film covering lower part of hot horizontal tube wall and coordinates

4.1.2 Assumptions

The following assumptions are made:

(1) Incompressible homogeneous liquid and vapor

(2) Vapor film is very thin with comparison to the radius of CT ($\delta \ll R$)

(3) Inertial and convection effects in the vapor are negligible

(4) Viscous dissipation in the vapor film is negligible

(5) Vapor density is uniformly distributed

(6) Thermophysical properties of either vapor or liquid are uniform and are temperature dependent

(7) Thermophysical properties are evaluated at atmospheric pressure

(8) CT surface temperature are uniform; there is neither circumferential heat loss nor longitudinal heat loss at the film boiling and quenching spots

(9) Laminar vapor flow covers most of the CT surface

(10) Developed laminar liquid flow exists at the outside of the liquid-vapor interface

(11) Heat conduction from liquid-vapor interface to subcooled liquid occurs on a thin liquid boundary layer near the liquid-vapor interface

(12) Smooth liquid-vapor interface. This is a reasonable representation of the average vapor film heat transfer behavior.

(13) In the vicinity of stagnation point ($\theta < 5^o$)(refer to Figure 26), the variation in vapor film thicknesses are negligible

(14) The thickness of the liquid-vapor interface is in the order of atomic diameter and is negligible when compared to the vapor film thickness.

Assumption (8) is made considering a uniform ballooning PT/CT contact over a significant length of a fuel channel and the whole outer surface of CT is blanket by vapor film. The heat flux to the inner of the PT is uniform. If bundle deformation occurs it will be well after the PT/CT contact. In this scenario the longitudinal and circumferential heat losses will be small and can be ignored when compared to the radial heat transfer.

Assumption (10) represents the free stream velocity by a fully developed flow. In Chapter three a correlation between the fluid velocity normal to the CT surface and the free stream liquid velocity was derived based on an assumption of fully developed flow. To maintain consistency, the same assumption is therefore made here. More discussions

about this assumption can be found in Chapter Seven.

4.1.3 Dynamic Pressure Near the Stagnation Point

At a point X that is neighborhood to the stagnation point, the static pressure, $P_{x,static}$, and the total pressure, $P_{x,total}$, have the following relationship

$$P_{x,total} = P_{x,static} + \rho_L u_N^2 / 2 \tag{56}$$

where u_N is the velocity component normal to the vapor interface. We have already derived Equation (35) in Chapter Three as

$$u_N^2 = (u_\infty + \dot{\delta})^2(1 - 4\sin^2\theta)$$

Substituting Equation (35) into (56), yields

$$P_{x,total} = P_{x,static} + \rho_L (u_\infty + \dot{\delta})^2(1 - 4\sin^2\theta) / 2 \tag{57}$$

From fluid mechanics [28], the static pressure P_x can be expressed as

$$P_{x,static}(x, \delta_x) = P_0(0, \delta) - \rho_L g \Delta h \tag{58}$$

Substituting equation(58) into equation(57), yields

$$P_{x,total} = P_0 - \rho_L g \Delta h + \frac{1}{2}\rho_L (u_\infty + \dot{\delta})^2(1 - 4\sin^2\theta) \tag{59}$$

Bradfield [29] investigated the wavy characteristics of the interface in stable laminar film boiling both experimentally and analytically. His analysis showed that the disturbances of vapor-liquid interface originating at the neighborhood of lower stagnation point of an

immersed hot tube are dominated by local acceleration effects rather than by viscous effects. In the neighborhood region of stagnation point, the corresponding equation of motion is

$$\frac{P_{x,static}}{g}\ddot{\delta} = -P_{x,total} + p_v + \frac{2\sigma}{R} \tag{60}$$

where $\ddot{\delta}$ is the acceleration of vapor-liquid interface; p_v is the vapor pressure distributed in the vapor film; σ is the water surface tension; and R is the tube outer radius.

Substituting equation(58) into (60) and rearranging, gives

$$P_{x,total} = -\frac{\ddot{\delta}}{g}(P_0 - \rho_L g\Delta h) + p_v + \frac{2\sigma}{R} \tag{61}$$

Equating equation(61) and (59) to cancel $P_{x,total}$, yields

$$-\frac{\ddot{\delta}}{g}(P_0 - \rho_L g\Delta h) + p_v + \frac{2\sigma}{R} = P_0 - \rho_L g\Delta h + \frac{1}{2}\rho_L (u_\infty + \dot{\delta})^2(1-4\sin^2\theta)$$

Rearrange,

$$p_v = (1+\frac{\ddot{\delta}}{g})(P_0 - \rho_L g\Delta h) + \frac{1}{2}\rho_L (u_\infty + \dot{\delta})^2(1-4\sin^2\theta) - \frac{2\sigma}{R} \tag{62}$$

Refer to Figure 26, Δh can be calculated as

$$\Delta h = (R+\delta_0) - (R+\delta_x)\cos\theta = (R+\delta_x)(1-\cos\theta) + \delta_0 - \delta_x$$

$$= \frac{(R+\delta_x)^2}{(R+\delta_x)}\frac{(1-\cos^2\theta)}{(1+\cos\theta)} + \delta_0 - \delta_x = \frac{[(R+\delta_x)\sin\theta]^2}{(R+\delta_x)(1+\cos\theta)} + \delta_0 - \delta_x$$

$$= \frac{d^2}{(R+\delta_x)(1+\cos\theta)} + \delta_0 - \delta_x$$

where the subscription 0 indicates the stagnation point and the subscription x indicates somewhere on the liquid-vapor interface at the vicinity of the stagnation point.

Considering $\delta_0 \approx \delta_x \approx \delta$, $r \approx d$ in the neighborhood region of stagnation point, the above equation reduces to

$$\Delta h \approx \frac{r^2}{(R+\delta)(1+\cos\theta)} \tag{63}$$

If the vicinity of the stagnation point is of interest, since $\theta \approx 0$, Equation (63) results in $\frac{r^2}{R+\delta}$. Equation (63) for Δh is applied for generality.

Substituting equation(63) into (62) and noting that $sin\ \theta = r/(R+\delta)$, yields

$$p_v = (1+\frac{\ddot{\delta}}{g})\left[P_0 - \rho_L g \frac{r^2}{(R+\delta)(1+\cos\theta)}\right] + \frac{1}{2}\rho_L (u_\infty + \dot{\delta})^2 \left[1 - \frac{4r^2}{(R+\delta)^2}\right] - \frac{2\sigma}{R}$$

Rearranging the above equation we obtain

$$p_v = -\frac{\rho_L}{(R+\delta)}\left(\frac{g+\ddot{\delta}}{1+\cos\theta} + \frac{2(u_\infty+\dot{\delta})^2}{R+\delta}\right)r^2 + \left(1+\frac{\ddot{\delta}}{g}\right)P_0 + \frac{1}{2}\rho_L(u_\infty+\dot{\delta})^2 - \frac{2\sigma}{R} \tag{64}$$

Differentiating in terms of r, yields a partial derivative of vapor pressure as

$$\frac{\partial p_v}{\partial r} = -\frac{2\rho_L}{(R+\delta)}\left(\frac{g+\ddot{\delta}}{1+\cos\theta} + \frac{2(u_\infty+\dot{\delta})^2}{R+\delta}\right)r \tag{65}$$

Later, this equation will be compared with another expression for $\frac{\partial p_v}{\partial r}$ to remove the dependence on p_v.

4.1.4 Governing Equations

From Navier-Stokes equations for the vapor film [15], the vapor pressure can be evaluated. This vapor pressure must match the vapor pressure calculated in Section 4.1.3.

The Navier-Stokes equations can be written as

Continuity

$$\frac{1}{r}\frac{\partial}{\partial r}(ru) + \frac{\partial v}{\partial z} = 0 \tag{66}$$

r momentum

$$\rho_v\left(\frac{\partial u}{\partial t} + u\frac{\partial u}{\partial r} + v\frac{\partial u}{\partial z}\right) = -\frac{\partial p_v}{\partial r} + \mu_v\left[\frac{\partial}{\partial r}\left(\frac{1}{r}\frac{\partial (ru)}{\partial r}\right) + \frac{\partial^2 u}{\partial z^2}\right] \tag{67}$$

z momentum

$$\rho_v\left(\frac{\partial v}{\partial t} + u\frac{\partial v}{\partial r} + v\frac{\partial v}{\partial z}\right) = \rho_v g - \frac{\partial p_v}{\partial z} + \mu_v\left[\frac{1}{r}\frac{\partial}{\partial r}\left(r\frac{\partial v}{\partial r}\right) + \frac{\partial^2 v}{\partial z^2}\right] \tag{68}$$

Boundary Conditions

At r = *0:* $u = 0$, (69)

At $z = 0$: $u=0$, $v = 0$, (70)

At $r=0$ and $z=\delta$: $u=0$, $v=\dot{\delta}-V_{evap}$ (71)

At the neighborhood of stagnation point, the vapor velocity field is strongly dominated by mass addition effects through the evaporating interface. This infers that the vapor velocity component v is independent of r. i.e. $v \neq v(r)$, in other words, $v = v(z,t)$.

To satisfy the boundary conditions (70) and (71), the velocity component $v(z,t)$ is expressed as a power function by

$$v(z,t)=\sum_{i=1}^{\infty} c_i z^i \psi(t) \tag{72}$$

where c_i is an arbitrary constant, and $\psi(t)$ is an unknown function. If c_1 =1 and i = 1 are taken into account, then equation(72) becomes

$$v(z,t)=z\cdot\psi(t) \quad \text{or} \quad \frac{\partial v}{\partial z}=\psi(t) \tag{73}$$

This assumption is called the von Karman assumption [30] and is applied as a boundary condition to solve inertial-dominant Navier-Stokes equations.

Substituting(73) into the continuity equation(66), yields

$$u=-\frac{r}{2}\psi(t) \tag{74}$$

Calculate the derivatives of u in terms of r, z, t, respectively, yields

$$\frac{\partial u}{\partial t}=-\frac{r}{2}\dot{\psi}, \quad \frac{\partial u}{\partial r}=-\frac{1}{2}\psi, \quad \frac{\partial u}{\partial z}=0 \tag{75}$$

where $\dot{\psi} = \frac{\partial \psi(t)}{\partial t}$

Substituted Equations (73),(74) and (75) into the into Equation(67) and rearranging, yields

$$\frac{\partial p_v}{\partial r} = \rho_v \left(\frac{r}{2}\dot{\psi} - \frac{r}{4}\psi^2 \right) \tag{76}$$

The vapor pressure from Equation(76) at the interface, where $y=\delta$, must match the vapor side pressure evaluated from Equation (65). Equating the two equations results in

$$\rho_v \left(\frac{1}{2}\dot{\psi} - \frac{1}{4}\psi^2 \right) = -\frac{2\rho_L}{(R+\delta)} \left(\frac{g+\ddot{\delta}}{1+\cos\theta} + \frac{2(u_\infty + \dot{\delta})^2}{R+\delta} \right) \tag{77}$$

From equation(73), $\frac{v(z,t)}{z} = \psi(t)$, one obtains

$$\dot{\psi}(t) = v(z,t)\frac{\partial \left[z^{-1} \right]}{\partial t} + \frac{1}{z}\frac{\partial v(z,t)}{\partial t}$$

$$= -\frac{v(z,t)}{z^2}\left(\frac{\partial z}{\partial t} \right) + \frac{1}{z}\frac{\partial v(z,t)}{\partial t} \tag{78}$$

and

$$\psi^2(t) = \left[\frac{v(z,t)}{z} \right]^2 \tag{79}$$

Substituting boundary condition (71) into Equation (78) yields,

$$\psi(t)\Big|_{y=\delta} = -\frac{\dot{\delta}-V_{evap}}{\delta^2}\dot{\delta} + \frac{1}{\delta}\frac{\partial}{\partial t}\left[\dot{\delta}-V_{evap}\right] = -\frac{\dot{\delta}-V_{evap}}{\delta^2}\dot{\delta} + \frac{1}{\delta}\left[\ddot{\delta}-\dot{V}_{evap}\right]$$

$$= -\frac{\dot{\delta}^2}{\delta^2} + \frac{V_{evap}\dot{\delta}}{\delta^2} + \frac{\ddot{\delta}}{\delta} - \frac{\dot{V}_{evap}}{\delta} \tag{80}$$

Substituting boundary condition (71) into Equation (79), yields

$$\psi^2(t)\Big|_{y=\delta} = \left[\frac{\dot{\delta}-V_{evap}}{\delta}\right]^2 = \frac{\dot{\delta}^2}{\delta^2} - \frac{2V_{evap}\dot{\delta}}{\delta^2} + \frac{V_{evap}^2}{\delta^2} \tag{81}$$

Substituting equations (80)and (81) into equation(77) yields

$$\rho_v\left(\frac{3\dot{\delta}^2}{4\delta^2} + \frac{V_{evap}-4\dot{\delta}}{4\delta^2}V_{evap} - \frac{\ddot{\delta}-\dot{V}_{evap}}{2\delta}\right) = \frac{2\rho_L}{(R+\delta)}\left(\frac{g+\ddot{\delta}}{1+\cos\theta} + \frac{2(u_\infty+\dot{\delta})^2}{R+\delta}\right) \tag{82}$$

Equation (82) needs information on V_{evap} (evaporation velocity at the vapor-liquid interface) for further derivation. In the following Section 4.2 we are going to determine this evaporation velocity based on the heat balance analysis in the vapor-liquid interface. The resultant expression for V_{evap} is expected to be a function of δ and the derivatives of δ.

Equation (82) requires information on free stream velocity, u_∞, as well. In Section 4.5 we derive this free stream velocity as function of subcooling.

4.2 Heat Balance and Vaporization Velocity

A solution for Equation(82) is required in order to finalize the vapor-film-thickness. This section starts from the heat balance analysis in the vapor film and on the both sides of the vapor-liquid interface, and arrives an expression for the vaporization velocity as function of the vapor film thickness.

4.2.1 Heat Balance

The heat transfer model is shown in Figure 27. All heat transferred from the outside of calandria tube is balanced by two heat transfer components, namely radiation heat transfer to the bulk liquid and the conduction heat transfer across the vapor film. The conduction heat transfer through vapor film heats the vapor film region. This heat transfer is indicated as q''_{sh} in Figure 27. At the liquid-vapor interface part of the conduction heat evaporates liquid to maintain the vapor film; while the remainder of the conduction heat is transferred to the bulk liquid by convection.

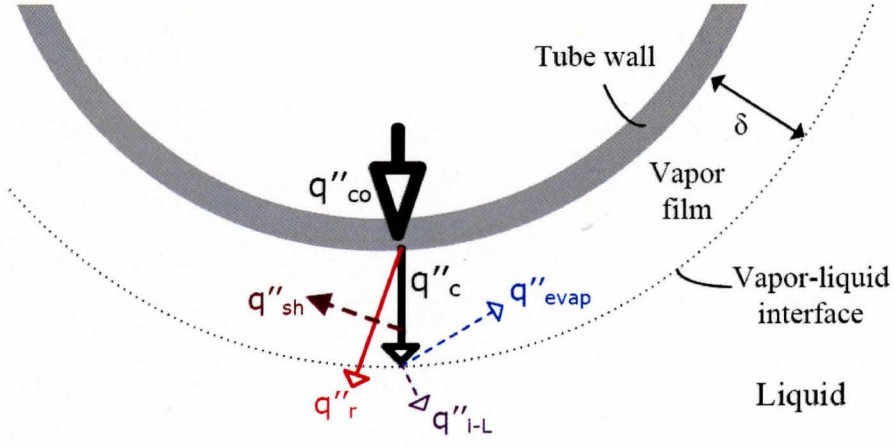

Figure 27: Model of film-boiling heat transfer mechanism

The definitions of symbols in Figure 27 are listed as below:

q''_{co} = total heat flux emitted from CT outer surface (same as q''_w in figures in Chapter Five)

q''_r = radiation heat flux from CT wall to bulk liquid

q''_{sh} = heat flux to superheat steam vapor

q''_c = conduction heat flux from CT wall across vapor film

q''_{evap} = heat flux used to evaporate saturated liquid

q''_{i-L} = heat flux transferred from the interface to thin liquid layer

4.2.1.1 heat balance across the vapor film

Conduction heat flux is expressed as

$$q''_c = k_v \frac{T_w - T_{sat}}{\delta} \tag{83}$$

The saturated liquid absorbs heat at the vapor-liquid interface and evaporates to become vapor with saturated temperature. The vaporization heat flux which is due to latent heat can be expressed as

$$q''_{evap} = \rho_v V_{evap} h_{fg} \tag{84}$$

where V_{evap} = evaporation velocity

h_{fg} = latent heat of vaporization

Part of the thermal energy conducted across the vapor film is used to evaporate liquid to vapor and the remaining thermal energy conducted across the vapor film is dissipated from the interface to the bulk liquid.

$$q''_{co} = q''_{c} + q''_{r} \tag{85}$$

$$q''_{c} = q''_{evap} + q''_{i-L} + q''_{sh} \tag{86}$$

Since the water is an excellent heat absorber, an assumption is therefore made here that the heat transferred from the interface to a very thin subcooled liquid layer. This assumption was also used by Bradfield in his research of two phase interface instability [12].

When calculating the CT (total) heat flux, q''_{co}, and (total) heat transfer coefficient, the radiation heat effects should be taken into account even though it contributes only a fairy small part in most quenching cases, which will be observed in Chapter Five.

The vapor inside the vapor film is superheated when heat is conducted through the vapor film. This results in the vapor with higher temperature near the CT wall surface and saturation temperature at the vapor-liquid interface. The superheating heat flux can be given by the specific heat of vapor multiplied by the vapor superheat temperature and multiplied by the vapor density. The average vapor temperature can be taken as $(T_w+T_{sat})/2$. The reason of using it as the representing vapor temperature has already been discussed in Section 3.5.2. The heat flux used for vapor superheating is

$$q''_{sh} = \rho_v V_{evap}\, c_{p,v}(T_v - T_{sat}) = \rho_v V_{evap}\, c_{p,v}\left[(T_w + T_{sat})/2 - T_{sat}\right]$$
$$= 0.5\rho_v V_{evap}\, c_{p,v}(T_w - T_{sat}) \quad (87)$$

where the specific heat of vapor, $c_{p,v}$ is evaluated at the average vapor temperature.

This expression is based on the definition of conduction heat flux with the assumption that the vapor temperature linearly drops across the vapor film. It is analogous to heat conduction in a solid body.

4.2.1.2 vaporization velocity and its derivatives

Substituting Equations (54),(83) and (84) into Equation (86), we have

$$q''_c = \rho_v V_{evap} h_{fg} + 0.5\rho_v V_{evap}\, c_{p,v}(T_w - T_{sat}) + 2k_L\sqrt{\frac{u_\infty + \dot{\delta}}{\pi R\alpha_L}}\cdot\cos\frac{\theta}{2}\cdot\Delta T_{sub} \quad (88)$$

Combining $\rho_v V_{evap}$ in the right hand side of Equation (88), yields

$$q''_c = \rho_v V_{evap} h'_{fg} + 2k_L\sqrt{\frac{u_\infty + \dot{\delta}}{\pi R\alpha_L}}\cdot\cos\frac{\theta}{2}\cdot\Delta T_{sub} \quad (89)$$

where h'_{fg} = modified latent heat of vaporization ($=h_{fg}+0.5c_{p,v}(T_w - T_{sat})$)

Substituting Equation (83) in to (89)

$$k_v\frac{T_w - T_{sat}}{\delta} = h'_{fg}\,\rho_v V_{evap} + 2k_L\sqrt{\frac{u_\infty + \dot{\delta}}{\pi R\alpha_L}}\cdot\cos\frac{\theta}{2}\cdot\Delta T_{sub} \quad (90)$$

where k_v, k_L = thermal conductivities of vapor and fluid, respectively

Rearranging yields

$$V_{evap} = \frac{k_v(T_w - T_{sat})}{h'_{fg}\,\rho_v \delta} - \frac{2k_L \cdot \cos\frac{\theta}{2} \cdot \Delta T_{sub}}{h_{fg}\rho_v\sqrt{\pi R \alpha_L}}\sqrt{u_\infty + \dot{\delta}} \tag{91}$$

Consequently obtains

$$\dot{V}_{evap} = \frac{\partial V_{evap}}{\partial t} = \frac{\partial V_{evap}}{\partial \delta}\cdot\frac{\partial \delta}{\partial t} = -\frac{k_v(T_w - T_{sat})}{h'_{fg}\,\rho_v \delta^2}\dot{\delta} - \frac{k_L \cdot \cos\frac{\theta}{2} \cdot \Delta T_{sub}}{h'_{fg}\,\rho_v\sqrt{\pi R \alpha_L}\sqrt{u_\infty + \dot{\delta}}}\ddot{\delta} \tag{92}$$

Having obtained the expression for the evaporation velocity and its derivative, one can utilize the information to formulate the vapor film thickness equation.

4.2.1.3 incident heat flux from PT to CT and emitted heat flux from CT wall

As described earlier by Equation (43) in Chapter 3, the radiation heat flux is simply as

$$q''_r = \varepsilon\ \sigma_{s-b}\left(T_w^4 - T_b^4\right) \tag{93}$$

where σ_{s-b} = the Stefan-Boltzmann constant ($= 5.67\times10^{-11}\ kW/m^2/K^4$)

ε = the surface emissivity of unoxidized calandria tube ($= 0.19$)

The heat balance equation describing the entire system can be written as

$$q''_{co} = q''_r + q''_{sh} + q''_c \tag{94}$$

where q''_{co} is mentioned earlier the total heat flux emitted from CT outer surface.

Substituting equation(87) and (93) into (94), the expression for the total heat emitted from outer surface of CT wall can be written as

$$q''_{co} = q''_{c} + \varepsilon\sigma_{s-b}\left(T_w^4 - T_b^4\right) + 0.5\rho_v V_{evap} C_{p,v}(T_w - T_{sat}) \tag{95}$$

Special attention should be paid when using Equation(95). The q''_{co} is the heat flux emitted from outer calandria tube, rather than that emitted from outer pressure tube to inner calandria tube. The latter is usually termed as "incident heat flux from pressure tube to calandria tube", $q''_{in,pt}$. It has a close relationship with the pressure tube heat-up rate, which can be easily measured in experiments. Reader can refer to Appendix 7.0 for more information about the converting from pressure tube heat-up rate to pressure tube incident heat flux. In order to relate q''_{co} and $q''_{in,pt}$ together, the transient PT/CT contact conductance may need to know. In this thesis, $q''_{co} = q''_{in,pt}$ is assumed as a premise.

4.3 Solution of Governing Equations

We have derived an intermediate vapor film thickness expression as Equation (82). Substituting equations (91) and (92) into Equation (82) and rearranging in terms of $\ddot{\delta}$ and $\dot{\delta}$ yields a vapor-film-thickness equation with regard to the calandria tube wall temperature, T_w, the location angle, θ, and the fluid subcooling, ΔT_{sub}, etc. as:

$$\langle 1\rangle + \langle 2\rangle + \langle 3\rangle + \langle 4\rangle + \langle 5\rangle + \langle 6\rangle + \langle 7\rangle + \langle 8\rangle = 0 \tag{96}$$

where

$$\langle 1\rangle = \ddot{\delta}\left[1+\frac{\chi(R+\delta)}{\delta}+\frac{1}{2}\chi C_1\frac{R+\delta}{\delta\sqrt{u_\infty+\dot{\delta}}}\right],$$

$$\langle 2\rangle = \left(\frac{\dot{\delta}}{\delta}\right)^2\left[-\frac{3}{4}\chi(R+\delta)\right],$$

$$\langle 3\rangle = \frac{\dot{\delta}}{\delta^2}\left[-2C_1(R+\delta)\sqrt{u_\infty+\dot{\delta}}\right],$$

$$\langle 4\rangle = \frac{\dot{\delta}}{\delta^3}\left[\frac{3}{2}\chi C_2(R+\delta)\right],$$

$$\langle 5\rangle = \frac{1}{\delta^2}\left[-\chi C_1^2(R+\delta)(u_\infty+\dot{\delta})\right],$$

$$\langle 6\rangle = \frac{1}{\delta^3}\left[\chi C_1C_2(R+\delta)(u_\infty+\dot{\delta})\right],$$

$$\langle 7\rangle = \frac{1}{\delta^4}\left[-\frac{1}{4}\chi C_2^2(R+\delta)\right],$$

$$\langle 8\rangle = g(R+\delta)+4(u_\infty+\dot{\delta})^2$$

In the terms above, χ, C_1 and C_2 are defined as, respectively,

$$\chi = \frac{\rho_v}{\rho_L},$$

$$C_1 = \frac{k_L\cdot\cos\frac{\theta}{2}\cdot\Delta T_{sub}}{h'_{fg}\,\rho_v\sqrt{\pi R\alpha_L}},$$

$$C_2 = \frac{k_v(T_w-T_{sat})}{h'_{fg}\,\rho_v}$$

4.4 Steady State Equation

By assigning $\ddot{\delta} = \dot{\delta} = 0$, the steady state equation for vapor film thickness can be achieved from Equation(96) as,

$$\frac{1}{\delta^2}\left[-\chi C_1^2 U_\infty\right]+\frac{1}{\delta^3}\left[\chi C_1 C_2 U_\infty\right]+\frac{1}{\delta^4}\left[-\frac{1}{4}\chi C_2^2\right]+g+\frac{4U_\infty{}^2}{R+\delta}=0 \tag{97}$$

To evaluate Equation(97), we need to know the liquid free stream velocity, u_∞.

4.5 Free Stream Velocity

The liquid free stream velocity, u_∞, is dominated by two components, namely the liquid phase buoyancy-driven flow and the relative bubble rise velocity of vapor in liquid. Natural convection happens when the driving force is the buoyancy force due to the density gradients. The density gradients originate from temperature gradients. The buoyancy-driven flow arises from the temperature-dependent density gradient between the liquid surrounding the cylinder and the bulk liquid and it is a function of liquid subcooling temperature. The bubble rise velocity is dependent upon the vapor bubble size. The effective free steam velocity is given by:

$u_\infty = u_{sub}(\Delta T_{sub}) + u_{br}(R_b)$

4.5.1 Bubble Rise Velocity

The bubble rises from the bottom of the calandria tube to the top of the calandria tube. In this section, we are going to investigate the bubble rise velocity by two methods. One is

a direct substitution to an empirical correlation and the other is theoretical derivation from a model. The results from the two methods agree with each other.

4.5.1.1 Wallis empirical correlation

The effect of bubble rise is an effective increase in the relative velocity at the vapor-liquid interface. The bubble-rise velocity for a large bubble as given by Wallis [31] is a simple correlation of the form

$$u_{br} = 1.00\sqrt{g\,R_b} \tag{98}$$

where R_b is the equivalent spherical bubble radius. Since the vapor surrounds the calandria tube, the characteristic bubble radius is equal to the calandria tube radius we have

$$u_{br} = 0.8 \text{ m/s.} \tag{99}$$

4.5.1.2 derivation of bubble rise velocity

A vertical plate is employed here to start with this derivation. A horizontal cylinder will be given later. Similarly to the analysis done in Reference [32], we have

$$\frac{1}{2}\rho_L \frac{d(u_{br}^{\,2})}{dx} = (\rho_v - \rho_L)g \tag{100}$$

Integrating yields

$$u_{br}^{\,2} = \int 2\frac{(\rho_v - \rho_L)g}{\rho_L}dx + c \tag{101}$$

We can now Apply Equation (101) to the geometry of a horizontal tube— a large cylinder — submerged in liquid. Since the calandria tube is relatively large, we may use the above result to estimate the rise velocity of the bubbles.

The outer surface of a calandria tube is a curve surface and the gravitational acceleration g along the surface direction x should be replace by $gsin\theta$, where θ is the angle of inclination (the angle departing from the vertical symmetry line of cross-section of CT). And dx changes to $d(R\theta)$, where R is the CT radius. Equation (101) evolves to

$$u_{br}{}^2 = \int 2\frac{(\rho_v - \rho_L)\, g \sin\theta}{\rho_L} d(R\theta) + c \tag{102}$$

It follows that

$$u_{br}{}^2 = 2\frac{(\rho_v - \rho_L)\, Rg}{\rho_L} \int \sin\theta d\theta + c \tag{103}$$

Simplifying, yields

$$u_{br}{}^2 = 2\frac{(\rho_L - \rho_v)\, Rg}{\rho_L} \cos\theta + c \tag{104}$$

If $\rho_L = \rho_v$, then $u_{br} = 0$. therefore the constant $c = 0$. Calculating the average value of $u_{br}{}^2$, in the range of θ from 0 to ξ, yields,

$$\overline{u}_{br}{}^2 = \frac{2\frac{(\rho_L - \rho_v)Rg}{\rho_L} \int_0^{\xi} \cos\theta d\theta}{\xi} \tag{105}$$

The value of ξ is decided by the separation point of the laminar flow developing into turbulent on the outside of calandria tube. Let's call it separation angle. It has been usually considered between $1/2\ \pi$ and $3/4\ \pi$. Figure 2 shows separation angle ξ.

Assigning the density values and radius value of CT into equation(105), yields the value of velocity at 0°C sub-cooling temperature as

U_{br}=0.78 $(\xi = 5\pi / 8)$ (106)

Comparing Equation(99) and Equation (106) we can conclude that the bubble rise velocities obtained from the two methods match with each other.

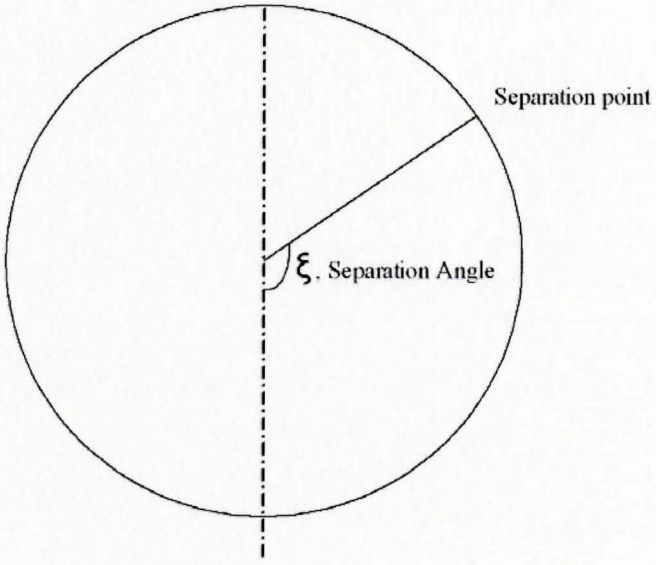

Figure 28: Separation angle

4.5.2 The Dependence of Free Steam Velocity upon Subcooling

Here we focus on the sub-cooling effect on velocity of the fluid in a fully developed liquid flow next to the vapor film. Figure 27 shows a vertical surface with constant temperature 100°C (at atmospheric pressure) in a quiescent fluid pool with subcooling temperature T_{sub} ranging from 0°C to 50°C.

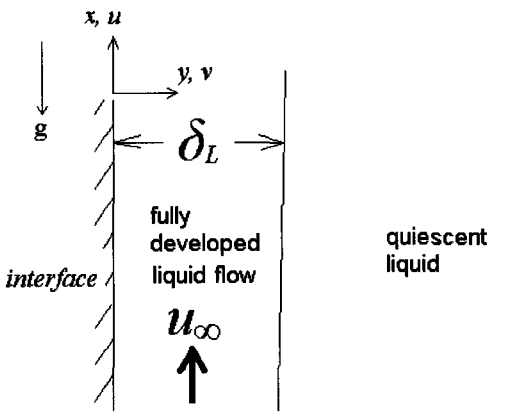

Figure 29: Fully developed liquid flow

The natural convection flow is induced by buoyancy forces, which is initially induced by temperature differences. The heated fluid rises upward while cold fluid is supplied from the surrounding quiescent region. Therefore the fluid motion is upward. Assume two-dimensional, incompressible and fully developed steady liquid flow with constant thermalhydraulic properties, and assume the body force is only the gravity force acting vertically downward in negative x direction.

The general equations governing the fluid are, respectively,

Mass conservation equation

$$\frac{\partial u}{\partial x}+\frac{\partial v}{\partial y}=0 \tag{107}$$

the x-momentum equation

$$\rho_L\left(u\frac{\partial u}{\partial x}+v\frac{\partial u}{\partial y}\right)=-\frac{\partial P}{\partial x}+\mu_L\left(\frac{\partial^2 u}{\partial x^2}+\frac{\partial^2 u}{\partial y^2}\right)+\mathrm{B_x} \tag{108}$$

and the y-momentum

$$\rho_L\left(u\frac{\partial v}{\partial x}+v\frac{\partial v}{\partial y}\right)=-\frac{\partial P}{\partial y}+\mu_L\left(\frac{\partial^2 v}{\partial x^2}+\frac{\partial^2 v}{\partial y^2}\right) \tag{109}$$

Figure 29 shows the fully developed steady liquid velocity. The heat is conducted from the liquid-vapor interface to the neighboring sub-cooled fluid. Assuming that the flow is close to fully developed flow in the x direction means that

$\partial u/\partial x = 0$

The boundary condition is that the shear stress at the free stream is zero,

$$\left.\frac{\partial u}{\partial y}\right|_{y=\delta_L}=0 \tag{110}$$

where δ_L is the fully developed liquid layer thickness.

Knowing $B_x=-\rho_L g$ and, and applying the concept from Prandtl's boundary layer theory [33]($u >> v$, $\partial u/\partial y >> \partial u/\partial x$ and $\partial v/\partial y >> \partial v/\partial x$) to derive an analogous developed flow layer in the liquid such that velocity component u is constant in the x direction, equations (108) and(109) become, respectively

$$\cancel{\frac{\partial u}{\partial x}}^{=0}+\frac{\partial v}{\partial y}=0 \text{ result in v = const} \tag{111}$$

$$0=(\rho_\infty-\rho_{L,sat})g+\mu_L\frac{\partial^2 u}{\partial y^2} \tag{112}$$

$$\frac{\partial P}{\partial y}=0 \tag{113}$$

Now introducing volumetric thermal expansion coefficient β and applying Boussinesq approximation, yields.

$$\beta = -\frac{1}{\rho_L}\left(\frac{\partial \rho_L}{\partial T}\right)_P \approx -\frac{1}{\rho_L}\frac{\Delta \rho_L}{\Delta T} = -\frac{1}{\rho_L}\frac{\rho_\infty - \rho_{L,sat}}{T_\infty - T_{sat}}$$

It follows that $(\rho_\infty - \rho_{L,sat}) \approx \rho_L \beta (T_{sat} - T_\infty)$. Substituting it into equation(112), yields

$$\frac{d^2u}{dy^2} \approx -\frac{\rho_L \beta g}{\mu_L}(T_{sat} - T_\infty)$$

Substituting $\Delta T_{sub} = T_{sat} - T_\infty$, and integrating,

$$\frac{du}{dy} = -\frac{\rho_L \beta g}{\mu_L}\Delta T_{sub} y + c_1 \tag{114}$$

Integrating again, yields

$$u = -\frac{1}{2}\frac{\rho_L \beta g}{\mu_L}\Delta T_{sub} y^2 + c_1 y + c_0 \tag{115}$$

The constant c_1 can be evaluated from equation (114) by applying the second boundary condition that the shear stress at the free stream is zero, it follows that

$$c_1 = \frac{\beta \rho_L g}{\mu_L}\Delta T_{sub}\delta_L \tag{116}$$

Again, δ_L is the fully developed liquid layer thickness.

Substituting equation (116) into equation(115), obtains

$$u = \frac{1}{2}\frac{\rho_L \beta g}{\mu_L}(2\delta_L y - y^2)\Delta T_{sub} + c_0 \tag{117}$$

The interest is to find the maximum value of liquid free stream velocity, so let $y=\delta_L$, given that the maximum of u occurs at $y = \delta_L$.

Let

$$b = \frac{1}{2}\frac{\rho_L \beta g}{\mu_L}(2\delta_L y - y^2) = \frac{1}{2}\frac{\rho_L \beta g}{\mu_L}\delta_L{}^2 \tag{118}$$

then equation(117) becomes

$$u = b\Delta T_{sub} + c_0 \tag{119}$$

It shows that u is a linear function of ΔT_{sub}.

The constant b and c_0 need to be defined. First, c_0 should correspond to zero subcooling. From the foregoing analysis one concludes that at zero sub-cooling temperature, the fluid close to the liquid-vapor interface is not stagnant; instead, the fluid either moves to replace the space where vapor left or evaporates into the vapor film. And the quantitative value of this velocity, given by Equation(106), was 0.78 m/s. In another word, it can be simply understood as $c_0 = u_{br}$ =0.78 m/s.

The value of constant b can be evaluated approximately through the *Blasius's solution*[34]. This solution suggested the liquid boundary layer thickness. If δ_L is known

then b is readily calculated. The solution for liquid boundary layer thickness δ_L in equation(118) was given as

$$\delta_L = \frac{5.0x}{\sqrt{\mathrm{Re}_\xi}} \tag{120}$$

where the local Reynolds number, Re_ξ, is evaluated at the position on the circumference from the bottom of calandria tube at separation angle ξ.

$$\mathrm{Re}_\xi = \frac{\rho_L U_{\Delta Tsub=0} L_\xi}{\mu_L} = \frac{U_{\Delta Tsub=0} L_\xi}{\gamma_L} \tag{121}$$

where L_ξ equals ξR_{CT}; γ_L is the kinematic viscosity of liquid.

Table 3 shows D_2O fluid properties with respect to temperatures. The properties at 20 K, subcooling are chosen for calculations of parameter *'b'*.

Table 3: Liquid properties with regard to subcooling

Subcooling Temperature [K]	Kinematic .Viscosity[35] γ =μ /ρ [m^2/s]	Thermal expansion[35],β [K^{-1}]	Liquid Density[36], ρ [kg/m^3]
0	$2.92x10^{-7}$	$750.1x10^{-6}$	$1.076x10^3$
20	$3.62x10^{-7}$	$641.0x10^{-6}$	$1.089x10^3$
30	$4.10\ x10^{-7}$	$585.0x10^{-6}$	$1.096x10^3$
50	$5.52\ x10^{-7}$	$458.8x10^{-6}$	$1.108x10^3$

Table 4: Values of b in terms of separation angle, ξ

Separation angle ξ [rad]	$U_{\Delta T_{sub}=0}$ [m/s]	Re_ξ	Liq B.L. Thickness δ_L [mm]	b [-]
(3/4) π	0.62	$2.66x10^5$	1.6	0.0233

"b" is calculated in Table 4. $b = 0.23$. Thus $u_{sub}(\Delta Tsub)=0.23\Delta Tsub$.

In conclusion, the free stream velocity can be related to function of sub-cooling temperature and take the form

$$u_{\infty} = u_{sub} + u_{br} = 0.0233\Delta T_{sub} + 0.78 \ \ [m/s] \tag{122}$$

Chapter Five

5.0 Steady State Analysis

Steady-State vapor film thickness equation (Equation (97)) coupled with information on V_{evap} and u provides the vapor film thickness as function of thermalhydraulic parameters, such as Subcooling, ΔT_{sub}, and wall temperature of the calandria tube, T_w. In this Chapter we first analyze and discuss the dependence of vapor film thickness upon these thermalhydraulic parameters, as well as the dependence of heat fluxes upon these thermalhydraulic parameters. In Section 5.1.2 a quenching conditions will be proposed and the substitution of the quenching conditions results in separation of quench or no-quench situations. The comparisons between model outputs and available experimental data are given in Section 5.3.

5.1 Heat Flux, Wall Temperature and Vapor Film Thickness

In this section, relationships between the variables of interest and specific thermalhydraulic parameters will be examined. The variables of interest include heat flux, wall temperature, and vapor film thickness. These relationships are derived from Equation (97)

5.1.1 Calandria Tube Wall Heat Flux vs Subcooling

Figure 30 shows the relationship between calandria tube wall heat flux and the subcooling at the steady state of vapor film thickness. It can be observed that at a particular thickness of vapor film, the heat flux increases as the subcooling increases. At the same subcooling, the heat flux is higher at a thicker steady state vapor film thickness.

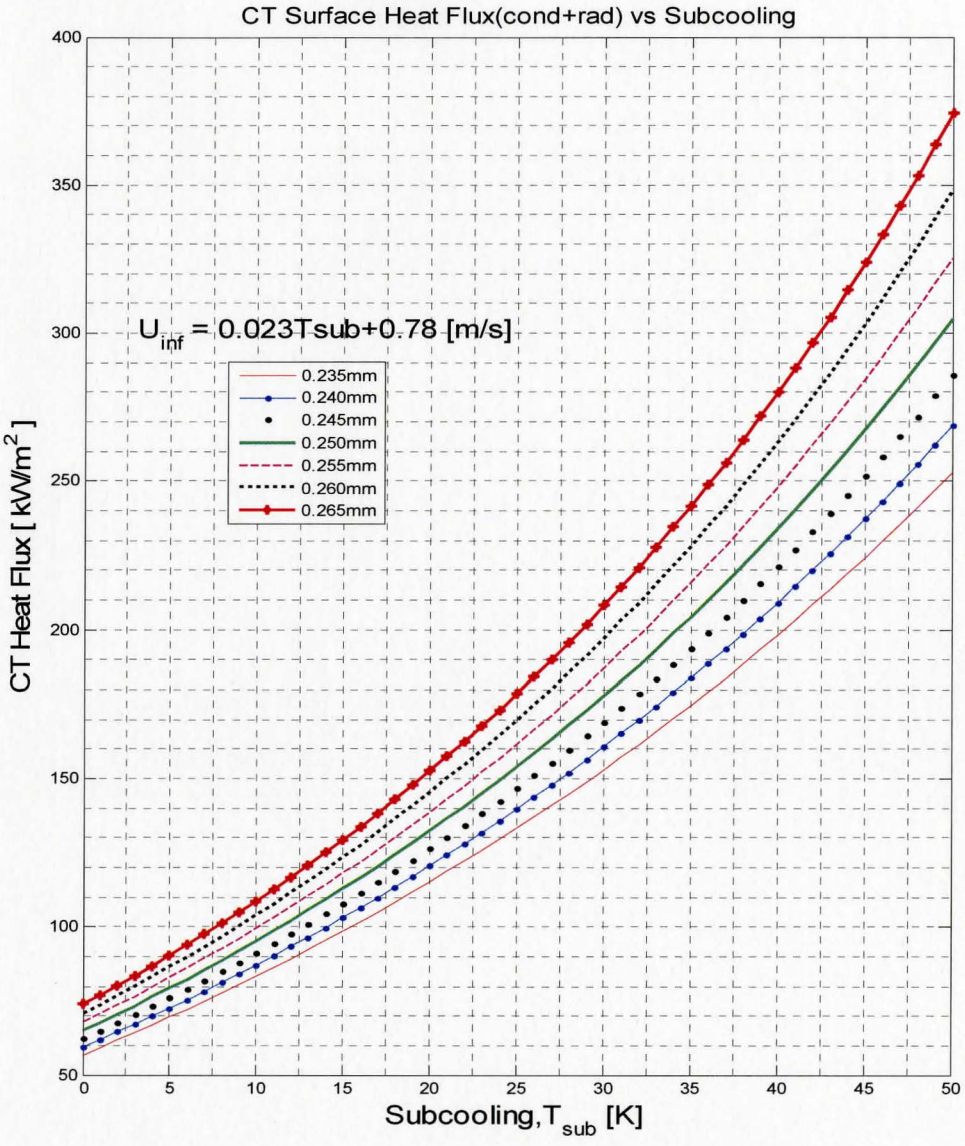

Figure 30: Calandria tube wall heat flux vs subcooling

5.1.2 Calandria Tube Wall Temperature vs Subcooling

The Calandria tube wall temperature is linearly proportional to the subcooling as can be seen from Figure 31. At the same subcooling, the thicker the steady state vapor film thickness, the higher the wall temperature is.

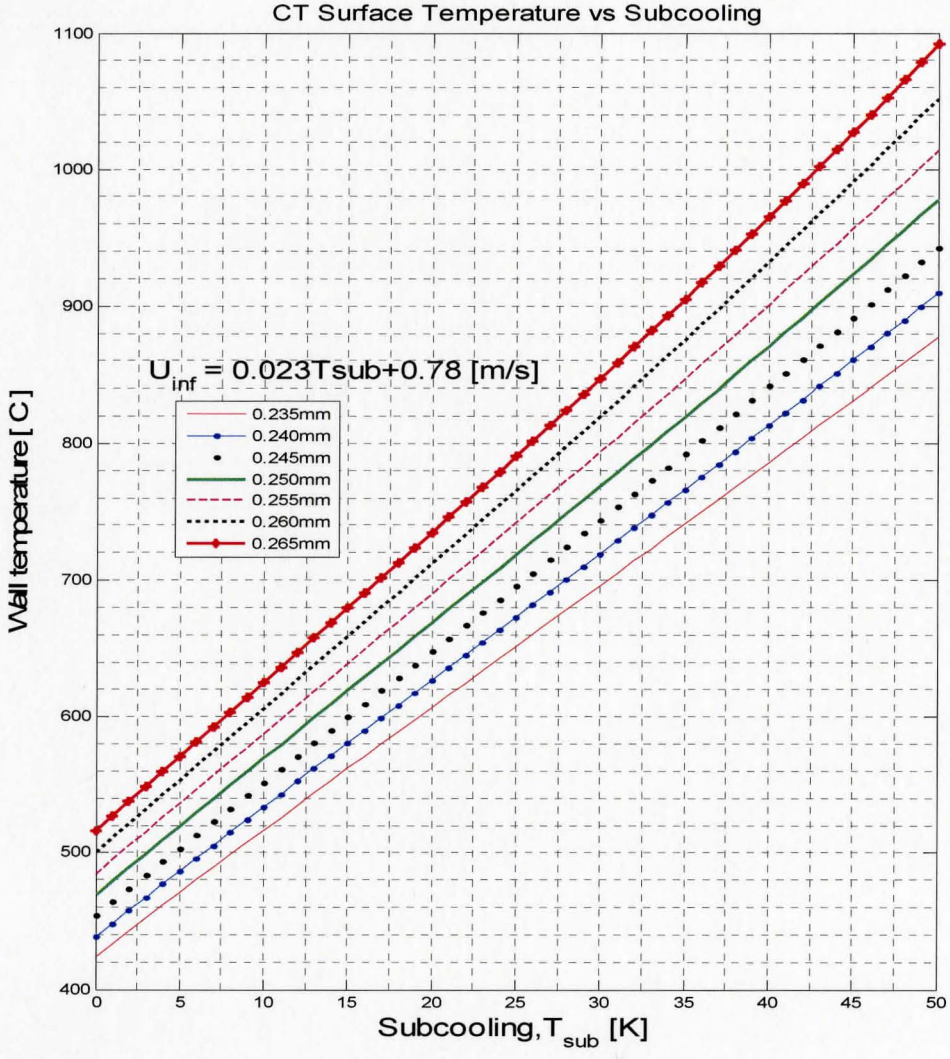

Figure 31: Calandria tube wall temperature vs subcooling

A MatLab code is attached in Appendix B for iteratively calculating the vapor film temperature and the CT wall temperature.

5.1.3 Vapor Film Thickness vs Wall Superheat

It can be observed from Figure 32 that the vapor film thickness increases as the wall superheat increases at a fixed subcooling. At the same wall superheat, the vapor film thickness increases as the subcooling decreases.

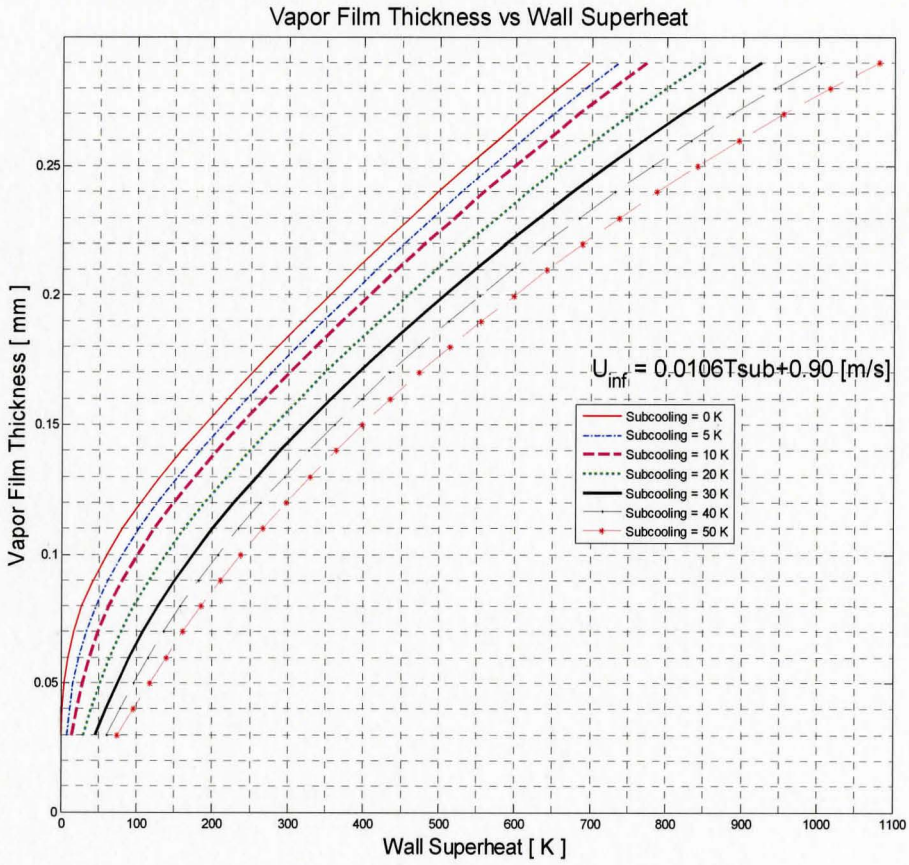

Figure 32: Vapor film thickness vs wall superheat

5.1.4 Calandria Tube Wall Heat Flux vs Calandria Tube Wall Temperature

At a constant wall temperature, the Calandria tube wall heat flux decreases with the increase in the vapor film thickness. As shown in Figure 33. The increase in vapor film thickness will create a higher heat resistance of the vapor film outside of the calandria wall. Vapor heat resistance dominates the total heat resistance for the heat emitted out of the calandria tube, thus it results in a lower calandria tube wall heat flux.

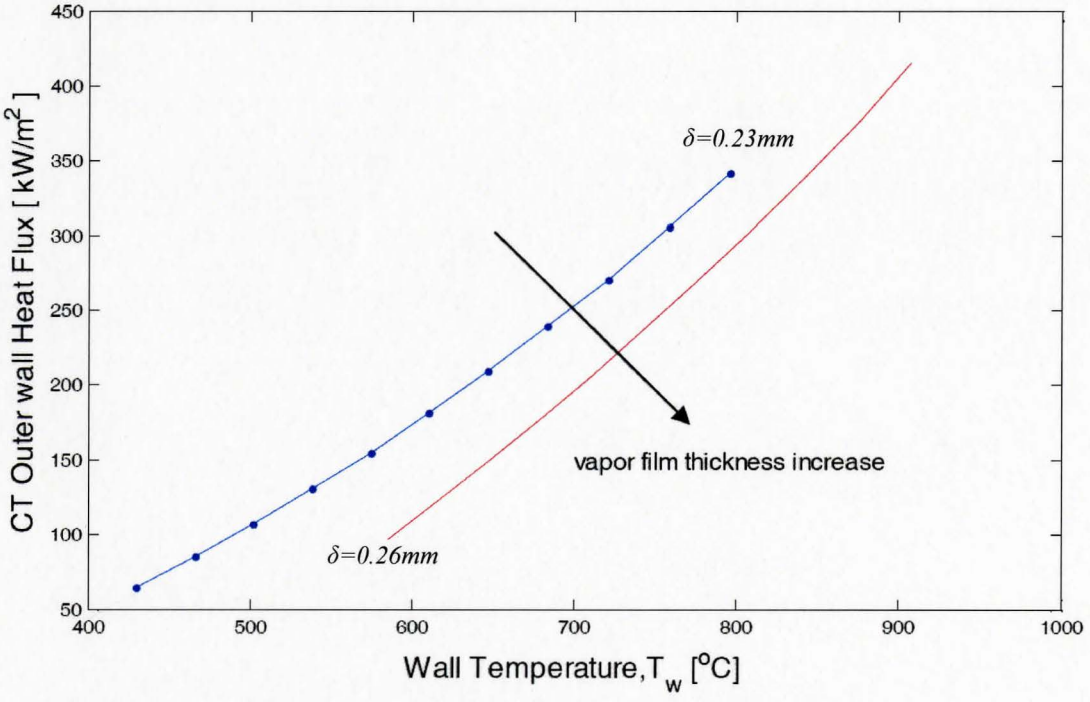

Figure 33: Influence of vapor film thickness increase on CT wall temperature

5.1.5 Vapor Film Thickness vs Subcooling Temperature

In Figure 34, it can be observed that the vapor film thickness decreases with the increase in the subcooling, as might be expected. The tendency of vapor film thickness decrease is exhibited by a decrease in the calandria tube surface temperature.

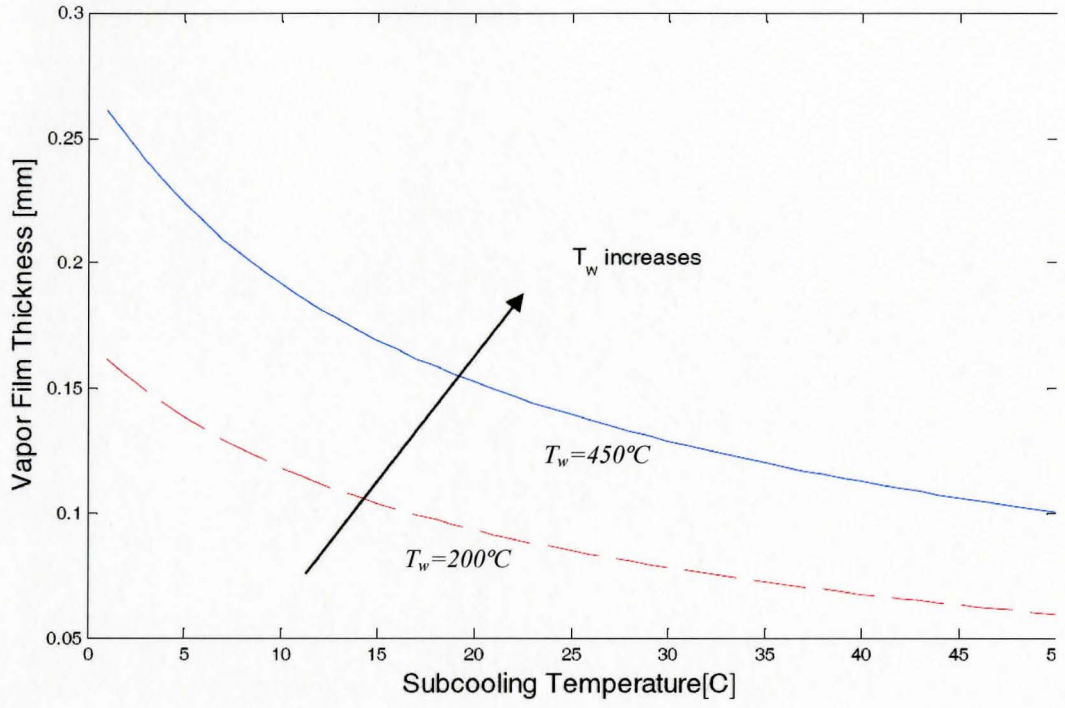

Figure 34: Vapor film thickness (U_∞=0.0233ΔT_{sub}+0.78 m/s)

5.2 Quench or No-Quench

5.2.1 Quench Conditions

It is of interest to possibly find the lower bound of vapor film thickness as it is relevant to the critical thickness of the vapor film prior to its quench. It can be approached by assigning equation (91) with $V_{evap}=0$. This condition implies that the vapor film has to continuously decrease due to no vapor generation until liquid rewets the wall surface. A relationship between calandria wall temperature and the subcooling then can be established,

$$T_w = T_{sat} + \frac{2k_L}{k_v\sqrt{\pi R\alpha_L}}\sqrt{u_\infty}\ \delta\cdot\Delta T_{sub} \tag{123}$$

Equation (97) and (123) now are ready to computer the lower bound vapor film thickness in terms of a number of thermalhydraulic parameters, some of which will be varied to investigate their impacts on the vapor film thickness.

5.2.2 Curves Demarcate Quench and No-Quench

Figure 35 presents a curve that demarcates a boundary between quench and no-quench of the CT outside surface based upon the relationship between vapor film thickness and the heat conducted in the vapor film. A quench will initiate at heat fluxes below the line, while heat fluxes above the line are likely to maintain stable film boiling.

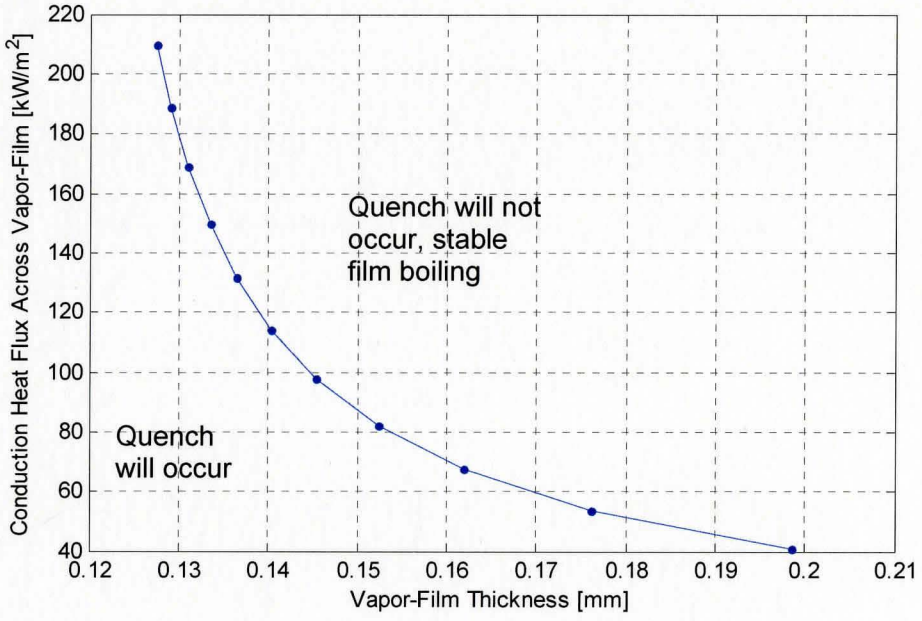

Figure 35: Conduction heat flux vs vapor film thickness

In Figure 36 any CT wall heat fluxes below the line will lead to quenching of the CT wall surface due to an inability to maintain a stable vapor film. Conversely, heat fluxes above the line are likely to result in formation of a stable film and probable dryout of the CT

surface. As indicated in Figure 36 higher heat fluxes on the CT wall are required for film boiling when the bulk liquid subcooling temperature increases.

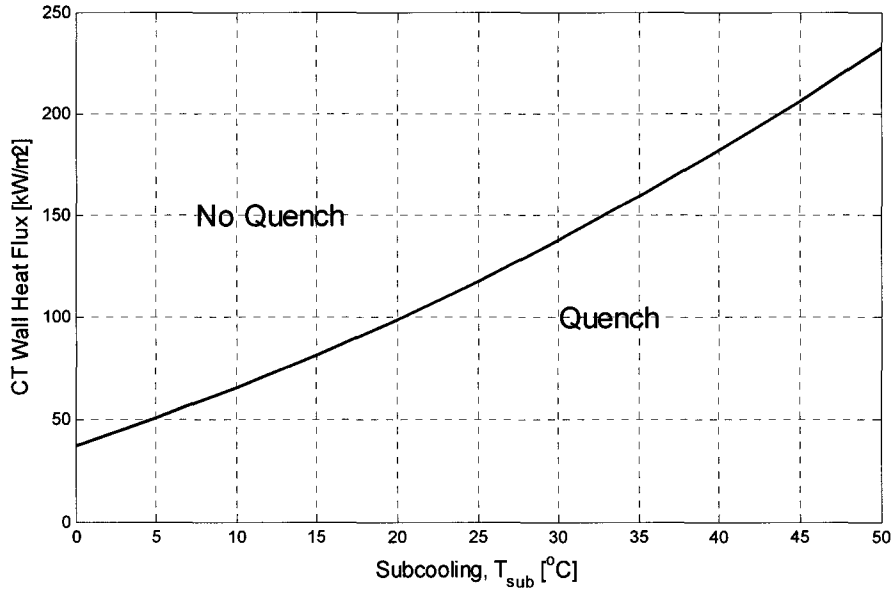

Figure 36: CT outside surface heat flux at quenching vs subcooling

5.2.3 Heat Flux Contribution

Figure 37 shows the fractional contribution of the radiation and conduction heat transfer components of the total heat out of the calandria tube outside surface as a function of liquid subcooling at conditions where a quench is about to be initiated. Both components are essentially independent of liquid subcooling with radiation heat transfer contributing around 4% and conduction heat transfer contributing 96% of the total heat transfer from CT outside surface.

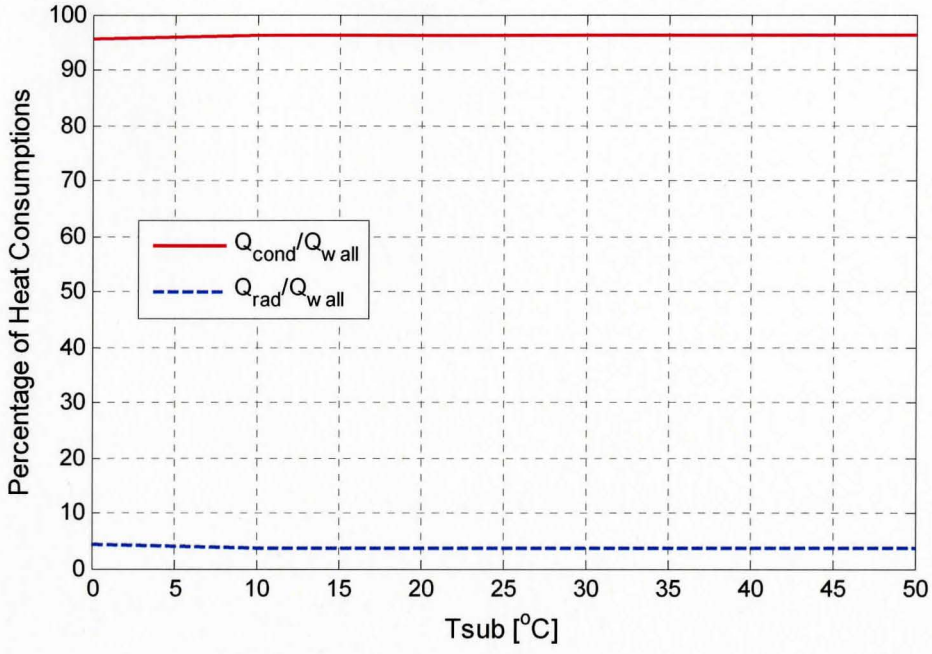

Figure 37: The contribution of radiation heat flux to the total CT outside surface heat flux

For example, at subcooling (T_{sub}) of 0 °C , T_{sat} =100 °C, and the wall temperature (T_w) 328 °C, the vapor film thickness (δ) when it changes from the steady state to quench is modeled to be 0.25 mm. Hence, the conduction heat transfer coefficient is

$$h_{cond} = \frac{k_v}{\delta} = 0.1413 \ (kW / m^2 / K)$$

where k_v can be calculated from Equations (55) and (51).

The radiation heat transfer coefficient under the same conditions is

$$h_{rad} = \varepsilon \sigma_{s-b} (T_w^2 + T_{sat}^2)(T_w + T_{sat}) = 0.0069 \ (kW / m^2 / K)$$

where T_w and T_{sat} are in absolute temperature.

Another conditions are for T_{sub}=50 °C, T_w=623 °C, T_{sat} =100 °C and δ= 0.144 mm. The conduction heat transfer coefficient (h_{cond}) and radiation heat transfer coefficient (h_{rad}) can be calculated as 0.3547 and 0.0157, respectively.

The two cases above, one is for lowest subcooling conditions and the other for highest subcooling conditions. Both results in ratios of h_{rad} to h_{cond} less than 5 %, which are compatible with Figure 37.

Figure 38 shows that the majority of heat transferred to the vapor-liquid interface is used to vaporize saturated liquid to maintain vapor film boiling. With increase in subcooling from 0°C to 50°C, the percentage of vaporization heat drops from 90% to 73%. During this process the contribution of heat to super-heat the vapor region gradually increases to 18% at 50 °C subcooling from 9% at 0 °C subcooling. The interface-to-liquid heat also gradually increases from 0% subcooling to 10% at 50 °C subcooling.

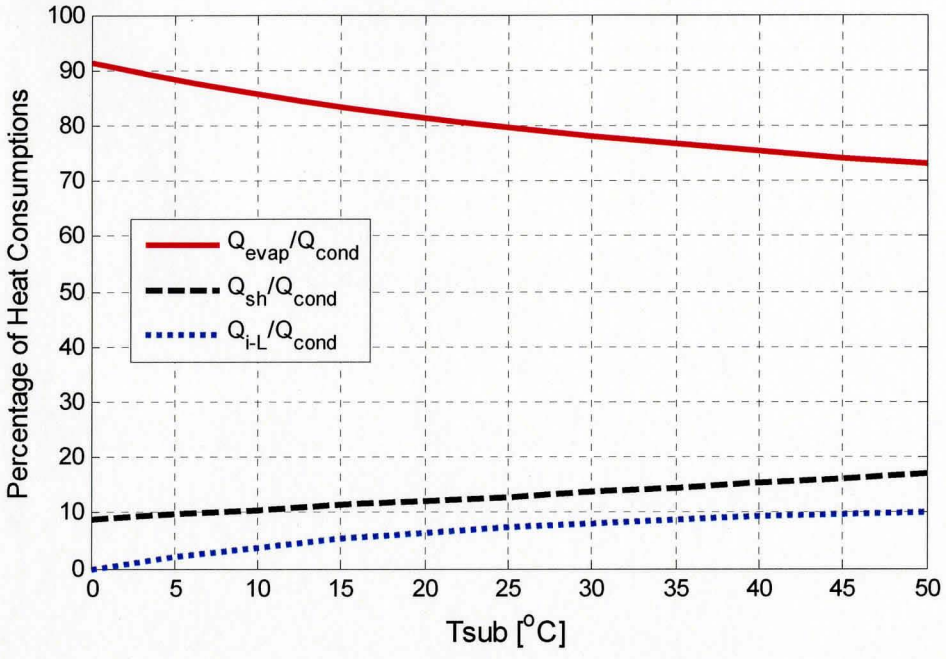

Figure 38: Contribution of vaporization, super-heating and interface-to-liquid heat to the heat conducted through the vapor film

5.3 Comparison to Available Experimental Data

Three plots shown in Figure 39, Figure 40 and Figure 41, generated from application of the model to evaluate quench behavior, are compared to the open literature and to contact boiling test data.

5.3.1 Heat Flux on the Calandria Tube Outside Surface

In Figure 39 the solid line represents the heat flux on the calandria tube outside surface obtained from the model, while the dotted line is obtained by converting the heatup rates [3] of the pressure tube to equivalent heat fluxes on the calandira tube outside surface. The model underestimates by 2.2% the heat fluxes for the subcooling ranging from 0 °C

to 30 °C. At higher subcooling up to 50 °C the model underestimates heat flux to a maximum of 5%. The agreement between the model and the experimental data is considered to be good.

At the same incident heat flux this model predicts a slightly higher subcooling for a quench to occur. For example, at the incident heat flux of 150kW/m^2, the model predicts an occurrence of quench at the subcooling of 33.5 °C, which is 2 °C higher than experiment data. The maximum over-prediction on subcooling for quench occurrence is 4 °C at the subcooling of 50 °C. This implies that the predicted quenching requirement on subcooling is conservative.

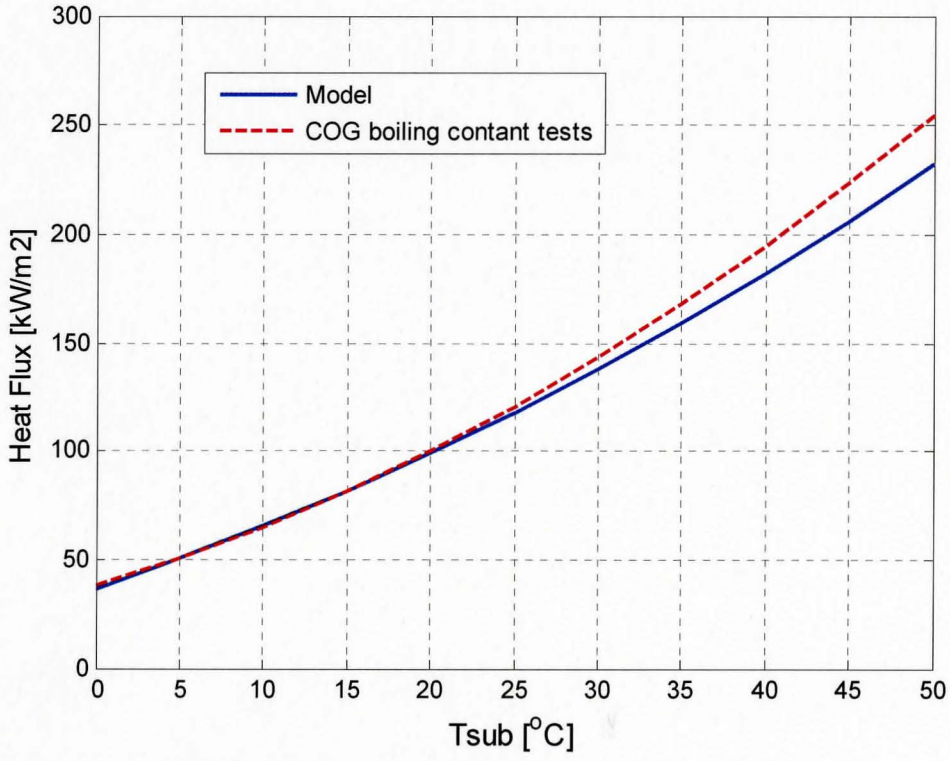

Figure 39: Prediction of heat flux at quench with comparison to COG experimental data

5.3.2 Effective Film-boiling Heat Transfer Coefficient

Figure 40 compares the effective film-boiling heat transfer coefficient derived from the model with the Gillespie & Moyer correlation [37], given as $h_{fb}=0.2(1+0.031*\Delta T_{sub})$ [kW/(m^2℃)]

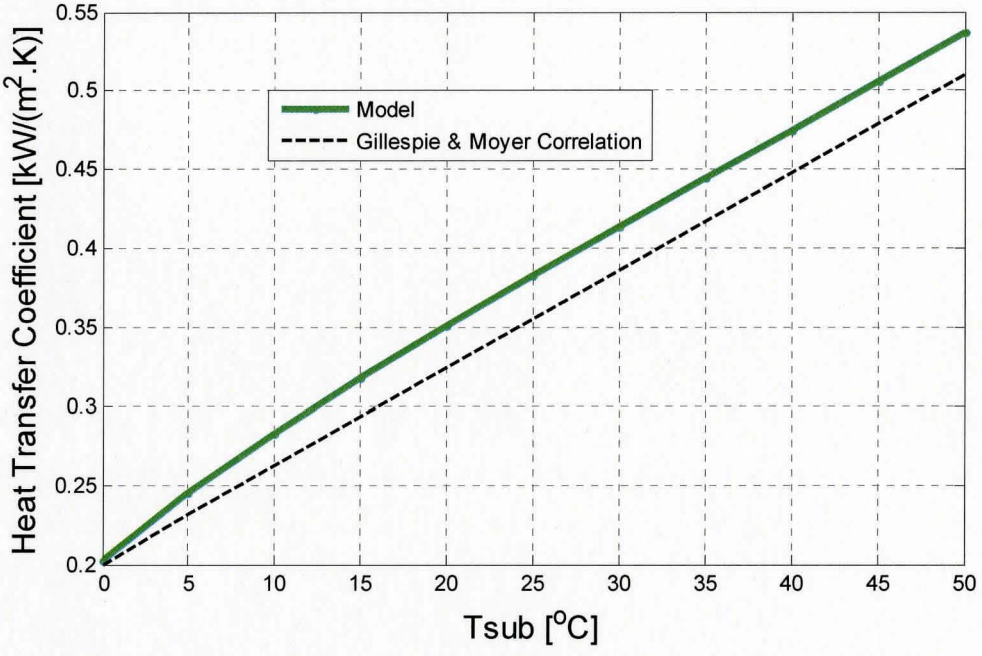

Figure 40: Prediction on effective film-boiling heat transfer coefficient with comparison to Gillespie & Moyer correlation

A relatively constant 7% over-prediction by the model exists for all subcoolings. This difference is not surprising since that the Gillespie & Moyer correlation is defined for the stable film-boiling, whereas the model predicts the conditions for onset of quench and is therefore expected to yield a somewhat higher heat transfer coefficient. The transition from stable film-boiling to quench is associated with an unstable reduction in the vapor film thickness. In Section 6.3 of Chapter Six, It shows two examples that increase in

subcooling affects the reduction of vapor film thickness with a high frequency oscillation. The conduction heat flux, $k_v(T_w-T_{sat})/\delta$, will increase due to the reduction of vapor film thickness. As shown in Figure 37, approximately 96% of heat transfer from the CT wall is due to conduction through the vapor film and any increase in conduction heat flux ultimately results in a higher effective heat transfer coefficient at quench than that at stable film-boiling. This behavior is expected to occur at all subcoolings.

The maximum over-prediction error is 8.6 % at subcooling 15 °C and the minimum overprediction error is 0 % at subcooling 0 °C.

5.3.3 Minimum Film-Boiling Temperature

At the evaluated quench heat fluxes, the model can also predict wall temperature of the Calandria tube at quench initiation. Several empirical correlations for minimum film-boiling temperature, T_{mfb}, from open literatures are plotted in Fig.14, as well as the values predicted by the model. The empirical correlations at atmospheric pressure with a unit of °C are listed below:

- Ohnishi [17]: $T_{mfb}=5.1\Delta T_{sub}+450$
- Bradfield [12]: $T_{mfb}=6.15\Delta T_{sub}+300$
- Groeneveld & Stewart [15]: $T_{mfb}=6.3\Delta T_{sub}+289$
- Adler [13]: $T_{mfb}=7\Delta T_{sub}+275$
- Mori [11]: $T_{mfb}=7.5\Delta T_{sub}+240$
- Lauer/COG experiment [14]: $T_{mfb}=5.893\Delta T_{sub}+328.6$
- Dhir and Purohit [18] $T_{mfb}=8\Delta T_{sub}+301$
- Nishio [19] $T_{mfb}=200$

Note that in Figure 41 the last two empirical correlations are not included. The model predictions are in general agreement with the majority of the correlations and are higher than the lower bound Mori correlation over most of the subcooling range. The quench temperatures predicted from the model are lower than the quench temperatures inferred from the contact boiling experiment data with a maximum underprediction of 41°C at a subcooling of 10°C. The following four reasons may possibly account for this difference.

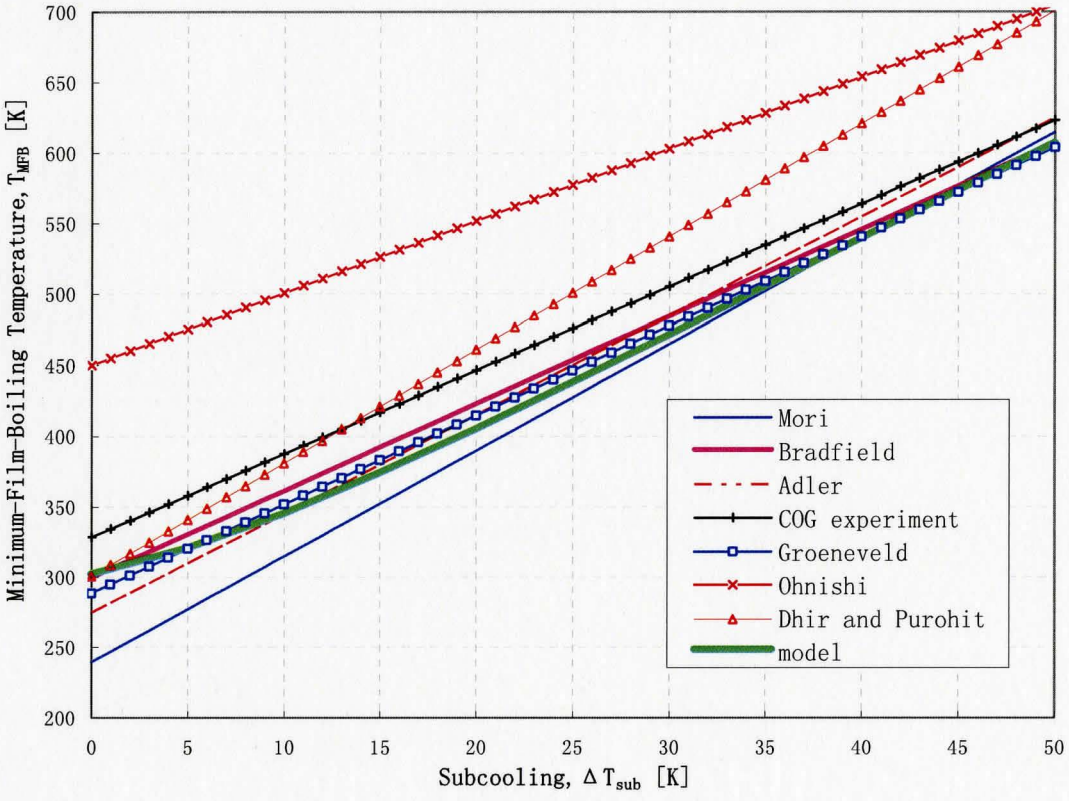

Figure 41: Prediction on minimum film boiling temperature with comparison to existing correlations

(1) As mentioned by Carbajo [38], the minimum film boiling temperature differs from the quench temperature. Due to the installation locations of the thermal couples

being a certain distance away under the CT surface, the measured temperature may be higher than the instantaneous quench temperature.

(2) The definition of quench temperature may vary with individual judgments. There are two ways of defining quench temperature that prevail over others. Point A in Fig.5 corresponds to the temperature at which an increase in negative slope of the temperature transient is observable. Point B is a projected temperature based on the intersection of the two distinct slopes in the temperature transient. The experimenters presented above may refer to Point A for their correlations. The quench temperatures predicted from the model are very likely to close to the temperature at Point B, based on the prerequisite that the evaporation velocity being zero at quench initiation.

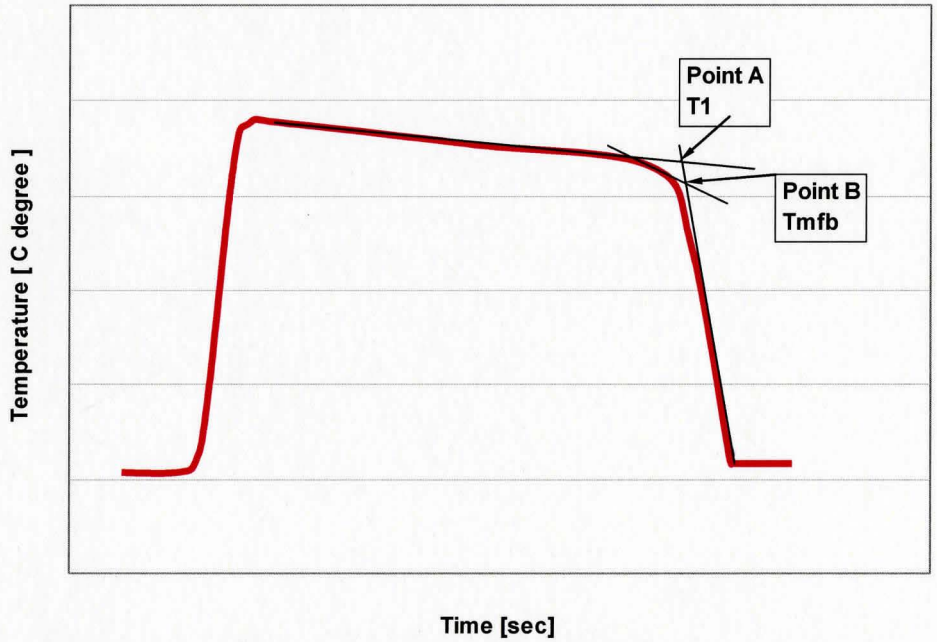

Figure 42: A typical quench curve transient [3]

(3) The geometry has influence on the minimum film-boiling temperature or quench temperature. It was reported [39] that small diameter heaters have higher

minimum film temperature (T_{mfb}) or higher quench temperature than large heaters do. The correlations above are based on tube data and these tubes are smaller than the CANDU calandria tube.

(4) Surface conditions, such as surface roughness and oxidization, affect the T_{mfb} or quench temperature as well. The surface conditions were not mentioned in some correlations above. In the model, the non-oxidized Zircaloy with emissivity of 0.19 was used. In general, both T_{mfb} and quench temperature increase as the surface becomes oxidized.

Overall, the model predictions are most similar to Groeneveld & Stewart's correlation.

5.4 Prediction Error

This model matches available experimental data quite well. The accuracy of predictions by the model is summarized in Table 5.

Table 5: Error percentage in prediction

	ΔT_{sub}										
	0°C	5°C	10°C	15°C	20°C	25°C	30°C	35°C	40°C	45°C	50°C
Error % in Prediction of CT Wall Heat Flux (compared to COG contact boiling tests)	-1.0	0.7	0.9	0.4	-0.4	-1.3	-2.2	-3.1	-3.8	-4.4	-4.8
Error % in Prediction of Effective film-boiling Heat Transfer Coefficient (compared to Gillespie & Moyer correlation)	1.3	6.13	8.1	8.6	8.4	7.9	7.2	6.6	6.0	5.5	5.2
Error % in Prediction of Calandria tube outside wall temperature (compared to Lauer correlation)	-4.2	-5.9	-6.7	-6.8	-6.5	-6.0	-5.4	-4.6	-3.9	-3.2	-2.5

Chapter Six

6.0 Vapor Film Transient Function of Step Change

In Chapter Five, all conclusions are based on the quench conditions applied on steady-state equation. In this chapter, a preliminary investigation of the transient vapor-film-thickness equation in terms of a step change in subcooling will be performed. It is noted that the detailed analysis of the transient behavior is beyond the objectives of this thesis. Therefore, the investigation presented here may be considered to be preliminary. The intention is to show the complexity of the vapor-film-thickness transient equation — a highly unstable non-linear Ordinary Differential Equation (ODE). A detailed analysis may be considered in a further project to study the oscillatory behavior and the stability of liquid-vapor interface.

6.1 Transient Vapor Film Thickness Equation

The transient vapor-film-thickness equation was given in Equation (96) in Chapter Four as below.

$$\langle 1\rangle + \langle 2\rangle + \langle 3\rangle + \langle 4\rangle + \langle 5\rangle + \langle 6\rangle + \langle 7\rangle + \langle 8\rangle = 0$$

$$\langle 1\rangle = \ddot{\delta}\left[1 + \frac{\chi(R+\delta)}{\delta} + \frac{1}{2}\chi C_1 \frac{R+\delta}{\delta\sqrt{u_\infty + \dot{\delta}}}\right],$$

$$\langle 2\rangle = \left(\frac{\dot{\delta}}{\delta}\right)^2\left[-\frac{3}{4}\chi(R+\delta)\right],$$

$$\langle 3\rangle = \frac{\dot{\delta}}{\delta^2}\left[-2C_1(R+\delta)\sqrt{u_\infty + \dot{\delta}}\right],$$

$$\langle 4\rangle = \frac{\dot{\delta}}{\delta^3}\left[\frac{3}{2}\chi C_2(R+\delta)\right],$$

$$\langle 5\rangle = \frac{1}{\delta^2}\left[-\chi C_1^2(R+\delta)(u_\infty+\dot{\delta})\right],$$

$$\langle 6\rangle = \frac{1}{\delta^3}\left[\chi C_1 C_2(R+\delta)(u_\infty+\dot{\delta})\right],$$

$$\langle 7\rangle = \frac{1}{\delta^4}\left[-\frac{1}{4}\chi C_2^2(R+\delta)\right],$$

$$\langle 8\rangle = g(R+\delta)+4(u_\infty+\dot{\delta})^2$$

In the terms above, χ, C_1 and C_2 are defined as, respectively,

$$\chi = \frac{\rho_v}{\rho_L},$$

$$C_1 = \frac{k_L \cdot \cos\frac{\theta}{2}\cdot \Delta T_{sub}}{h'_{fg}\,\rho_v\sqrt{\pi R\alpha_L}},$$

$$C_2 = \frac{k_v(T_w - T_{sat})}{h'_{fg}\,\rho_v}$$

It is a second order, no homogeneous nonlinear ODE in terms of time. Note that the free steam velocity u can be substituted by $u_\infty = aT_{sub} + b$, where a and b are constants. In such a way a step change in subcooling can be made to exam the influence on vapor film thickness, given that the other parameters are kept unchanged.

6.2 4th Order Runge-Kutta Method

The 4th Order Runge-Kutta method is used to integrate the differential equation. This is a widely used method. A brief description of this method is presented here. To bridge the gap between the first-order Euler method and this fourth order method, readers are recommended to review a relevant chapter from a math book. Given that f(x,y) is only a function of x, one of the most commonly used is described below [40]

$$y_{i+1} = y_i + \frac{1}{6}(k_1 + k_2 + k_3 + k_4)h$$

where

$$k_1 = h f(x_i, y_i),$$

$$k_2 = h f(x_i + \frac{h}{2}, y_i + \frac{1}{2}k_1),$$

$$k_3 = h f(x_i + \frac{h}{2}, y_i + \frac{1}{2}k_2),$$

$$k_4 = h f(x_{i+1}, y_i + k_3),$$

A function in MatLab, called `ode45`, which implements the 4th order Runge-Kutta method, was used to solve ODEs.

6.3 Influence of Subcooling Step Change on Vapor Film Thickness

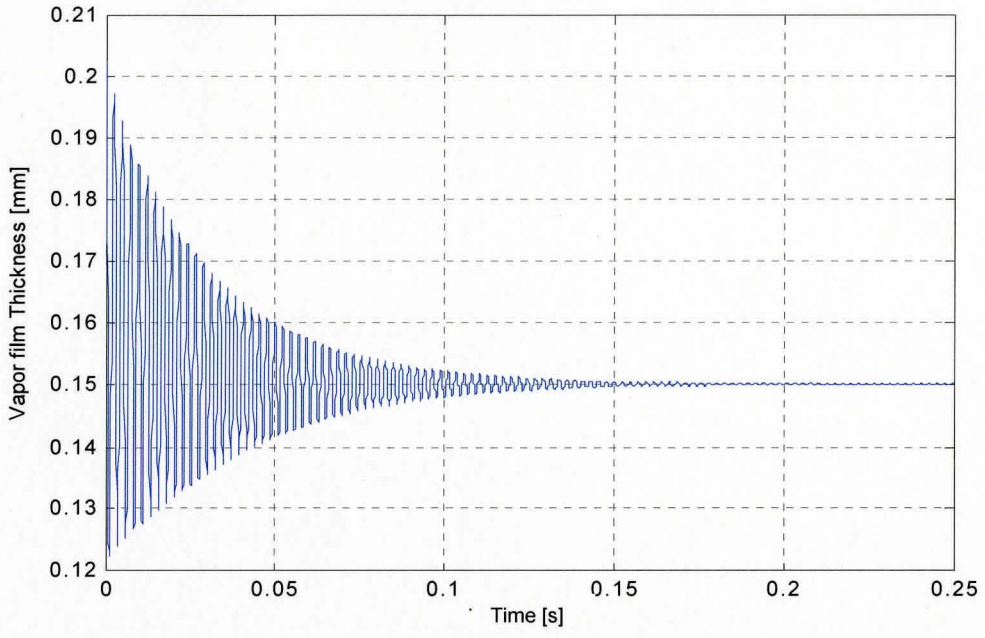

Figure 43: Vapor film oscillation and stabilization due to 15 ˚C increase of subcooling

Figure 43 presents a vapor film oscillation and stabilization triggered by 15 ˚C drop in subcooling (from 20 ˚C to 35 ˚C). The initial condition is the vapor film at 0.165 mm. The final stabilized thickness stay at about 0.150 mm.

Figure 44 shows how a 10˚C increase of subcooling (from 15˚C to 25˚C) affects the vapor film thickness. A sudden increase occurs at time 0.06 second and then stabilizes ultimately. The initial thickness was 0.18 mm. Compared to a 15˚C drop in subcooling,

the lower subcooling drop (10˚C) has less influence on the reduction of vapor film thickness and seems to be less able to stabilize the vapor film at a lower thickness level.

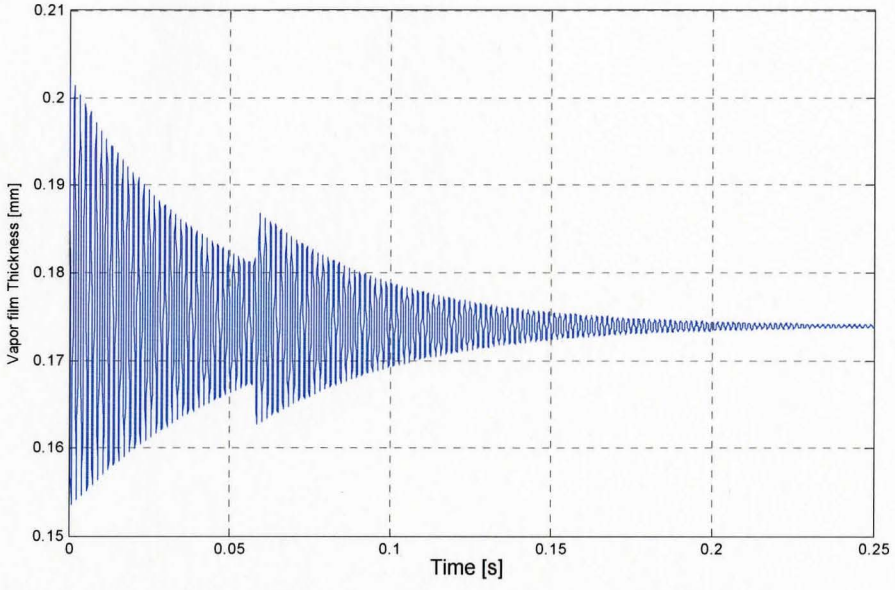

Figure 44: Vapor film oscillation and stabilization due to 10 ˚C increase of subcooling

If the subcooling decreases, the vapor film thickness exhibits an unstable response. Figure 45 shows that the vapor film oscillates and grows to a fixed layer thickness when the subcooling decreases from 30 ˚C to 20 ˚C. This behavior indicates that film thickness increases with reduction in subcooling, thereby making quench less likely to occur.

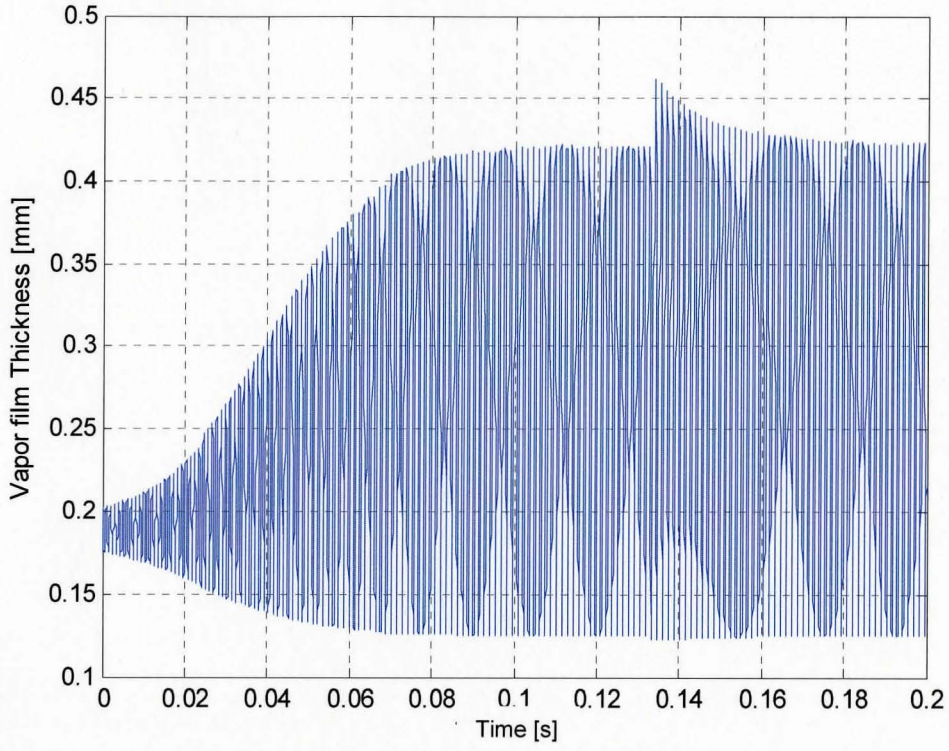

Figure 45: Vapor film oscillation and instability due to 10 °C reduction of subcooling

Chapter Seven

7.0 Conclusions and Recommendations

The proposed model characterizes the pool film-boiling and quench on the outside of a calandria tube. It provides an understanding of the influence of thermalhydraulic parameters on the film-boiling heat transfer.

At given conditions, such as subcooling, wall temperature (or heat flux), the steady state vapor film thickness can be calculated. Those results are plotted as Figure 30 through Figure 34.

The model clearly demarcates the requirements for the occurrence of quench. There are tow plots (Figure 35 and Figure 36) show the requirements on heat flux as function of either subcooling or vapor film thickness.

A relationship between quench temperature and subcooling is provided which is close to Groeneveld & Stewart's correlation for minimum film-boiling temperature. And the reasons are also provided for the under-prediction of quench temperature when compared to the result of COG boiling contact tests.

Considering future work, the transient vapor film equation should be quantitatively investigated in terms of subcooling step changes. The influence of step change in incident wall heat flux or heatup rate on vapor film stability is also of interest for future study. In addition, research into the inherent instability behavior of the vapor film may

start with the sensitivity evaluation of the transient vapor-film-thickness equation.

It is author's opinion that an experimentally based study relevant to this dissertation would be an interesting work to examine and assess behavior that has been theoretically derived and modeled in this dissertation.

In Chapter Four, we assumed that a fully developed laminar liquid flow exists at the outer surface of the vapor-liquid interface. If a turbulent flow is assumed, the Navier-Stokes equations can not be solved analytically. Also assuming developed laminar flow rather than turbulent flow will lead to lower heat transfer from the interface to the liquid, which tends to retard quench. Therefore, the assumption of fully developed laminar liquid flow bounds the case in which an assumption of turbulent flow is assumed.

Appendixes

Appendix A: Calculate CT Outer Surface Heat Flux from a PT Heatup Rate

The volumetric heat rate of pressure tube is

$$q'''_p = \frac{q_{pi}}{V_p} = \frac{q_{pi}}{\pi(R_{po}^2 - R_{pi}^2)L} \tag{124}$$

where q_{pi} = incidental heat to pressure-tube inner surface

R_{po} = outer radius of pressure-tube

R_{pi} = inner radius of pressure-tube

V_p = volume of pressure-tube

L = Length of pressure-tube or calandria-tube

The heat flux to inner wall of pressure-tube from the fuel core:

$$q''_{pi} = \frac{q_{pi}}{A_{pi}} = \frac{q_{pi}}{2\pi R_{pi} L} \tag{125}$$

where A_{pi} = inner area of pressure-tube

From Equation (124)and(125),

$$(R_{po}^2 - R_{pi}^2) q'''_p = 2R_{pi}\, q''_{pi}$$

$$So \quad q''_{pi} = \frac{(R_o^2 - R_i^2)}{2R_i} q'''_p \tag{126}$$

The other expression for pressure-tube volumetric heat rate is given by

$$q'''_p = \rho_p c_{p,p} \frac{dT_p}{dt} \tag{127}$$

where $c_{p,p}$ = specific heat of pressure-tube, 0.35kJ/kg/°K

dT_p/dt = the heat up rate of pressure-tube

Substituting Equation (127) into(126), yields:

$$q''_{pi} = \frac{(R_{po}^2 - R_{pi}^2)}{2R_{pi}} \rho_p c_{p,p} \frac{dT_p}{dt} \tag{128}$$

Density of the pressure-tube is:

$$\rho_p = \frac{m_p}{V_p} = \frac{m_p}{\pi(R_{po}^2 - R_{pi}^2)L} = \frac{m'_p}{\pi(R_{po}^2 - R_{pi}^2)} \tag{129}$$

where m_p = mass of pressure-tube

m'_p = mass per unit length of pressure-tube, 9.164 kg/m.

Substituting Equation (129) into(128), yields

$$q''_{pi} = \frac{m'_p}{2\pi R_{pi}} c_{p,p} \frac{dT_p}{dt} \tag{130}$$

The heat flux emitted from outer surface of CT is given by

$$q''_{ct} = \frac{q_{co}}{A_{co}} = \frac{q_{co}}{2\pi R_{co} L} \tag{131}$$

where A_{co} = area of calandria-tube outer surface

R_{co} = Radius of calandria-tube outer surface

At the steady state, the incidental heat to calandria-tube outter surface, q_{co}, equals the heat emitted from pressure-tube inner surface, q_{pi}.

$$q_{co} = q_{pi} \tag{132}$$

From Equation (125),(131) and (132), it follows that

$$q''_{co} = q''_{pi} \frac{R_{pi}}{R_{co}} \tag{133}$$

Substituting Equation (130) into (133), yields

$$q''_{co} = \frac{m'_p}{2\pi R_{co}} c_{p,p} \frac{dT_p}{dt} \tag{134}$$

Substituting values of m'_p, R_{co} and $c_{p,p}$, into Equation (134) gives

$$q''_{co} = \frac{9.164\ kg/m}{2\pi(6.5875\times10^{-2})m} \cdot 0.35kJ/(kg\cdot°C)\frac{dT_p}{dt} = 7.75(kJ/m^2/°C)\frac{dT_p}{dt} \tag{135}$$

If the unit of dT_p/dt is given as "$°C/s$", then the heat flux has a unit of kW/m^2.

Therefore, under the steady state situation the emitting heat flux from the calandria-tube outer surface can be converted from the heat up rate of the pressure-tube.

Figure 46 shows the heat flux, from the calandria-tube outer surface, in accordance with the heat up rate given in Figure 47.

Note that the above result may rely on the assumption that the contact between CT and PT is tight enough — there is no-gap in between (the contact conductance=0).

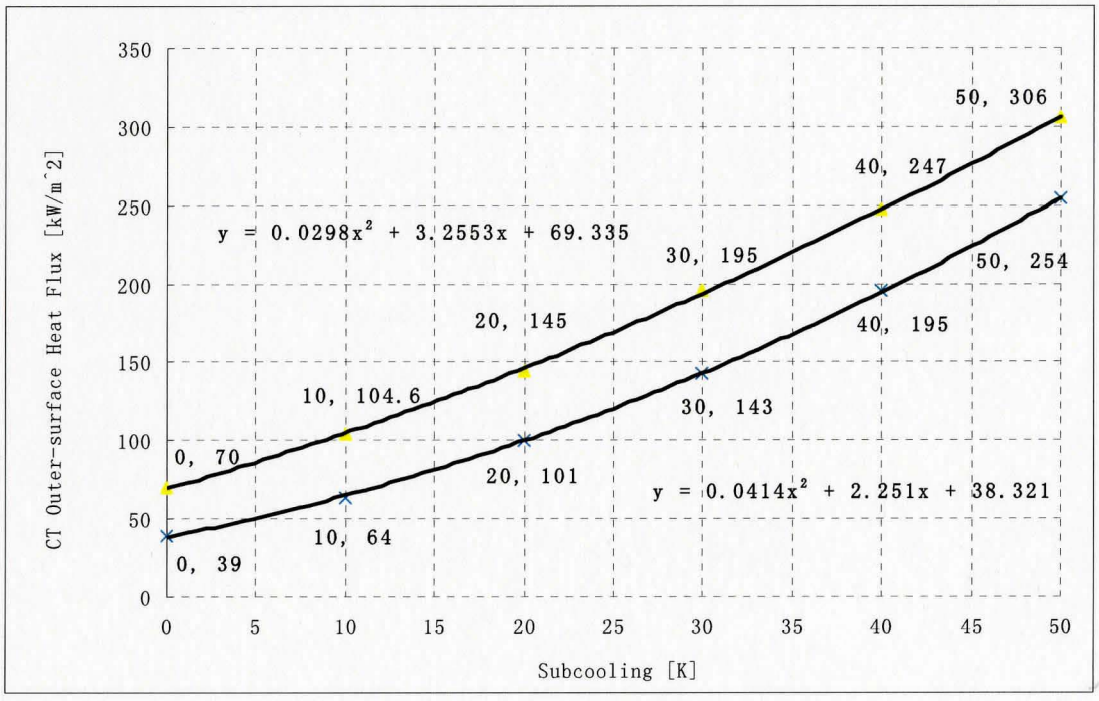

Figure 46: Heat flux in terms of subcooling

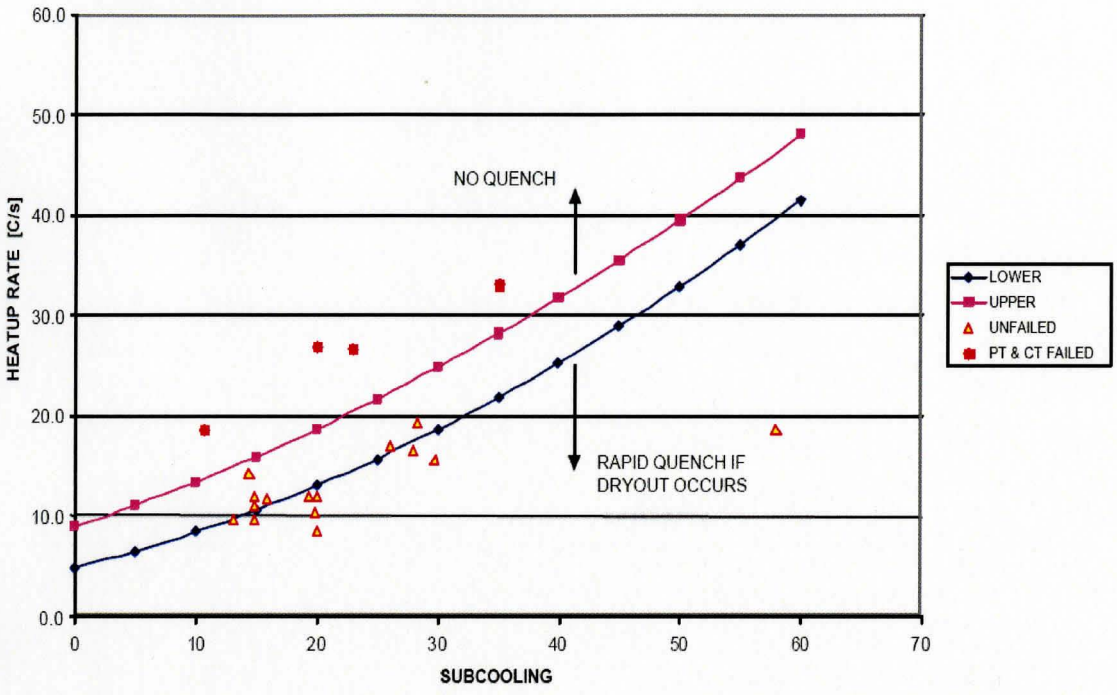

Figure 47: Heat-up rate in terms of subcooling [3]

Appendix B: A MatLab Code for Calculating Vapor Film Temperature

```
%% Calculates the vapor tempterature and given situation of                %
% subcooling temp, free stream liquid velocity and vapor film thickness.  %
% Code Author: Jiantao Jiang                                               %
% June 2007
% MatLab 7.01
%%%%%%%%%%%%%%%%%%%%%%%%%%%%%%%%%%%%%%%%%%%%%%%%%%%%%%%%%%%%%%%%%%%%%%%%%%%%


clc;
clear all;

% Sat Water properties are estimated at 373.15K (or 100C deg)
% rho_l = 0.9579*10^3; % [kg/m^3]H2O. if D2O -> 1.0829 *10^3 kg/m^3
rho_l = 1.093 *10^3;   % [kg/m^3]D2O at 75C
h_fg = 2257; % [kJ/kg] latent heat of vaporization
k_l = 680*10^(-6); % [kW/m/K)] liquid thermal conductivity
emisv = 0.2 ; % emissivity of non-oxidated Calandria Tube
s_bolzm = 5.670*10^(-11);  % Stefan-Boltzmann Constant [kW/(m^2*K^4)]
Rco=0.065875;    % [m] CT Outer Radius    % Rci = 0.064478 m
Rpi=0.051689;    % [m] PT Inner Radius    % Rpo = 0.056032 m

R = 6.5875*10^(-2); % [m] CT outside radius
g = 9.8; % [m/s^2] gravity
Tsat = 100; % [C] water saturation temp
% Tsub=zeros(50,6);
d=10^(-3).*[    0.2610    0.2133
    0.2259    0.1878
    0.2034    0.1716
    0.1879    0.1607
    0.1766    0.1530
    0.1681    0.1473
    0.1614    0.1429
    0.1561    0.1396
    0.1517    0.1369
    0.1481    0.1348
    0.1450    0.1330
];

for      n=1:1:2
        % d(n,1)=0.225*10^(-3)+ 0.01*10^(-3)*(n-1);  % [m] Thickness of Vapor Film ranges
from 0.105mm - 0.135 mm

        for     i=1:1:11
                Tsub(i,n)=(i-1)*5;        % Tsub range from 0 - 50C deg

                Tv(i,1,n)=400;        % [C] Initiate a value for Vapor Temperature

                Uinf(i,n)=0.023*Tsub(i,n)+0.78;  % [m/s] Given Velocity of Free Stream
Liquid.

                T_error(i,1,n) = 5;  % Arbitrary value to let while-loop begin

                j=1;                 % Initiate j starting from 1
                while      ( abs(T_error(i,j))>0.01 )    % Loop Condition : if absolute
```

```
temp error is bigger than 0.01 C deg
                            Kv(i,j,n)= 10^(-10)*Tv(i,j,n).^2+5*10^(-8)*Tv(i,j,n)+2*10^(-5);
%[C] Calculate Kv - vapor conductivity
                            % rho(i,j,n)= -0.213*reallog(Tv(i,j,n)) + 1.6388;  % [kg/m^3]
vapor density
                            rho(i,j,n) = -10^(-9)*Tv(i,j,n).^3 + 3*10^(-6)*Tv(i,j,n).^2 -
0.002*Tv(i,j,n) + 0.8237;
                             Cp(i,j,n) = -3*10^(-9)*Tv(i,j,n).^3+4*10^(-6)*Tv(i,j,n).^2-
0.0008*Tv(i,j,n)+1.9146; %[kJ/kg/K] vapor heat apacity
                            % Cp(i,j,n) = -3E-14*Tv(i,j,n)^5 + 6E-11*Tv(i,j,n)^4 - 5E-
08*Tv(i,j,n)^3 + 2E-05*Tv(i,j,n)^2 - 0.0045*Tv(i,j,n)^ + 2.1481;
                            % a(i,j,n) = Kv(i,j,n)/(rho(i,j,n)*Cp(i,j,n)); % [m^2/s] vapor
thermal diffusivity
                            a(i,j,n)=1.63*10^(-4);              %  [m^2/s] H2O thermal
diffusivity at 345K(71.85C)
                            u(i,j,n) = 4*10^(-8)*Tv(i,j,n)+8*10^(-6);  %[N.s/m^2 ]dynamic
viscosity
                            v(i,j,n)=u(i,j,n)./rho(i,j,n);               % [m^2/s] vapor
kinamatic viscosity

                            % h_fg_m(i,j,n)=h_fg*(1+0.4*Cp(i,j,n)*(Tv(i,j,n)-Tsat)/h_fg)^2;

                            B1(i,j,n) = 12*2^(1/2)*v(i,j,n)*R .*k_l*Tsub(i,n)./(rho_l*h_fg
*(3.14159/2*R*a(i,j,n))^(1/2)).*Uinf(i,n)^(1/2);
                            B2_star(i,j,n) = 12*v(i,j,n)*R .*Kv(i,j,n)/(h_fg*rho_l);
                            B3(i,n) = g + 4*Uinf(i,n).^2/R;

                            Tw_calc(i,j,n) = Tsat + (B3(i,n).*d(i,n)^4 +
B1(i,j,n).*d(i,n))./B2_star(i,j,n); % Calculate Wall Temperature
                            Tv_calc(i,j,n) = (Tw_calc(i,j,n)+Tsat)/2;
                            T_error(i,j+1,n) = Tv_calc(i,j,n)-Tv(i,j,n);    % Temperature
error
                            Tv(i,j+1,n) = Tv(i,j,n)+ 0.5*T_error(i,j+1,n);  % Update Tv
                            j=j+1;

                end
        Tvap(i,n)=Tv(i,j,n); j;
        Tw(i,n)=2*Tv(i,j,n)-Tsat;

        syms K T;
        a2=10^(-10);  a1=5*10^(-8);  a0=2*10^(-5);
        K=a2*T^2+a1*T+a0;  % Vapor conductivity as a function of Vapor Temperature.
        % Qc(i,n)= double( -int(K,T,Tw(i,n),Tsat)/d(i,n) );
        Qc(i,n)= Kv(i,j-1,n).*(Tw(i,n)-Tsat)./d(i,n);                % Conduction heat
alone
        Qr(i,n)= emisv*s_bolzm*((Tw(i,n)+273).^4-((Tsat-Tsub(i,n))+273).^4); %Radiation
heat
        h_sh(i,n)=0.5*Cp(i,j-1,n).*(Tw(i,n)-Tsat);
        V_evap(i,j,n)= rho_l*d(i,n).^3/(12*u(i,j-1,n)*R).*(g+4*Uinf(i,n).^2/R)
        Qsh(i,n)=h_sh(i,n).*rho(i,j-1,n).*V_evap(i,j,n);           % Super-heatting the
vapor
        Qct(i,n)=Qc(i,n)+Qr(i,n)+Qsh(i,n);              % Total heat flux emitting from CT
        Qpt_in(i,n)=Qct(i,n)*(Rco/Rpi);        % Corresponding PT-inner-wall incident Heat
Flux
        % Qin2(i,n)= (a2*Tv(i,j,n)^2+a1*Tv(i,j,n)+a0)*(Tw(i,n)-Tsat)/d(n,1);
        % Qcond(i,n)=d(n,1)^3*(g+B3(i,n))/12/v(i,j-1,n)/R*(h_fg_m(i,j-
1,n)*rho_l)+2*k_l*Tsub(i,n)*Uinf(i,n)^(1/2)/(3.14159*R*a(i,j-1,n))^(1/2);
        r_c_persentage(i,n)=Qr(i,n)./Qc(i,n)*100;
        sh_c_persentage(i,n)=Qsh(i,n)./Qc(i,n)*100;
        hc(i,n)=Qc(i,n)./(Tw(i,n)-Tsat);
        hr(i,n)=Qr(i,n)./(Tw(i,n)-(Tsat-Tsub(i,n)));
        hr_eff(i,n)=hr(i,n)*(Tw(i,n)-(Tsat-Tsub(i,n)))/(Tw(i,n)-Tsat);
        hsh(i,n)=Qsh(i,n)./(Tw(i,n)-Tsat);
        % ratio_of_h(i,n)=hr(i,n)/hc(i,n);
        h(i,n)=hc(i,n)+ hr_eff(i,n)+ hsh(i,n);
        h_aecl(i,n)=0.2*(1+0.031*Tsub(i,n));
        end
```

```
        if    n==1
              figure(1), plot(Tsub(:,n),Qc(:,n),'r-','LineWidth',1)
              hold on
              figure(2), plot(Tsub(:,n),Qr(:,n),'r-','LineWidth',1)
              hold on
              figure(3), plot(Tsub(:,n),Qsh(:,n),'r-','LineWidth',1)
              hold on
              figure(4), plot(Tsub(:,n),Qc(:,n)+Qr(:,n)+Qsh(:,n),'r-','LineWidth',1)
              hold on
              figure(5), plot(Tsub(:,n),Qpt_in(:,n),'r','LineWidth',1)
              hold on
              figure(7), plot(Tsub(:,n),h(:,n),'r-')
              hold on
              figure(6), plot(Tw(:,n),Qct(:,n),'r-')
              hold on
              figure(8), plot(Tsub(:,n),Tw(:,n),'r-','LineWidth',1)
              hold on
        end

        if    n==2
              figure(1), plot(Tsub(:,n),Qc(:,n),'b.-','LineWidth',1)
              hold on
              figure(2), plot(Tsub(:,n),Qr(:,n),'b.-','LineWidth',1)
              hold on
              figure(3), plot(Tsub(:,n),Qsh(:,n),'b.-','LineWidth',1)
              hold on
              figure(4), plot(Tsub(:,n),Qc(:,n)+Qr(:,n)+Qsh(:,n),'b.-','LineWidth',1)
              hold on
              figure(5), plot(Tsub(:,n),Qpt_in(:,n),'b.-','LineWidth',1)
              hold on
              figure(6), plot(Tw(:,n),Qct(:,n),'b.-')
              hold on
              figure(7), plot(Tsub(:,n),h(:,n),'b.-')
              hold on
              figure(8), plot(Tsub(:,n),Tw(:,n),'b.-','LineWidth',1)
              hold on
        end


end

figure(7), plot(Tsub(:,1),h_aecl(:,1),'k--')

     for m=1:1:5
        figure(m),legend('Upper Bound','Lower Bound')
        figure(m),xlabel('Subcooling,T_s_u_b [K]','FontSize',16)
        ylabel('Heat Flux [ kW/m ^2 ]','FontSize',16)
     end
     for m=1:1:8
         figure(m),grid
         figure(m),hold off
     end

        figure(1),title('Conduction Heat Flux vs Subcooling','FontSize',14)
        figure(2),title('Radiation Heat Flux vs Subcooling','FontSize',14)
        figure(3),title('SuperHeatting Heat Flux vs Subcooling','FontSize',14)
        figure(4),title('CT Total Heat Flux(cond+rad+superheat) vs
Subcooling','FontSize',14)
        figure(5),title('Corresponding PT Inner Wall Incident Heat Flux','FontSize',14)
        figure(6),title('CT Outer wall Heat Flux vs Wall Temperature','FontSize',14)
        figure(6),xlabel('Wall Temperature,T_w [K]','FontSize',14)
        figure(6),ylabel('CT Outer wall Heat Flux [ kW/m ^2 ]','FontSize',14)
        figure(6),legend('Upper Bound','Lower Bound')
         figure(7),title('Effective Total Heat Transfer Coefficient','FontSize',14)
         figure(7),xlabel('Subcooling,T_s_u_b [K]','FontSize',14)
         figure(7),ylabel('Effective Total Heat Transfer Coefficient
```

```
[kW/m^2/K]','FontSize',14)
         figure(7),legend('Upper Bound', 'Lower Bound','Gillespie&Moyer Correlation')
        figure(8),xlabel('Subcooling Temperature,T_s_u_b [ C ]','FontSize',16)
        figure(8),ylabel('Wall temperature, T_w [ C ]','FontSize',16)
```

Appendix C: Tables of Thermophysical Properties of D_2O

(Taken from Hill et al, AECL [36])

Table C1: Volume

Table 3. Liquid and Vapour

	Volume, m^3/kg			Enthalpy, kJ/kg			Energy, kJ/kg			Entropy, kJ/kg.K			
p(kPa)	90.	95.	100.	90.	95.	100.	90.	95.	100.	90.	95.	100.	p(kPa)
t sat	96.17	99.64	101.05	96.17	99.64	101.05	96.17	99.64	101.05	96.17	99.64	101.05	t sat
Liq.sat	0.0009391	0.0009402	0.0009412	397.5	403.6	409.5	397.4	403.5	409.4	1.2354	1.2518	1.2675	Liq.sat
Vap.sat	1.6881	1.6048	1.5295	2476.6	2478.8	2480.9	2324.7	2326.3	2327.9	6.8347	6.8184	6.8031	Vap.sat
t(C)													t(C)
3.8	0.0009045	0.0009045	0.0009045	0.1	0.1	0.1	0.0	0.0	0.0	0.0	0.0	0.0	3.8
4.	0.0009045	0.0009045	0.0009045	0.9	0.9	0.9	0.8	0.8	0.8	0.0030	0.0030	0.0030	4.
6.	0.0009043	0.0009043	0.0009043	9.4	9.4	9.4	9.3	9.3	9.3	0.0332	0.0332	0.0332	6.
8.	0.0009042	0.0009042	0.0009042	17.8	17.8	17.8	17.7	17.7	17.7	0.0635	0.0635	0.0635	8.
10.	0.0009042	0.0009042	0.0009041	26.3	26.3	26.3.	26.2	26.2	26.2	0.0935	0.0935	0.0935	10.
12.	0.0009041	0.0009041	0.0009041	34.7	34.7	34.7	34.6	34.6	34.6	0.1233	0.1233	0.1233	12.
14.	0.0009042	0.0009042	0.0009042	43.2	43.2	43.2	43.1	43.1	43.1	0.1529	0.1529	0.1529	14.
16.	0.0009043	0.0009043	0.0009043	51.7	51.7	51.7	51.6	51.6	51.6	0.1823	0.1823	0.1823	16.
18.	0.0009046	0.0009045	0.0009045	60.2	60.2	60.2	60.1	60.1	60.1	0.2115	0.2115	0.2115	18.
20.	0.0009047	0.0009047	0.0009047	68.6	68.6	68.7	68.6	68.6	68.6	0.2406	0.2406	0.2406	20.
22.	0.0009049	0.0009049	0.0009049	77.1	77.1	77.1	77.0	77.0	77.0	0.2694	0.2694	0.2694	22.
24.	0.0009052	0.0009052	0.0009052	85.6	85.6	85.6	85.5	85.5	85.5	0.2981	0.2981	0.2981	24.
26.	0.0009056	0.0009056	0.0009056	94.1	94.1	94.1	94.0	94.0	94.0	0.3265	0.3265	0.3265	26.
28.	0.0009060	0.0009060	0.0009060	102.6	102.6	102.6	102.5	102.5	102.5	0.3548	0.3548	0.3548	28.
30.	0.0009064	0.0009064	0.0009064	111.1	111.1	111.1	111.0	111.0	111.0	0.3829	0.3829	0.3829	30.
32.	0.0009068	0.0009068	0.0009068	119.5	119.5	119.6	119.5	119.5	119.5	0.4107	0.4107	0.4107	32.
34.	0.0009074	0.0009074	0.0009074	128.0	128.0	128.0	127.9	127.9	127.9	0.4384	0.4384	0.4384	34.
36.	0.0009079	0.0009079	0.0009079	136.5	136.5	136.5	136.4	136.4	136.4	0.4659	0.4659	0.4659	36.
38.	0.0009085	0.0009085	0.0009085	145.0	145.0	145.0	144.9	144.9	144.9	0.4932	0.4932	0.4932	38.
40.	0.0009091	0.0009091	0.0009091	153.4	153.4	153.4	153.3	153.3	153.3	0.5203	0.5203	0.5203	40.
42.	0.0009098	0.0009097	0.0009097	161.9	161.9	161.9	161.8	161.8	161.8	0.5473	0.5473	0.5473	42.
44.	0.0009104	0.0009104	0.0009104	170.3	170.3	170.4	170.3	170.3	170.3	0.5740	0.5740	0.5740	44.
46.	0.0009111	0.0009111	0.0009111	178.8	178.8	178.8	178.7	178.7	178.7	0.6006	0.6006	0.6006	46.
48.	0.0009119	0.0009119	0.0009119	187.2	187.2	187.3	187.2	187.2	187.2	0.6270	0.6270	0.6270	48.
50.	0.0009127	0.0009127	0.0009127	195.7	195.7	195.7	195.6	195.6	195.6	0.6532	0.6532	0.6532	50.
52.	0.0009135	0.0009135	0.0009135	204.1	204.1	204.1	204.0	204.0	204.0	0.6792	0.6792	0.6792	52.
54.	0.0009143	0.0009143	0.0009143	212.6	212.6	212.6	212.5	212.5	212.6	0.7051	0.7051	0.7051	54.
56.	0.0009152	0.0009152	0.0009152	221.0	221.0	221.0	220.9	220.9	220.9	0.7308	0.7307	0.7307	56.
58.	0.0009160	0.0009160	0.0009160	229.4	229.4	229.4	229.3	229.3	229.3	0.7563	0.7563	0.7563	58.
60.	0.0009170	0.0009170	0.0009170	237.8	237.8	237.8	237.7	237.7	237.7	0.7816	0.7816	0.7816	60.
62.	0.0009179	0.0009179	0.0009179	246.2	246.2	246.2	246.2	246.2	246.2	0.8068	0.8068	0.8068	62.
64.	0.0009189	0.0009189	0.0009189	254.6	254.6	254.6	254.6	254.6	254.6	0.8318	0.8318	0.8318	64.
66.	0.0009199	0.0009198	0.0009198	263.0	263.0	263.0	263.0	263.0	263.0	0.8566	0.8566	0.8566	66.
68.	0.0009209	0.0009209	0.0009209	271.4	271.4	271.4	271.4	271.4	271.4	0.8813	0.8813	0.8813	68.
70.	0.0009219	0.0009219	0.0009219	279.8	279.8	279.8	279.7	279.7	279.7	0.9058	0.9058	0.9058	70.
72.	0.0009230	0.0009230	0.0009230	288.2	288.2	288.2	288.1	288.1	288.1	0.9302	0.9302	0.9302	72.
74.	0.0009241	0.0009241	0.0009241	296.6	296.6	296.6	296.5	296.5	296.5	0.9544	0.9544	0.9544	74.
76.	0.0009252	0.0009252	0.0009252	305.0	305.0	305.0	304.9	304.9	304.9	0.9785	0.9784	0.9784	76.
78.	0.0009263	0.0009263	0.0009263	313.3	313.3	313.3	313.3	313.3	313.2	1.0024	1.0024	1.0023	78.
80.	0.0009275	0.0009275	0.0009275	321.7	321.7	321.7	321.6	321.6	321.6	1.0261	1.0261	1.0261	80.
82.	0.0009287	0.0009287	0.0009287	330.1	330.1	330.1	330.0	330.0	330.0	1.0497	1.0497	1.0497	82.
84.	0.0009299	0.0009299	0.0009299	338.4	338.4	338.4	338.3	338.3	338.3	1.0732	1.0732	1.0732	84.
86.	0.0009311	0.0009311	0.0009311	346.8	346.8	346.8	346.7	346.7	346.7	1.0965	1.0965	1.0965	86.
88.	0.0009324	0.0009324	0.0009324	355.1	355.1	355.1	355.0	355.0	355.0	1.1197	1.1197	1.1197	88.
90.	0.0009337	0.0009337	0.0009337	363.5	363.5	363.5	363.4	363.4	363.4	1.1427	1.1427	1.1427	90.
92.	0.0009350	0.0009350	0.0009350	371.8	371.8	371.8	371.7	371.7	371.7	1.1656	1.1656	1.1656	92.
94.	0.0009363	0.0009363	0.0009363	380.1	380.1	380.1	380.0	380.0	380.0	1.1884	1.1883	1.1883	94.
96.	0.0009377	0.0009377	0.0009377	388.5	388.5	388.5	388.4	388.4	388.4	1.2110	1.2110	1.2110	96.
98.	0.0009390	0.0009390	0.0009390	396.8	396.8	396.8	396.7	396.7	396.7	1.2335	1.2335	1.2335	98.
100.	1.6970	1.6064	0.0009404	2480.1	2479.5	405.1	2327.3	2326.9	405.0	6.8440	6.8203	1.2558	100.
105.	1.7213	1.6295	1.5468	2488.5	2488.9	2488.4	2334.6	2334.1	2333.7	6.8690	6.8454	6.8230	105.
110.	1.7456	1.6524	1.5687	2496.8	2496.3	2497.8	2341.8	2341.4	2340.9	6.8927	6.8702	6.8478	110.
115.	1.7696	1.6753	1.5905	2508.2	2507.7	2507.2	2348.9	2348.6	2348.2	6.9180	6.8945	6.8722	115.
120.	1.7936	1.6982	1.6122	2517.5	2517.1	2516.6	2356.1	2355.7	2355.4	6.9418	6.9185	6.8962	120.
125.	1.8176	1.7209	1.6339	2526.8	2526.4	2526.0	2363.3	2362.9	2362.6	6.9654	6.9420	6.9199	125.

	Volume, m^3/kg			Enthalpy, kJ/kg			Energy, kJ/kg			Entropy, kJ/kg.K			
p(kPa)	90.	95.	100.	90.	95.	100.	90.	95.	100.	90.	95.	100.	p(kPa)
t(C)													t(C)
130.	1.8415	1.7436	1.6555	2536.1	2535.7	2535.3	2370.6	2370.1	2369.8	6.9886	6.9653	6.9432	130.
135.	1.8653	1.7662	1.6770	2546.4	2545.0	2544.6	2377.5	2377.2	2376.9	7.0114	6.9882	6.9662	135.
140.	1.8891	1.7888	1.6985	2554.7	2554.3	2553.8	2384.7	2384.4	2384.1	7.0340	7.0108	6.9888	140.
145.	1.9129	1.8113	1.7200	2564.0	2563.6	2563.2	2391.8	2391.5	2391.2	7.0563	7.0332	7.0112	145.
150.	1.9366	1.8338	1.7414	2573.2	2572.9	2572.5	2398.9	2398.7	2398.4	7.0783	7.0552	7.0333	150.
155.	1.9603	1.8563	1.7627	2582.5	2582.2	2581.8	2406.1	2405.8	2405.5	7.1001	7.0770	7.0551	155.
160.	1.9839	1.8787	1.7841	2591.7	2591.4	2591.1	2413.2	2412.9	2412.7	7.1216	7.0986	7.0767	160.
165	2.0075	1.9011	1.8054	2601.0	2600.7	2600.4	2420.3	2420.1	2419.8	7.1428	7.1199	7.0980	165.
170.	2.0311	1.9235	1.8267	2610.3	2610.0	2609.7	2427.5	2427.3	2427.0	7.1639	7.1409	7.1191	170.
175.	2.0546	1.9458	1.8479	2619.5	2619.2	2619.0	2434.6	2434.4	2434.2	7.1847	7.1618	7.1400	175.
180.	2.0782	1.9681	1.8691	2628.8	2628.5	2628.3	2441.8	2441.6	2441.4	7.2053	7.1824	7.1607	180.
185.	2.1017	1.9904	1.8903	2638.1	2637.9	2637.6	2449.0	2448.8	2448.6	7.2257	7.2028	7.1811	185.
190.	2.1251	2.0127	1.9115	2647.4	2647.2	2646.9	2456.2	2456.0	2455.8	7.2459	7.2230	7.2013	190.
195.	2.1486	2.0349	1.9326	2656.7	2656.5	2656.3	2463.4	2463.2	2463.0	7.2658	7.2430	7.2214	195.
200.	2.1720	2.0571	1.9538	2666.0	2665.8	2665.6	2470.6	2470.4	2470.2	7.2857	7.2629	7.2412	200.
210.	2.2188	2.1015	1.9960	2684.7	2684.5	2684.3	2485.0	2484.9	2484.7	7.3247	7.3019	7.2803	210.
220.	2.2656	2.1458	2.0381	2703.4	2703.3	2703.1	2499.5	2499.4	2499.3	7.3631	7.3403	7.3187	220.
230.	2.3123	2.1901	2.0802	2722.2	2722.0	2721.9	2514.1	2514.0	2513.9	7.4008	7.3781	7.3565	230.
240.	2.3589	2.2343	2.1222	2741.1	2740.9	2740.7	2528.8	2528.6	2528.5	7.4379	7.4152	7.3936	240.
250.	2.4055	2.2785	2.1642	2760.0	2759.8	2759.7	2543.5	2543.4	2543.2	7.4743	7.4517	7.4301	250.
260.	2.4521	2.3226	2.2061	2778.9	2778.8	2778.6	2558.2	2558.1	2558.0	7.5102	7.4876	7.4661	260.
270.	2.4986	2.3667	2.2480	2798.0	2797.8	2797.7	2573.1	2573.0	2572.9	7.5456	7.5230	7.5015	270.
280.	2.5451	2.4108	2.2899	2817.1	2816.9	2816.8	2588.0	2587.9	2587.8	7.5805	7.5578	7.5364	280.
290.	2.5915	2.4548	2.3318	2836.2	2836.1	2836.0	2603.0	2602.9	2602.8	7.6148	7.5922	7.5708	290.
300.	2.6380	2.4988	2.3736	2855.5	2855.4	2855.3	2618.1	2618.0	2617.9	7.6487	7.6261	7.6047	300.
310.	2.6844	2.5428	2.4154	2874.8	2874.7	2874.6	2633.2	2633.1	2633.1	7.6821	7.6595	7.6381	310.
320.	2.7308	2.5868	2.4572	2894.2	2894.1	2894.0	2648.4	2648.4	2648.3	7.7151	7.6925	7.6711	320.
330.	2.7772	2.6307	2.4989	2913.7	2913.6	2913.5	2663.7	2663.7	2663.6	7.7476	7.7251	7.7037	330.
340.	2.8235	2.6747	2.5407	2933.2	2933.1	2933.0	2679.1	2679.0	2679.0	7.7798	7.7572	7.7358	340.
350.	2.8699	2.7186	2.5824	2952.9	2952.8	2952.7	2694.6	2694.6	2694.4	7.8115	7.7890	7.7676	350.
360.	2.9162	2.7625	2.6241	2972.6	2972.5	2972.4	2710.1	2710.0	2710.0	7.8429	7.8204	7.7990	360.
370.	2.9625	2.8064	2.6658	2992.4	2992.3	2992.2	2725.7	2725.7	2725.6	7.8739	7.8514	7.8300	370.
380.	3.0088	2.8502	2.7075	3012.2	3012.1	3012.1	2741.4	2741.4	2741.3	7.9046	7.8820	7.8607	380.
390.	3.0551	2.8941	2.7492	3032.2	3032.1	3032.0	2757.2	2757.2	2757.1	7.9349	7.9124	7.8910	390.
400.	3.1014	2.9379	2.7909	3052.2	3052.1	3052.1	2773.1	2773.0	2773.0	7.9649	7.9424	7.9210	400.
420.	3.1939	3.0256	2.8742	3092.5	3092.4	3092.4	2805.0	2805.0	2805.0	8.0239	8.0014	7.9800	420.
440.	3.2864	3.1133	2.9575	3133.1	3133.1	3133.0	2837.4	2837.3	2837.3	8.0817	8.0592	8.0378	440.
460.	3.3789	3.2009	3.0407	3174.1	3174.1	3174.0	2870.0	2870.0	2869.9	8.1383	8.1158	8.0945	460.
480.	3.4714	3.2885	3.1240	3215.4	3215.4	3215.3	2903.0	2902.9	2902.9	8.1939	8.1714	8.1501	480.
500.	3.5638	3.3761	3.2072	3257.1	3257.0	3257.0	2936.3	2936.3	2936.2	8.2485	8.2260	8.2046	500.
520.	3.6562	3.4637	3.2904	3299.0	3299.0	3298.9	2970.0	2969.9	2969.9	8.3021	8.2796	8.2582	520.
540.	3.7486	3.5512	3.3736	3341.3	3341.3	3341.2	3003.9	3003.9	3003.9	8.3547	8.3322	8.3108	540.
560.	3.8411	3.6388	3.4567	3383.9	3383.9	3383.9	3038.2	3038.2	3038.2	8.4065	8.3840	8.3627	560.
580.	3.9334	3.7263	3.5399	3426.9	3426.8	3426.8	3072.9	3072.8	3072.8	8.4574	8.4350	8.4136	580.
600.	4.0258	3.8138	3.6231	3470.2	3470.1	3470.1	3107.8	3107.8	3107.8	8.5076	8.4851	8.4638	600.
620.	4.1182	3.9014	3.7062	3513.7	3513.7	3513.7	3143.1	3143.1	3143.1	8.5569	8.5345	8.5131	620.
640.	4.2106	3.9888	3.7894	3557.6	3557.6	3557.6	3178.7	3178.7	3178.6	8.6055	8.5831	8.5618	640.
660.	4.3029	4.0764	3.8725	3601.9	3601.8	3601.8	3214.6	3214.6	3214.6	8.6534	8.6310	8.6097	660.
680.	4.3953	4.1639	3.9556	3646.4	3646.4	3646.3	3250.8	3250.8	3250.8	8.7007	8.6782	8.6569	680.
700.	4.4876	4.2514	4.0387	3691.2	3691.2	3691.2	3287.3	3287.3	3287.2	8.7472	8.7247	8.7034	700.
720.	4.5800	4.3389	4.1219	3736.4	3736.3	3736.3	3324.2	3324.1	3324.1	8.7931	8.7706	8.7493	720.
740.	4.6723	4.4263	4.2050	3781.8	3781.8	3781.7	3361.3	3361.3	3361.2	8.8384	8.8158	8.7946	740.
760.	4.7646	4.5138	4.2881	3827.5	3827.5	3827.5	3398.7	3398.7	3398.6	8.8831	8.8605	8.8393	760.
780.	4.8570	4.6013	4.3712	3873.5	3873.5	3873.5	3436.4	3436.4	3436.3	8.9272	8.9047	8.8834	780.
800.	4.9493	4.6888	4.4543	3919.8	3919.8	3919.7	3474.3	3474.3	3474.2	8.9707	8.9482	8.9269	800.

Table C2: Specific Heat

Table B. Specific Heat at Constant Pressure

Specific Heat, J/g.K

p(kPa)	10.	20.	30.	40.	60.	80.	100.	200.	300.	400.	600.	800.	p(kPa)
t sat	47.93	62.00	70.92	77.60	87.54	95.01	101.05	121.41	134.56	144.53	159.57	171.02	t sat
Liq.sat	4.223	4.204	4.193	4.184	4.173	4.165	4.160	4.153	4.158	4.167	4.189	4.215	Liq.sat
Vap.sat	1.772	1.799	1.819	1.834	1.861	1.882	1.902	1.979	2.043	2.100	2.205	2.302	Vap.sat
t(C)													t(C)
20.	4.243	4.243	4.242	4.242	4.242	4.242	4.242	4.242	4.242	4.241	4.240	4.240	20.
30.	4.240	4.240	4.240	4.240	4.240	4.240	4.240	4.240	4.240	4.239	4.239	4.238	30.
40.	4.232	4.232	4.232	4.232	4.232	4.232	4.232	4.231	4.231	4.231	4.230	4.230	40.
50.	1.771	4.220	4.220	4.220	4.220	4.220	4.220	4.220	4.220	4.219	4.219	4.218	50.
60.	1.767	4.207	4.207	4.207	4.207	4.207	4.207	4.207	4.207	4.206	4.208	4.205	60.
70.	1.766	1.783	4.194	4.194	4.194	4.194	4.194	4.193	4.193	4.193	4.193	4.192	70.
80.	1.767	1.788	1.810	1.831	4.181	4.181	4.181	4.181	4.181	4.180	4.180	4.180	80.
90.	1.770	1.787	1.804	1.821	1.857	4.170	4.170	4.170	4.169	4.169	4.169	4.168	90.
100.	1.774	1.787	1.802	1.816	1.845	1.874	4.161	4.161	4.161	4.160	4.160	4.160	100.
110.	1.778	1.790	1.801	1.813	1.837	1.861	1.886	4.155	4.165	4.166	4.154	4.154	110.
120.	1.783	1.793	1.803	1.813	1.833	1.853	1.874	4.153	4.153	4.153	4.152	4.152	120.
130.	1.789	1.798	1.806	1.814	1.831	1.848	1.866	1.956	4.155	4.155	4.154	4.154	130.
140.	1.795	1.803	1.810	1.817	1.831	1.846	1.861	1.940	2.026	4.162	4.161	4.161	140.
150.	1.802	1.808	1.814	1.821	1.833	1.846	1.859	1.927	2.000	2.080	4.173	4.173	150.
160.	1.809	1.814	1.820	1.825	1.836	1.847	1.858	1.917	1.981	2.049	2.203	4.190	160.
170.	1.816	1.821	1.825	1.830	1.840	1.848	1.859	1.911	1.968	2.025	2.156	4.212	170.
180.	1.823	1.827	1.831	1.836	1.844	1.853	1.862	1.907	1.955	2.007	2.120	2.249	180.
190.	1.830	1.834	1.838	1.842	1.849	1.857	1.865	1.905	1.947	1.992	2.091	2.201	190.
200.	1.838	1.841	1.845	1.848	1.855	1.862	1.869	1.904	1.942	1.982	2.068	2.163	200.
210.	1.845	1.848	1.851	1.854	1.861	1.867	1.873	1.905	1.939	1.974	2.049	2.133	210.
220.	1.853	1.856	1.859	1.861	1.867	1.872	1.878	1.907	1.937	1.968	2.035	2.108	220.
230.	1.861	1.863	1.866	1.868	1.873	1.878	1.883	1.909	1.936	1.964	2.024	2.088	230.
240.	1.869	1.871	1.873	1.876	1.880	1.886	1.889	1.913	1.937	1.962	2.015	2.072	240.
250.	1.877	1.879	1.881	1.883	1.887	1.891	1.895	1.917	1.938	1.961	2.009	2.058	250.
260.	1.885	1.887	1.889	1.891	1.894	1.898	1.902	1.921	1.941	1.961	2.004	2.049	260.
270.	1.893	1.895	1.896	1.898	1.902	1.905	1.908	1.926	1.944	1.962	2.001	2.041	270.
280.	1.901	1.903	1.904	1.906	1.909	1.912	1.915	1.931	1.948	1.964	1.999	2.036	280.
290.	1.910	1.911	1.912	1.914	1.917	1.920	1.922	1.937	1.952	1.967	1.999	2.032	290.
300.	1.918	1.919	1.920	1.922	1.924	1.927	1.930	1.943	1.957	1.971	1.999	2.029	300.
310.	1.926	1.927	1.929	1.930	1.932	1.935	1.937	1.949	1.962	1.974	2.001	2.028	310.
320.	1.935	1.936	1.937	1.938	1.940	1.942	1.945	1.956	1.967	1.979	2.003	2.027	320.
330.	1.943	1.944	1.945	1.946	1.948	1.950	1.952	1.962	1.973	1.984	2.005	2.028	330.
340.	1.951	1.952	1.953	1.954	1.956	1.958	1.960	1.969	1.979	1.989	2.009	2.029	340.
350.	1.960	1.961	1.962	1.962	1.964	1.966	1.968	1.976	1.985	1.994	2.013	2.032	350.
360.	1.968	1.969	1.970	1.971	1.972	1.974	1.976	1.984	1.992	2.000	2.017	2.034	360.
370.	1.977	1.978	1.978	1.979	1.981	1.982	1.984	1.991	1.999	2.006	2.022	2.038	370.
380.	1.985	1.986	1.987	1.987	1.989	1.990	1.992	1.999	2.006	2.013	2.027	2.042	380.
390.	1.994	1.995	1.995	1.996	1.997	1.998	2.000	2.006	2.013	2.019	2.032	2.046	390.
400.	2.002	2.003	2.004	2.004	2.005	2.007	2.008	2.014	2.020	2.026	2.038	2.051	400.
420.	2.020	2.020	2.021	2.021	2.023	2.023	2.024	2.029	2.035	2.040	2.050	2.061	420.
440.	2.037	2.037	2.038	2.038	2.039	2.040	2.041	2.045	2.050	2.054	2.063	2.073	440.
460.	2.054	2.054	2.054	2.055	2.056	2.056	2.057	2.061	2.065	2.069	2.077	2.085	460.
480.	2.071	2.071	2.071	2.072	2.072	2.073	2.074	2.077	2.081	2.084	2.091	2.098	480.
500.	2.088	2.088	2.088	2.088	2.089	2.090	2.090	2.093	2.096	2.099	2.105	2.112	500.
520.	2.104	2.105	2.105	2.105	2.106	2.106	2.107	2.109	2.112	2.115	2.121	2.126	520.
540.	2.121	2.121	2.121	2.122	2.122	2.123	2.123	2.126	2.128	2.131	2.136	2.140	540.
560.	2.138	2.138	2.138	2.138	2.139	2.139	2.139	2.142	2.144	2.146	2.151	2.155	560.
580.	2.154	2.154	2.154	2.154	2.155	2.155	2.156	2.158	2.160	2.162	2.166	2.170	580.
600.	2.170	2.170	2.170	2.171	2.171	2.171	2.172	2.174	2.175	2.177	2.181	2.185	600.
620.	2.186	2.186	2.186	2.187	2.187	2.187	2.188	2.189	2.191	2.193	2.196	2.199	620.
640.	2.202	2.202	2.202	2.202	2.203	2.203	2.203	2.205	2.206	2.208	2.211	2.214	640.
660.	2.218	2.218	2.218	2.218	2.218	2.219	2.219	2.220	2.222	2.223	2.226	2.229	660.
680.	2.233	2.233	2.233	2.233	2.234	2.234	2.234	2.236	2.237	2.238	2.241	2.244	680.
700.	2.248	2.248	2.248	2.248	2.249	2.249	2.249	2.251	2.252	2.253	2.256	2.258	700.

Table C3: Dynamic Viscosity

TABLE 9 DYNAMIC VISCOSITY (16) $(10^{-7}$ Pa.s) μ

T/K	276.95	300	350	400	450	500	550	600	625	650	675	700	750	800
P/MPa			$\times 10^{-7}$											
0.1	20461	10481	4321	183.3	157.5	177.5	197.9	218.8	229.4	240.1	250.8	261.7	283.7	306.1
1	20451	10481	4323	2555	1746	175.2	196.3	217.8	228.8	239.8	250.8	261.9	284.2	306.6
2.5	20435	10481	4328	2560	1750	171.2	193.5	216.2	227.7	239.3	250.8	262.1	284.9	307.6
5	20408	10481	4335	2568	1757	1320	188.6	213.6	226.3	238.7	250.9	262.8	286.3	309.7
7.5	20381	10481	4342	2575	1764	1327	1057	211.3	225.1	238.5	251.3	263.7	287.9	311.6
10	20353	10481	4349	2583	1771	1334	1066	209.6	224.5	238.8	252.1	264.9	289.6	314.1
15	20295	10481	4362	2598	1785	1348	1082	836.2	227.5	241.8	255.4	268.5	293.9	319.5
20	20236	10480	4376	2613	1799	1362	1097	865.3	723.9	255.5	263.4	274.9	299.7	326.1
25	20175	10479	4389	2628	1812	1375	1111	889.7	773.0	562.5	286.1	286.8	307.6	334.4
30	20113	10478	4403	2642	1826	1387	1125	910.9	809.3	665.9	394.3	312.3	318.8	345.0
35	20048	10474	4416	2657	1839	1400	1137	929.9	838.0	721.6	550.4	372.8	335.3	358.5
40	19982	10472	4429	2671	1852	1411	1149	947.1	862.2	761.6	629.4	467.7	359.8	375.6
50	19846	10464	4454	2699	1877	1434	1172	977.8	902.6	820.5	722.9	610.5	441.2	426.3
60	19703	10456	4479	2727	1902	1455	1193	1005	936.2	865.9	785.8	698.4	544.8	501.2
70	19554	10445	4503	2754	1926	1475	1212	1028	965.1	903.5	834.8	763.4	639.3	590.9
80	19399	10433	4527	2781	1949	1494	1230	1050	990.3	935.4	875.7	815.9	719.1	686.7
100	19074	10404	4573	2833	1995	1531	1264	1088	1034	988.3	942.7	900.0	847.6	864.3

Table C4: Thermal Conductivity

TABLE 11 THERMAL CONDUCTIVITY (16) (10^{-3}W/m.K)

T/K	276.95	300.0	350.0	400.0	450.0	500.0	550.0	600.0
P/MPa								
0.1	571.2	597.6	630.4	26.23	30.38	35.24	40.67	46.63
1	571.7	598.0	630.9	634.7	612.7	37.41	41.80	47.31
2.5	572.6	598.8	631.6	635.5	613.7	43.47	44.60	48.87
5	573.9	600.1	632.8	636.8	615.3	570.0	53.36	53.04
7.5	575.3	601.4	634.0	638.2	616.9	572.3	509.1	60.15
10	576.7	602.6	635.2	639.5	618.5	574.6	512.6	72.38
15	579.4	605.2	637.6	642.1	621.7	579.1	519.2	428.6
20	582.1	607.7	640.0	644.7	624.7	583.3	525.4	442.6
25	584.7	610.2	642.3	647.3	627.8	587.4	531.2	454.0
30	587.4	612.6	644.7	649.8	630.8	591.3	536.6	463.9
35	590.0	615.1	647.0	652.3	633.7	595.1	541.9	472.6
40	592.6	617.5	649.2	654.8	636.6	598.8	546.9	480.6
50	597.8	622.3	653.7	659.7	642.3	605.9	556.2	494.9
60	602.8	627.0	658.1	664.4	647.7	612.5	564.9	507.5
70	607.8	631.6	662.5	669.1	653.0	618.9	573.1	518.8
80	612.7	636.2	666.7	673.7	658.2	625.0	580.7	529.1
100	622.3	645.1	675.0	682.5	668.2	636.6	595.1	547.7
150	646.0	665.3	694.5	702.8	691.1	663.9	627.1	585.2
200	664.5	683.8	713.0	722.3	712.5	688.0	654.5	616.7
250	680.1	700.1	730.2	740.5	732.2	709.9	679.2	644.3

T/K	625.0	650.0	675.0	700.0	750.0	800.0	850.0	900.0
P/MPa								
0.1	49.81	53.12	56.57	60.15	67.75	75.93	84.71	94.1
1	50.36	53.59	56.98	60.52	68.05	76.20	84.96	94.3
2.5	51.60	54.61	57.85	61.28	68.69	76.75	85.46	94.8
5	54.75	57.11	59.91	63.05	70.08	77.93	86.50	95.7
7.5	59.74	60.86	62.89	65.51	71.94	79.46	87.83	96.9
10	67.41	66.28	66.97	68.77	74.30	81.35	89.43	98.3
15	99.92	85.27	79.66	79.29	80.67	86.24	93.47	101.9
20	379.0	134.3	101.9	93.12	89.56	92.69	98.63	106.2
25	379.8	348.4	147.7	116.3	101.5	100.8	104.9	111.4
30	414.9	359.7	268.5	156.3	117.1	110.7	112.3	117.4
35	428.2	375.8	320.8	222.5	137.7	122.7	120.9	124.3
40	439.9	390.7	343.3	278.1	164.1	136.8	130.7	131.8
50	459.1	417.1	373.8	329.3	226.6	171.5	153.6	149.1
60	474.8	438.0	398.1	359.9	276.9	211.2	180.4	169.0
70	488.4	455.4	419.6	383.3	312.3	247.7	209.1	190.7
80	500.3	470.0	437.4	403.6	339.6	279.5	237.0	213.2
100	521.2	494.1	466.4	437.4	380.7	328.9	285.4	255.1
150	563.3	540.9	518.4	495.8	451.1	409.2	372.4	341.3
200	597.0	577.2	557.3	537.6	499.1	462.9	430.1	401.8
250	626.2	607.9	589.7	571.7	536.7	503.9	473.9	447.5

References

[1] CANDU Technical Description, AECL document 69-01371-TED-001 Rev1, Jan 1995

[2] F. J. Doria, Atomic Energy of Canada Limited, *CANDU Safety #16: Large Loss-of-Coolant Accident with Coincident: Loss of Emergency Core Cooling,* Retrieved from http://canteach.candu.org/library/19990116.pdf

[3] J. C. Luxat, *Mechanistic Modeling of Heat Transfer Processes Governing Pressure Tube-To-Calandria Tube Contact and Fuel Channel Failure*, Proceedings CNS Annual Conference, June 2-5, 2002

[4] D. Meneley, *Nuclear Safety and Reliability*. Retrieved in May 2007 from CANTEACH website http://canteach.candu.org/library/20032209.pdf (Oct 23, 2003)

[5] S. El-Genk and A. G. Glebov, *Film Boiling From A Downward-facing Curved Surface In Saturated And Subcooled Water*, Int. J. Heat Mass Transfer, Vol39, No.2, 1996, pp275-288.

[6] P. J. Berenson, *Film Boiling Heat Transfer From A Horizontal Surface*, Journal of Heat Transfer, Trans. ASME, August 1961, pp351-356.

[7] P. E. Liley, *Steam Table in SI Units, private communication, School of Mechanical Engineering*, Purdue University, West Lafayette, IN, March 1984.

[8] L. A. Bromely, *Heat Transfer In Stable Film Boiling*, Chem. Eng. Prog., Vol. 46, No.5,1950, pp221-227.

[9] L. A. Bromely, N. R. LeRoy, and J. A. Robbers, *Heat Transfer In Forced Convection Film Boiling*, Industrial And Engineering Chemistry, Vol.45, No.12, December 1953. pp2639-2646.

[10] Y. P. Chang, *Wave Theory of Heat Transfer in Film Boiling, Journal of Heat*

Transfer, Feb. 1959, pp1-8.

[11] M. Mori, S. Toda, M. Ochiai, and S. Saito, *Transient Cooling Process Of Fuel Rod In Reactivity Initiated Accident,* J. Nucl. Sci. Technol. 17(6), 1980, pp413-424.

[12] W. S. Bradfield, *On the Effect of Subcooling on Wall Superheat in Pool Boiling*, Trans. ASME, Journal of Heat Transfer, 89-C, 1967. pp269-270

[13] M. R. Adler, *The Influence of Water Purity and Subcooling on the Minimum Film Boiling Temperature*, M. S. thesis, University of Illinois, Urbana-Champaign(1979).

[14] H. Lauer and W. Hufschmidt, *Heat Transfer and Surface Rewet During Quenching,* European Two-Phase Flow Group Meeting, Erlangen, May31-June4, 1976.

[15] D. G.. Groeneveld and J. C. Stewart, *The Minimum Film Boiling Temperature for Water during Film Boiling Collapse,* Int. Topical Meeting on Nuclear Reactor Thermal-Hydraulics, Santa Barbara, Calif., 1983, pp393-398.

[16] L. H. K, Leung and D. G. Groeneveld (Editors), *Compendium of Thermal Hydraulic Correlations and Fluid Properties,* Version 1991, Revision 1, COG-90-86

[17] N. Ohnishi, K. Ishijima and S. Tanzawa, *A Study of Subcooled Film-Boiling Heat Transfer Under Reactivity-Initiated Accident Conditions in Light Water Reactors*, Nuclear Science & Engineering, 88, 1984, pp331-341.

[18] V. K. Dhir and G. P. Purohit, *Subcooled Film-Boiling Heat. Transfer from Sphere*, Nuclear Engineering and Design, Vol. 47, 1978, pp. 49-66

[19] S. Nishio, *Prediction Technique for Minimum-Heat-Flux(MHF)-Point Condition of Saturated Pool Boiling*, Int. J. Heat Mass Transf., Vol.30, No.10(1987), pp2045-2057

[20] R. W. Fox, A. McDonald & P. Pritchard, *Introduction to Fluid Mechanics*, 6 ed, 2004, S28 on CD. John Wiley & Sons Inc.

[21] C. Meskell, *Section 3 of 4B6 Fluid Mechanics*, Department of Mechanical and manufacturing engineering, Trinity College, University of Dublin. Retrieved on July 19, 2007 from http://www.mme.tcd.ie/~craigm/Cnotes/4b6/nodes/week3.php

[22] International Nuclear Safety Center, "*Zircaloy Emissivity Recommendation*", Available online: http://www.insc.anl.gov/matprop/zircaloy/zircalemis.pdf, Retrieved on Oct 16, 2007.

[23] F. P. Incropera, D. P. Dewitt, *Fundamentals of Heat and Mass Transfer,* 5 ed. John Wiley & Sons, p811.

[24] Samuel Sideman, *The Equivalence of the Penetration and Potential Flow Theories,* Industrial and Engineering Chemistry, Vol.58, No.2, Feb 1966, pp57 (54-68).

[25] Suhas V. Patankar, *Numerical Heat Transfer and Fluid Flow*, ISBN 0891165223, Taylor & Francis, 1980, pp102.

[26] L. C. Witte, J. Orozco, *The Effect of Vapor Velocity Profile Shape on Flow Film Boiling from Submerged Bodies,* ASME Journal of Heat Transfer, Vol.106, Feb 1984, pp193 (191-197).

[27] P. G. Hill, R. D. MacMillan and V. Lee, *Tables of Thermodynamic Properties of Heavy Water in SI Units*, Atomic Energy of Canada Limited, AECL-7531, 1981.

[28] R. Fox, A. T. McDonald and P. J. Pritchard, *Introduction to Fluid Mechanics,* 6th ed., Student Resource CD-ROM, S-22. John Wiley & Sons.

[29] W. S. Bradfield, *Wave Generation at a Stagnation Point in Stable Film Boiling,* Report No. 35, Spec TAI.N532, No. 35, C.2, April 1965, College of Engineering, State University of New York At Stony Brook.

[30] N. N. Huang, *Viscoelastic analysis of von Karman laminated plates under in-plane compression with initial deflection*, International Journal of Non-Linear Mechanics, Volume 32, Number 6, November 1997 , pp. 1065-1075(11)

[31] G. B. Wallis, *One-dimensional Two-phase Flow*, McGraw-Hill, 1969, pp249.

[32] W. K. Kays and M. E. Crawford, *Convective Heat and Mass Transfer*, 2nd Edition, McGraw-Hill Book Company.

[33] L. Prandtl, *Fluid Motion with Very Small Friction (in German)*, Proceedings of the Third International Congress on Mathematics, Heidelberg, 1904; English translation available as NACA TM 452, March 1982.

[34] H. Blasius, *Grenzschichten in Flussigkeiten mit kleiner Reibung*, Z. Math. Phys. Vol.56, pp. 1-37, 1908, http://naca.larc.nasa.gov/reports/1950/naca-tm-1256 (English translation). Retrieved from http://en.wikipedia.org/wiki/Blasius_boundary_ layer"

[35] F. P. Incropera, D. P. DeWitt, *Fundamentals of Heat and Mass Transfer,* 5 ed, 2002, pp923

[36] P. G. Hill, R. D. C. MacMillan, and V. Lee, *Tables of Thermodynamic Properties of Heavy Water in S.I. Units*, Report No. AECL-7531, Atomic Energy of Canada Limited (AECL), 1981.

[37] G. Gillespie & R. Moyer, *An Experimental Determination of Heat Transfer from large Cylinders: Film Boiling in Subcooled Water*, WNRE-569, AECL, February 1984

[38] J. J. Carbajo, *A Study of Rewetting Temperatures", Nuclear Engineering and Design*, Vol. 84, No.1, Jan.1985.

[39] F. S. Gunnerson and A. W. Cronenberg, *On the Minimum Film Boiling Conditions for Spherical Geometries*, Trans. ASME, Journal of Heat Transfer, 102(1980), pp335-341

[40] M. D. Greenberg, *Advanced Engineering Mathematics*, Hardcover, REV, 2, Pearson Education